

LOCKHEED MARTIN ENERGY RESEARCH LIBRARIES

ORNL/TM-5431



3 4456 0509659 8

Cy 86

LMFBR Safety and Core Systems Programs Progress Report for October-December 1975

M. H. Fontana
J. L. Wantland
P. A. Gnadt
W. H. Sides
R. W. McCulloch
G. F. Flanagan
R. E. MacPherson



OAK RIDGE NATIONAL LABORATORY
CENTRAL RESEARCH LIBRARY
DOCUMENT COLLECTION
LIBRARY LOAN COPY

DO NOT TRANSFER TO ANOTHER PERSON
If you wish someone else to see this
document, send in name with document
and the library will arrange a loan.

UCRL-7748
(S) (2-67)

OAK RIDGE NATIONAL LABORATORY
OPERATED BY UNION CARBIDE CORPORATION FOR THE ENERGY RESEARCH AND DEVELOPMENT ADMINISTRATION

Printed in the United States of America. Available from
the Energy Research and Development Administration,
Technical Information Center

P.O. Box 62, Oak Ridge, Tennessee 37830

Price: Printed Copy \$5.50 ; Microfiche \$2.25

This report was prepared as an account of work sponsored by the United States Government. Neither the United States nor the Energy Research and Development Administration/United States Nuclear Regulatory Commission, nor any of their employees, nor any of their contractors, subcontractors, or their employees, makes any warranty, express or implied, or assumes any legal liability or responsibility for the accuracy, completeness or usefulness of any information, apparatus, product or process disclosed, or represents that its use would not infringe privately owned rights.

ORNL/TM-5431
UC-79, -79e, -79p

Contract No. W-7405-eng-26

LMFBR SAFETY AND CORE SYSTEMS PROGRAMS PROGRESS
REPORT FOR OCTOBER-DECEMBER 1975

M. H. Fontana W. H. Sides
J. L. Wantland R. W. McCulloch
P. A. Gnadt G. F. Flanagan
 R. E. MacPherson

JULY 1976

NOTICE This document contains information of a preliminary nature and was prepared primarily for internal use at the Oak Ridge National Laboratory. It is subject to revision or correction and therefore does not represent a final report.

OAK RIDGE NATIONAL LABORATORY
Oak Ridge, Tennessee 37830
operated by
UNION CARBIDE CORPORATION
for the
ENERGY RESEARCH AND DEVELOPMENT ADMINISTRATION

LOCKHEED MARTIN ENERGY RESEARCH LIBRARIES



3 4456 0509659 8

CONTENTS

	<u>Page</u>
PREVIOUS LMFBR SAFETY PROGRESS REPORTS	v
SUMMARY	vii
1. PROGRAM COORDINATION	1
References	3
2. ANALYSIS AND DATA EVALUATION	4
2.1 Bundle 3B Boiling Tests	4
2.2 Bundle 7A Heater Thermal Modeling	4
2.3 Bundle 5D Flow-Coastdown Tests	10
References	42
3. WATER SYSTEM MOCKUP OF THE FFM	43
4. DETECTION METHODS DEVELOPMENT	44
4.1 Temperature Fluctuation Measurement with Stainless Steel-Sodium Fast-Response Thermocouples	44
4.1.1 Bundle 6A Instrumentation	44
4.1.2 Single-Pin Test Loop Measurements	47
4.1.3 Temperature Measurement Problems with Stainless Steel Sodium Thermocouples in the FFM	47
References	49
5. FFM FACILITY OPERATIONS	50
5.1 Test Facility Operation	50
5.2 Test Bundles	50
5.2.1 Bundle 6	50
5.2.2 Bundle 7	50
5.3 Facility Modifications	65
5.3.1 Bundle Power Supply and Control	65
5.3.2 Bundle 6 Operation	67
5.4 Investigation of Failure of Bundle 5D	67
References	90
6. HEATER DEVELOPMENT	91
6.1 LMFBR Heaters	91
6.1.1 FFM Heaters	91
6.1.2 Fuel Pin Simulators for Others	93
6.1.3 Advanced Fuel Pin Simulator Development	94
6.1.4 Nondestructive Testing	96

7.	NEUTRONICS ANALYSIS OF A DISRUPTED CORE	97
7.1	Effects of Bubble Collapse on Reactivity	97
7.2	Development of a Transient Monte Carlo Code	98
7.3	Reactivity Determinations of a Disrupted Core	98
	References	98
8.	CENTRAL COMPUTERIZED DATA BASE FOR LMFBR SAFETY CODES	99
	References	99

PREVIOUS LMFBR SAFETY PROGRESS REPORTS

Prior information on these projects was presented in the following:

ORNL Nuclear Safety Research and Development
Program Bimonthly Reports

<u>Period Covered</u>	<u>Report No.</u>
September-October 1968	ORNL/TM-2425
November-December 1968	ORNL/TM-2479
January-February 1969	ORNL/TM-2533
March-April 1969	ORNL/TM-2588
May-June 1969	ORNL/TM-2663
July-August 1969	ORNL/TM-2718
September-October 1969	ORNL/TM-2777
November-December 1969	ORNL/TM-2829
January-February 1970	ORNL/TM-2919
March-April 1970	ORNL/TM-2984
May-June 1970	ORNL/TM-3061
July-August 1970	ORNL/TM-3122
September-October 1970	ORNL/TM-3212
November-December 1970	ORNL/TM-3263
January-February 1971	ORNL/TM-3342
March-April 1971	ORNL/TM-3411
May-June 1971	ORNL/TM-3483
July-August 1971	ORNL/TM-3554
September-October 1971	ORNL/TM-3623
November-December 1971	ORNL/TM-3670
January-February 1972	ORNL/TM-3738
March-April 1972	ORNL/TM-3831
May-June 1972	ORNL/TM-3900
July-August 1972	ORNL/TM-3873

LMFBR Safety and Core Systems Programs
Progress Reports

<u>Period Covered</u>	<u>Report No.</u>
September-October 1972	ORNL/TM-4075
November-December 1972	ORNL/TM-4088
January-February 1973	ORNL/TM-4148
March-April 1973	ORNL/TM-4261
May-June 1973	ORNL/TM-4331
July-September 1973	ORNL/TM-4417
October-December 1973	ORNL/TM-4505
January-March 1974	ORNL/TM-4630
April-June 1974	ORNL/TM-4727
July-September 1974	ORNL/TM-4776
October-December 1974	ORNL/TM-4877
January-March 1975	ORNL/TM-4980
April-June 1975	ORNL/TM-5076
July-September 1975	ORNL/TM-5197

SUMMARY

1. Program Coordination

This report includes the progress of two new programs: Neutronics Analysis of a Disrupted Core and Central Computerized Data Base for LMFBR Safety Codes.

Coordination was maintained with the LMFBR Loss-of-Pipe-Integrity (LOPI) Task Force, and results were obtained from a set of tests at MIT on boiling, dryout, and rewetting under LOPI conditions, using a simple water experiment. Plans were made to investigate analogous behavior with a similar sodium experiment.

Installation of bundle 6 into the Fuel Failure Mockup (FFM) facility was completed, and unheated flow tests were started. Bundle 7 was canceled, and tests were combined with those of bundle 6. Plans were made to progress directly to the 61-rod bundle 9.

An expanded effort on electrical fuel simulator development was undertaken to place the technology on a sound footing. In particular, development of techniques for fabricating Nichrome V and Pt-8% W alloy and for fabricating boron nitride (BN) preforms for electrical insulation were started.

2. Analysis and Data Evaluation

A preliminary draft of the FFM bundle 3B data record has been written. Preliminary evaluation of results will be reported in the next quarterly report.

A thermal model of an FFM bundle 7A electrically heated rod has been formulated and is being used in conjunction with a heat-conduction computer code to analyze the causes of a bundle 7A prototype heater failure during high-temperature [980°C (1800°F)] preliminary testing.

Tests were performed on FFM bundle 5D to determine the effects of power skew and an overpowered pin. An analysis was made using the duct wall thermocouples, the wire-wrap thermocouples, and the heater internal thermocouples. The results showed temperature increases and increases in the rate of temperature increase in the vicinity of the

overpowered area as the skew was increased. Thermocouples located in the underpowered area of the skew showed decreases in temperature and in the rate of temperature increase as the skew was increased. The thermocouples located in the average-power area of the skew showed no appreciable temperature changes as the skew was increased.

The responses of duct wall thermocouples located above the 381-mm (15-in.) axial level showed large temperature fluctuations, but the responses of duct wall thermocouples located below this level continually increased in temperature as did all the responses of the wire-wrap and heater internal thermocouples. The maximum temperature reached by the duct wall thermocouples was sufficiently high to indicate the presence of a power skew but not high enough to indicate the presence of an overpowered pin. The overpowered pin affected the temperature responses of only those thermocouples that were located close to it.

3. Water System Mockup of the FFM

Work in this area has been temporarily suspended. Reporting will continue when work is resumed.

4. Detection Methods Development

Seven stainless steel-sodium, fast-response thermocouple assemblies were installed in bundle 6A for evaluation. The low sensitivity of these junctions ($<17 \mu\text{V}/^\circ\text{C}$) requires special care in the electrical shielding of signal leads to reduce electromagnetic interference from the bundle heater circuits. Noise signals from these assemblies will be recorded and analyzed. Recorded signals from two assemblies installed in the single-pin heater test loop are currently being analyzed. Preliminary results show that shunt resistance losses will be important in the bundle 6A installation.

5. FFM Facility Operation

Metallurgical analysis of bundle 5, which was partially melted during boiling experiments, is now complete. The study disclosed that

the material from the ruptured heater sheaths and the heater elements remained within a few inches of its point of origin. The sodium apparently cleaned the surfaces of the undamaged heaters, allowing the alloy residue, principally Nichrome V, to wet these surfaces and adhere readily. The flowing sodium also rapidly cooled the molten alloy, preventing it from flowing very far and from dissolving or penetrating the sheaths of undamaged heaters. The stainless steel sheath material of one of the heaters was heated to its melting point, and the flowing sodium caused some of the molten stainless steel to move downstream, thickening the heater sheath in some areas. The Kanthal heater element probably became hot enough to melt and react with the BN or to heat the stainless steel sheath material until it reacted with the BN, thereby creating pressures great enough to blow the heater apart in the hot zone.

Bundle 6 was completed and installed in the facility. The need for bundle 7, another 19-rod bundle, and bundle 8, a 37-rod bundle originally designed for support of the ANL Sodium Loop Safety Facility (SLSF) test program, is being evaluated. A possibility exists that these bundles will be delayed or canceled in order to proceed with the testing of larger bundles. Operational testing of the newly modified facility is in progress.

6. Heater Development

Analysis of the 6A fuel pin simulators with low insulation resistance revealed no significant levels of impurities. The insulation resistance returned to normal when the affected 12.7-mm (1/2-in.) sections were baked out in a vacuum, indicating that trapped moisture was the original cause of low insulation resistance. Sodium loop tests on a 6A heater indicated that the bundle should operate for long periods at the intended heat flux and temperature levels. Another 6A fuel pin simulator will be tested in February 1976 under sodium boiling conditions.

The 7A bundle heaters were found to have uncrushed BN cores. Swaging cracked the cores and elongated the simulator enough to cause

core gaps. Heat flux profiles and other operational capabilities are inadequate for program use, as indicated by infrared (IR) scans and by premature failure of two units tested in the sodium loop.

Premature melting of the Pt-8% W ribbons, apparently due to secondary grain growth and melting, has led to early failure of several fuel pin simulators. Studies are in progress on methods to retard grain growth in the material.

Difficulties are still being experienced in the machining of Pt-8% W variable-width ribbons. Two ribbons were machined, but excessive tool wear caused excessive dimensional variations. Nichrome V ribbon is being machined as a backup. The use of an alumina-template grinding machine to fabricate these ribbons on a volume basis is being studied and looks very promising.

An effort to fabricate a preform fuel pin simulator with the aid of the Y-12 Development Division is in progress. The first simulator, to be fabricated in February 1976, will contain a Nichrome V variable-width ribbon and will have no internal thermoelements.

Fabrication of a high-temperature conductivity cell test apparatus is complete and resistivity testing of conductivity cells will begin shortly.

The request for capital funds to support commercial fabrication of BN preforms has been approved, and the purchase requisition is being processed. Meanwhile, preforms are being fabricated locally to fill interim demand. The Metals and Ceramics Division has developed a BN-powder pretreatment that may allow high-volume fabrication of highly oriented preforms. A vacuum-drying and ammonia-baking process, developed at ORNL, appears to provide excellent purification of preforms. Plans to install such a process locally to purify commercially fabricated preforms are in progress.

Equipment to automate the IR scanning system is in the final testing stages and will be operational in February. A dc offset device that gives high-temperature, high-resolution IR scans is now operational. Cost quotations have been obtained on the equipment necessary for automation of the simulator x-ray examination. Automation will allow quick,

accurate data to be obtained during heater radiography on coil turns per inch, concentricity, width, and thickness.

7. Neutronics Analysis of a Disrupted Core

The analysis of the reactivity due to stainless steel vapor bubble collapse using transport techniques has been completed. All efforts to use Monte Carlo techniques have failed, except for the method employing an upper-bound approach. Efforts to estimate the quasi-static integral parameters using Monte Carlo have begun.

8. Central Computerized Data Base for LMFBR Safety Codes

The computer system JOSHUA has been obtained from Savannah River Laboratory and is being implemented on the ORNL computers. This system provides the necessary data management options needed for operation of the safety data base. The data base will be coordinated by a national committee composed of various evaluation groups whose task it is to collect and evaluate the data before they are entered into the system.

1. PROGRAM COORDINATION

M. H. Fontana

The LMFBR safety research and development effort at ORNL is composed of four programs: (1) Fuel Failure Mockup Facility (189a OH044), (2) Electric Heaters for Fuel Pin Simulation (189a OH033), (3) Neutronics Analysis of a Disrupted Core (189a OH069), and (4) Central Computerized Data Base for LMFBR Safety Codes (189a OH099).

The Fuel Failure Mockup (FFM), reported in Chaps. 1 to 5 of this report, is a sodium flow facility that has the capability of simulating LMFBR fuel subassemblies using electric cartridge heaters. Prototypic configuration, power density, pressure, specific flow, and temperature are obtained. The objectives of the program include (1) investigation of flow and temperature distributions within fuel rod assemblies under normal and accident conditions, such as partial flow blockages and flow-power mismatches; (2) detection of events that could lead to failure; (3) investigation of loop system dynamics; and (4) extrapolation of experimental results to predict the behavior of full-size reactors under hypothetical accident conditions.

The Electric Heaters for Fuel Pin Simulation task (Chap. 6) has as its objective the development and refinement of the technology of electric heaters for simulating LMFBR fuel assemblies over a wide range of conditions up to and including sodium boiling and dryout. An integral part of the program is the development of commercial sources of these heaters for the entire LMFBR thermal-hydraulic experimental community.

The purpose of the Neutronics Analysis of a Disrupted Core task (Chap. 7) is (1) to test and verify neutronics methods for analysis of disrupted LMFBR cores using existing computer codes, and (2) to develop a three-dimensional Monte Carlo quasi-static code appropriate for coupling with existing hydrodynamics codes for use in LMFBR core disassembly calculations.

The Central Computerized Data Base for LMFBR Safety Codes task (Chap. 8) has as its purpose the definition, development, and maintenance of a central computerized data base for LMFBR safety computer codes.

Coordination was maintained with the LMFBR Loss-of-Pipe-Integrity (LOPI) Task Force, and a test was funded at MIT to investigate dryout and rewetting under conditions approximating those subsequent to a LOPI, using a simple water rig. Plans are to duplicate the tests at ORNL, using sodium. FFM bundle 6 will be used to investigate thermal-hydraulic behavior associated with the LOPI, and a test program is being worked out with the LOPI Task Force.

Evaluations were made of the use of the old side of the FFM loop for testing instrumentation, such as flowmeters and pressure transducers, under severe transient and temperature conditions.

A meeting was held with personnel of the Clinch River Breeder Reactor (CRBR) project to acquaint them with ORNL capabilities in liquid-metal technology.

Midyear evaluation of the program indicated the need for an extensive effort in heater development to place the technology on a sound basis, to develop a smoothly variable axial heat-flux profile, and to develop boron nitride (BN) preforms for internal insulation to ensure greater reliability and consistency. It was also recommended that (1) bundle 7 be dropped and its test program combined with bundle 6, (2) the sodium analog of the MIT water LOPI tests be constructed, (3) the 37-rod bundle 8 be skipped, and (4) the 61-rod bundle 9 be constructed in sequence after bundle 6, with the timing dependent on the assurance of a quality supply of electric fuel pin simulators.

The first national meeting of the thermal-hydraulic working group, which was held at Westinghouse Advanced Reactors Division (WARD) on December 11, 1975, was attended by FFM project staff. The desirability of using the FFM as a loop dynamics, natural-convection test bed was discussed. Also, discussed was the need for larger bundle tests (up to 217 rods). Both of these items will be documented in CY 1976.

A summary of FFM program accomplishments during CY 1975 was transmitted to the ERDA Division of Reactor Development and Demonstration (RDD). Included in the summary were the boiling tests with bundle 5D; the boiling tests with the internally blocked bundle 3B; the expansion of the electrical power supply to 2.0 MW; the expansion of the loop for full-length experiments with a sodium-mixing plenum, bypass line,

and valving to allow for simulation of reactor primary-coolant loop systems; and construction at ORNL of a 2.0-MW dump heat exchanger to nuclear standards.

In the heater development program, development of techniques for the fabrication of variable-width ribbons of Nichrome V and Pt-8% W alloys was started at the Y-12 Plant. Also, in-house production of limited amounts of BN preforms was started prior to the placing of a commercial contract.

The FFM was filled with sodium, and unheated flow tests were performed. Of particular interest was the fact that the oscillations of the liquid levels in the pump bowl and within the sodium-mixing plenum were within tolerance, which is of importance should loss of power occur during unattended operation.

Close coordination with the LMFBR safety community was maintained in order to obtain input to the Central Computerized Data Base for LMFBR Safety Codes program.

Two papers directly related to the project were issued during this report period.^{1,2}

References

1. J. L. Wantland et al., "The Effect of Edge Configuration on Peripheral Flow in Sodium-Cooled 19-Rod Bundles with Helical Wire-Wrap Spacers," Trans. Am. Nucl. Soc. 22, 398 (1975).
2. W. H. Leavell and W. H. Sides, "Effects of Entrained Gas on the Acoustic Detection of Sodium Boiling in a Simulated LMFBR Fuel Bundle," Trans. Am. Nucl. Soc. 22, 399 (1975).

2. ANALYSIS AND DATA EVALUATION

M. H. Fontana N. Hanus
J. L. Wantland C. M. Smith

2.1 Bundle 3B Boiling Tests

A preliminary draft of the bundle 3B data record entitled Boiling Tests (With and Without Inert Gas Injection) in a 19-Rod Simulated LMFBR Fuel Assembly with a Central Blockage (Record of Experimental Data for Fuel Failure Mockup Bundle 3B) has been written and is being reviewed. This report contains graphs of the unevaluated experimental data for each of the 22 bundle 3B tests conducted in the LMFBR FFM in April 1975 along with a description of bundle 3B and the FFM facility. Bundle 3B consisted of 19 electrically heated rods spaced by wire wraps, with rod and spacer outside diameters being those of the Fast Test Reactor (FTR). A 6.3-mm-long (0.25-in.) stainless steel blockage covered the central six flow channels (approximately 12.5% of the total flow area) at an axial position 381 mm (15 in.) downstream from the start of the 533-mm-long (21-in.) heated section.

The primary purpose of the bundle 3B tests was to determine if stable sodium boiling (i.e., no propagation of the boiling zone during constant flow and heater power) could be maintained downstream of the blockage. Preliminary results of bundle 3B data analysis for stable boiling were discussed in the previous report in this series.¹ Other bundle 3B results, discussing inert-gas injection during boiling and nonboiling experiments, will be presented in a future report in this series.

2.2 Bundle 7A Heater Thermal Modeling

A mathematical model of the heated section of a bundle 7A heater was formulated and is being used in a transient heat-conduction computer code to theoretically determine the causes of a prototype FFM bundle 7A heater failure during full-power, high-temperature [approximately 982°C (1800°F)] testing in sodium.

The bundle 7A heater, shown in Fig. 2.1, consists of a variable-pitch, Pt-8% W alloy ribbon (heating element) that is helically wound around a premachined hot-pressed BN rod and centered in a tube clad with type 316 stainless steel. Granular BN is tamped into the annular space between the tube and the heating element, after which the entire assembly is compacted by swaging. The total length of the heated section is 914 mm (36 in.).

A three-phase approach is being taken to analyze heater failure.

Phase I — In order to establish the overall validity of the mathematical heater model, theoretical and experimental average outside cladding temperatures are to be compared for two preliminary tests in which the heater was placed in air and energized for 1 sec either through the heating element or through the cladding. The theoretical outside cladding temperatures are then to be matched to the experimental values (see Figs. 2.2 and 2.3) by varying the thermal conductivity (a function of density) of the granular BN located in the annular space between the heating element and the cladding. This approach assumes that the thermal conductivity is not completely known because of the process by which granular BN is compressed in the annular space.

Phase II — Further improvements in the model are to be made by including heater defects that were found in a postfailure examination² and consisted of gaps in the central BN rod; the local fluctuations in the experimental cladding temperatures in Figs. 2.2 and 2.3 can thus be reproduced theoretically.

Phase III — Causes of heating element failure during full-power, high-temperature [980°C (1800°F)] testing are to be determined by subjecting the heating element in the refined theoretical model to the same length of time and power at which failure occurred in the test.

The present status of the effort is in phase I, where the average theoretical outside cladding temperatures for the 1-sec cladding energization have been determined and are shown in Fig. 2.4 as a function of granular BN density. The relationship between the thermal conductivity and density of granular BN, as shown in Fig. 2.4, was taken from Ref. 3 and is used as a first estimate until a corresponding relationship is available for a prototype bundle 7A heater. A comparison

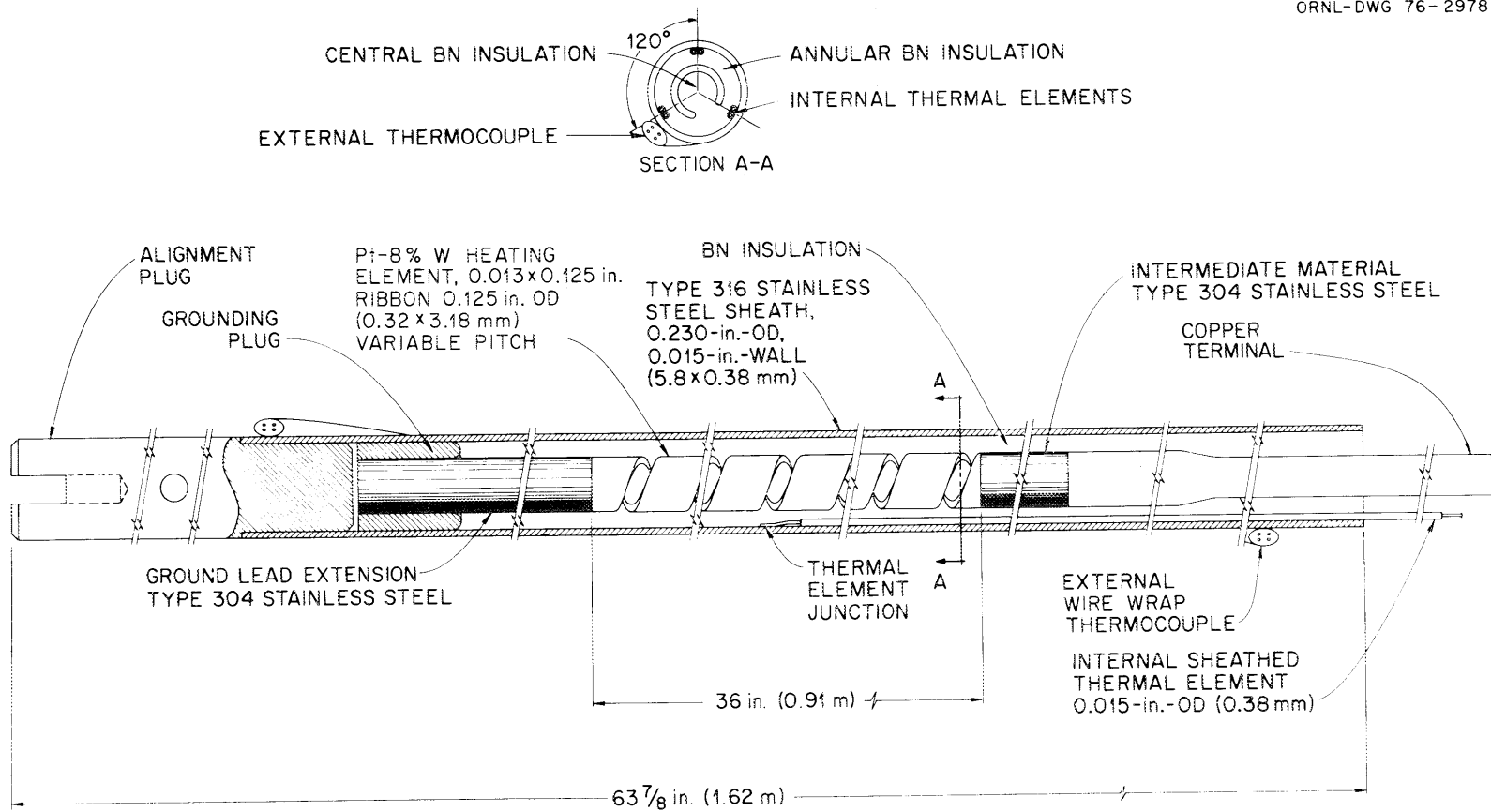


Fig. 2.1. LMFBR category III heater (bundle 6A and 7A heater).

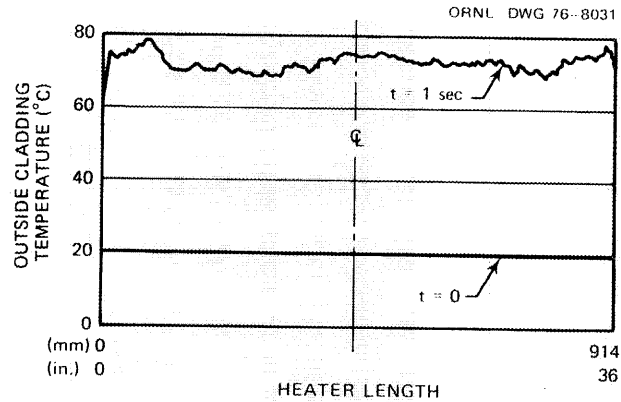


Fig. 2.2. Bundle 7A prototype heater experimental temperature profile after 1-sec cladding energization.

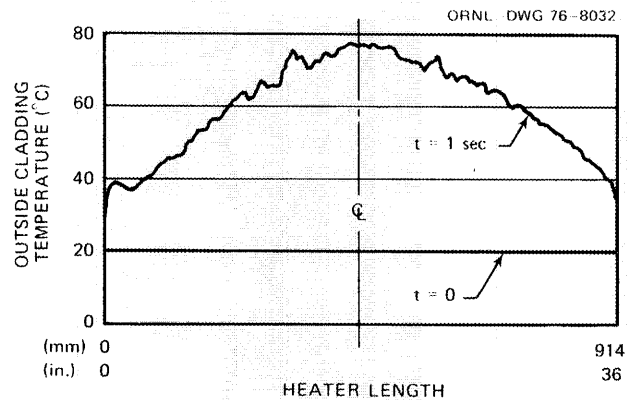


Fig. 2.3. Bundle 7A prototype heater experimental temperature profile after 1-sec heating element energization.

of Figs. 2.2 and 2.4 shows that the average theoretical outside cladding temperature after 1 sec [$\sim 75^{\circ}\text{C}$ (168°F)] matches the experimental value at a granular BN density of $\sim 86\%$ theoretical density (TD). The heater model used for cladding energization is shown in Fig. 2.5, where the helically wound heater element and the corresponding helical gaps have been lumped together every 50.8 mm (2 in.). The model includes assumptions of negligible free convection, negligible axial conduction away from the heated section, radial heater symmetry, and axial heater symmetry.

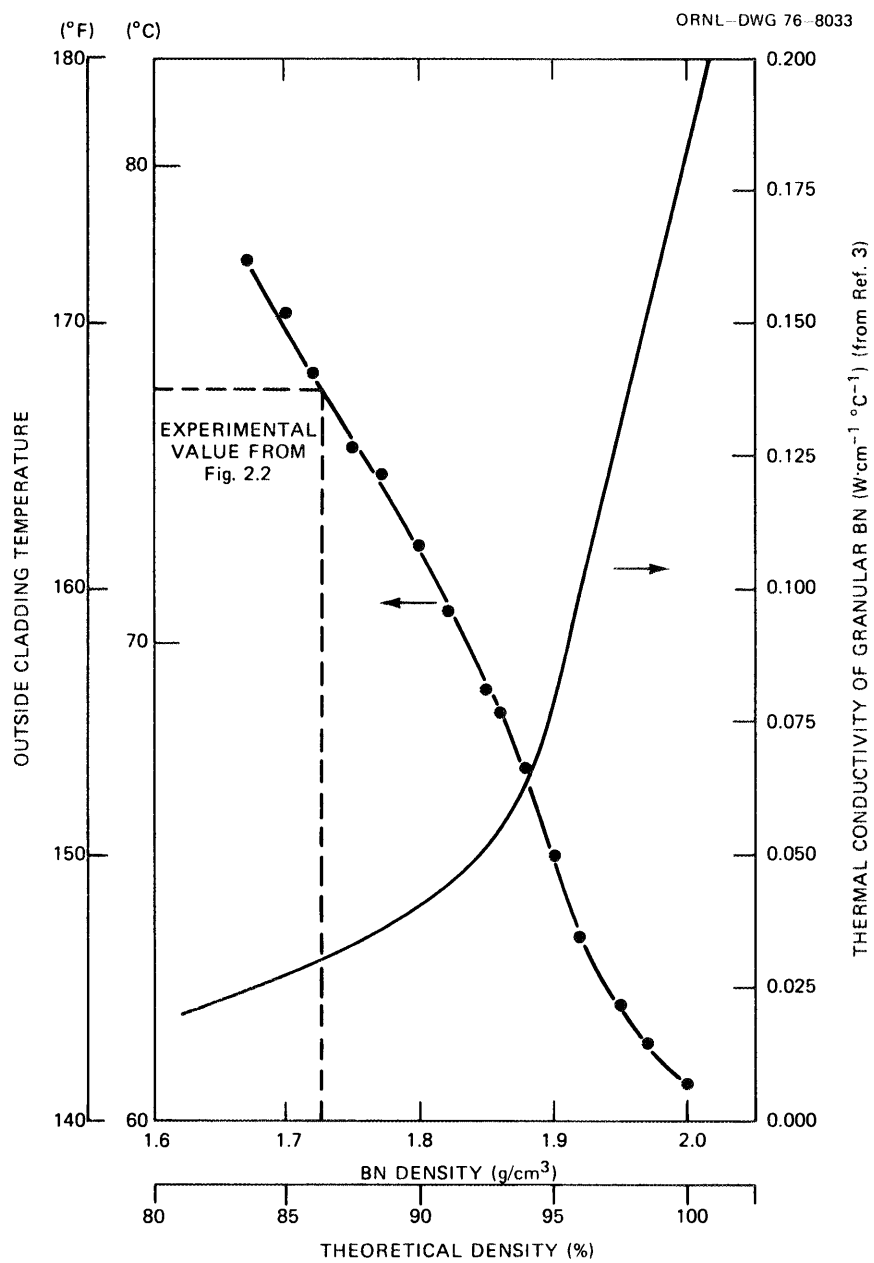


Fig. 2.4. Outside cladding temperatures after 1-sec cladding energization using lumped thermal model of bundle 7A prototype heater.

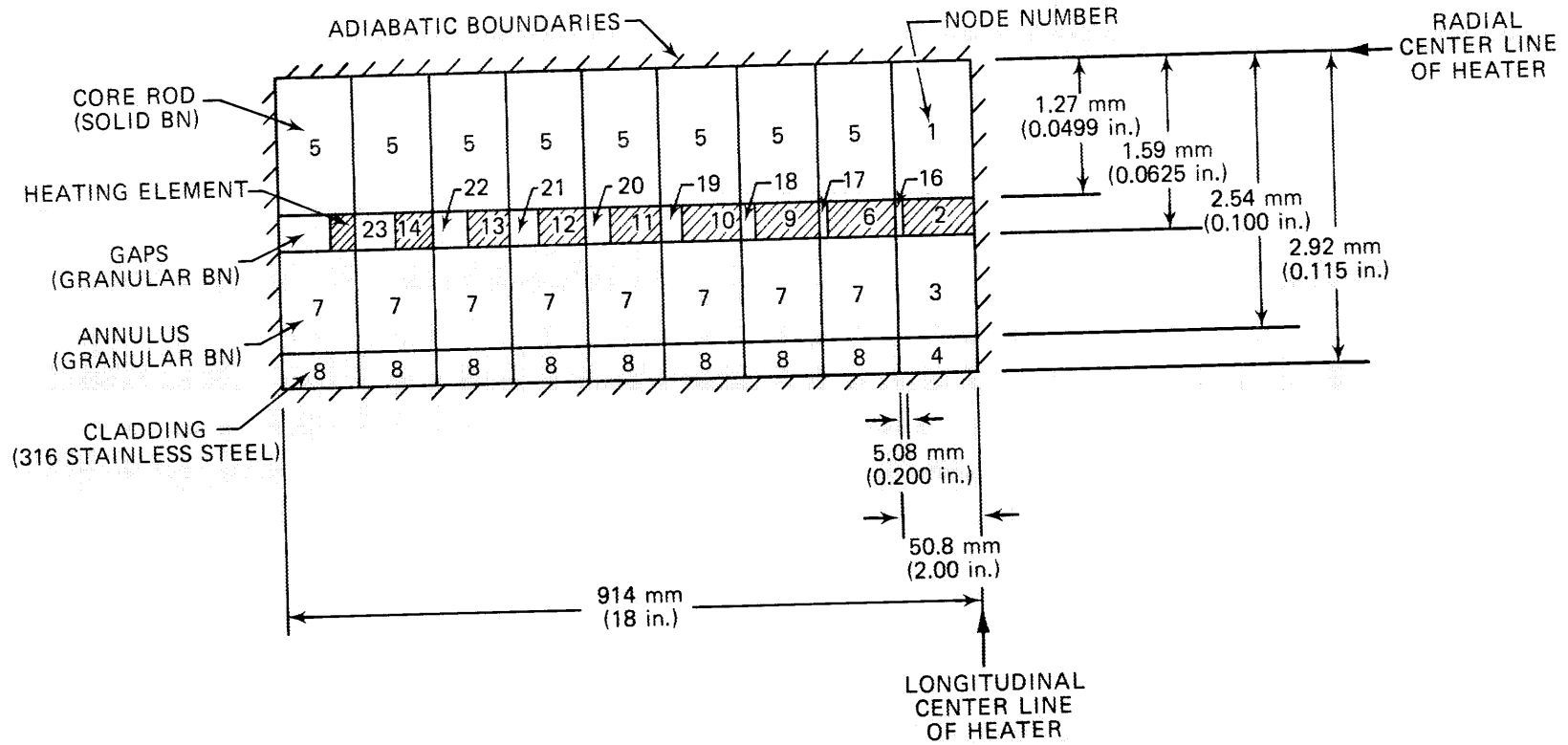


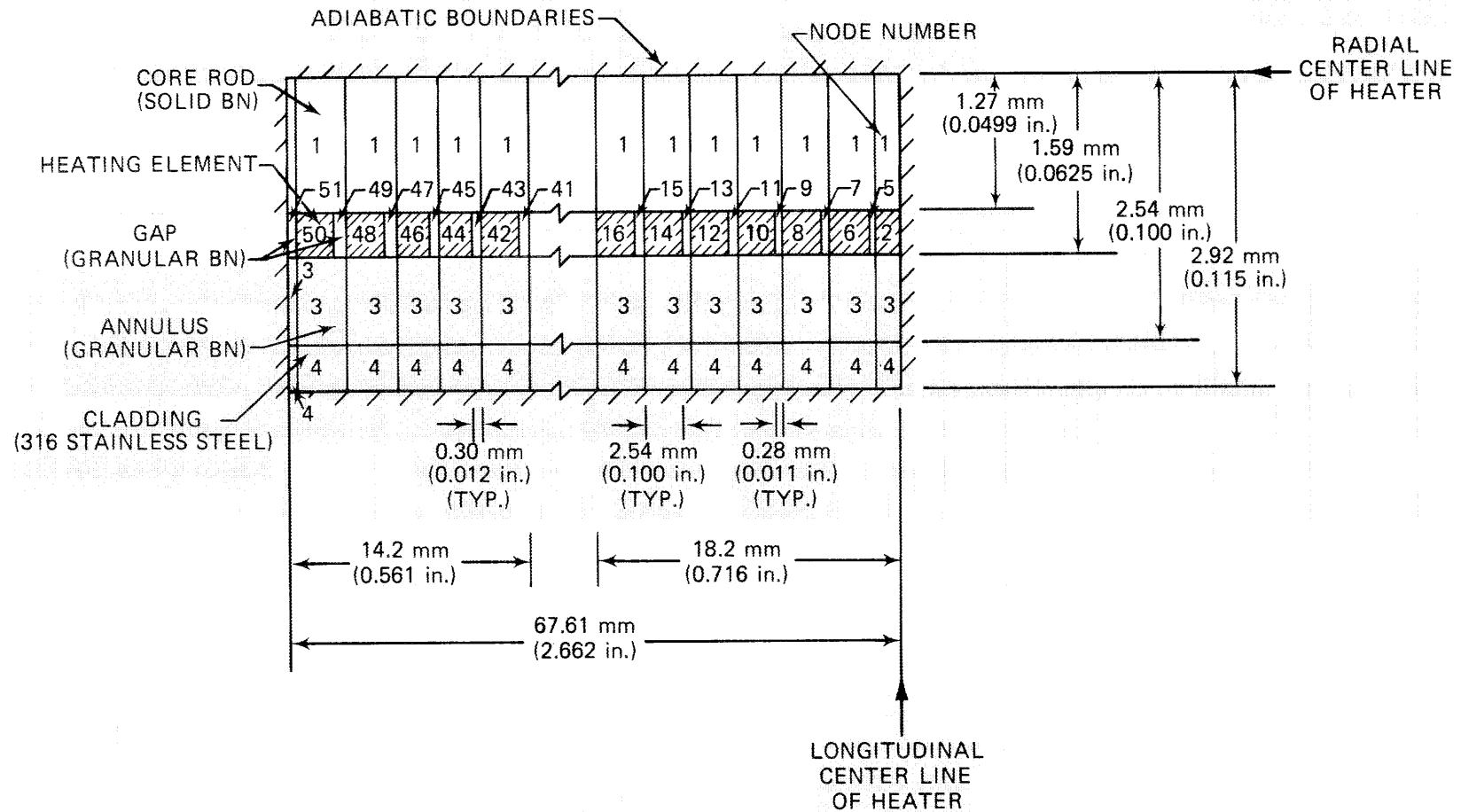
Fig. 2.5. Bundle 7A heater thermal model (lumped) for 1-sec cladding energization.

A more exact thermal model, shown in Fig. 2.6, was used to determine the outside cladding temperature for the 1-sec heater element energization. For this model, only 67.6 mm (2.66 in.) from the center of the heater could be modeled for any one computer run due to the nodal limitations in the computer code. Outside cladding temperatures during heater element energization are now being obtained with this model; Fig. 2.7 gives a preliminary outside cladding temperature profile near the longitudinal center of the heater for 100% TD of granular BN. By varying the percentage of theoretical density, the average experimental temperature of 76°C (169°F) in Fig. 2.3 will be matched theoretically. If the percentages of TD obtained theoretically for both cladding and heater element energization are almost equal, the model will be considered adequate; if the percentages of TD for the two transients disagree, further modifications to the thermal models will be necessary.

2.3 Bundle 5D Flow-Coastdown Tests

FFM bundle 5 was designed to match the configuration of the 19-rod bundle in the SLSF Pl in-reactor tests being conducted by ANL.⁴ This bundle consists of 19 electrically heated rods in a hexagonal duct. The rods are 5.84 mm (0.230 in.) in diameter and are spaced by 1.42-mm-diam (0.056-in.) helical wire wraps on a 305-mm (12-in.) pitch. The heated section of the bundle is 457 mm (18 in.) long. The gaps between the peripheral rods and the hexagonal duct are half as large as the nominal gaps [i.e., 0.71 mm (0.028 in.)], and an edge blockage plate could be inserted into the bundle 102 mm (4 in.) downstream from the start of the heated length. The test-section assembly and instrument layout are given in Figs. 2.8 and 2.9.

Steady-state tests were conducted with and without the blockage plate in the bundle.^{5,6} In October 1974, the unblocked bundle configuration plus an attenuator assembly was designated bundle 5D, and a series of flow-coastdown tests to simulate loss-of-pump conditions was run to determine the transient temperatures throughout the bundle



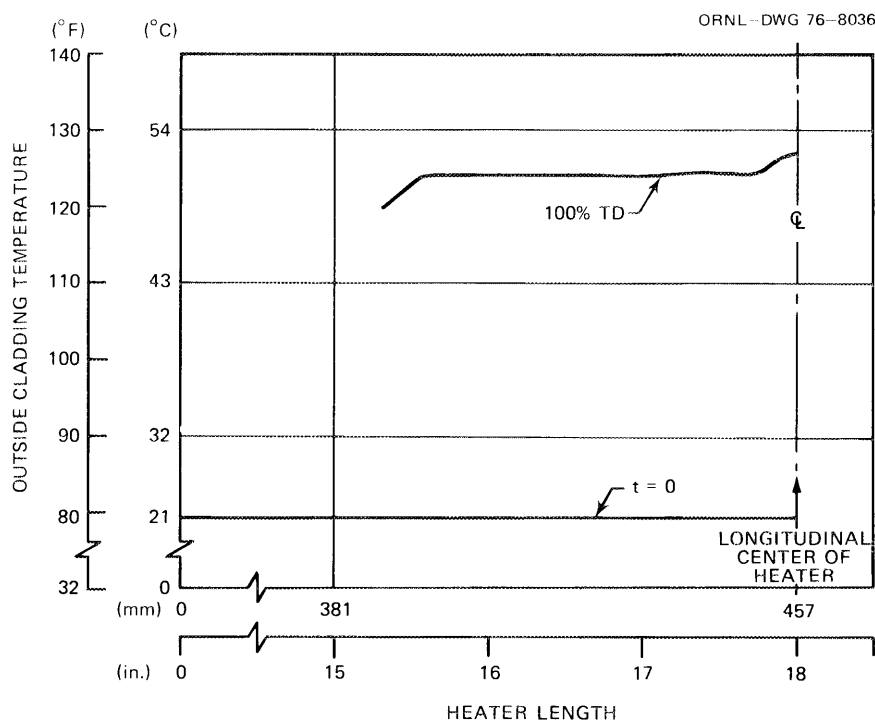


Fig. 2.7. Outside cladding temperature profile after 1-sec heater element energization using bundle 7A heater thermal model.

to the onset of boiling and to provide an acoustic signal for boiling-noise analysis. Table 2.1 presents a summary of the tests performed in October. When this series of tests was completed, a system that injects argon gas into the test section to simulate fission-gas release and cover-gas entrainment was installed. In January 1975, a series of flow-coastdown tests similar to the previous series was run to investigate the effects of gas injection. Table 2.2 presents a summary of the tests performed in January. Both series of tests were reported in previous reports in this series.^{7,8}

This section presents portions of the analysis of these test results to determine the effects of power skews and overheated pins. For the analysis, the responses of thermocouples during different tests were compared to determine if and how the varying test conditions changed the temperature responses. Table 2.3 compares test conditions of the tests made during the course of the analysis.

Table 2.1. Summary of tests performed on bundle 5D during October 1974

Test	Run	Power skew	Rod 10 overpowered	Boiled (sec)	Gas injection	Initial temperature [°C (°F)]	Date	Time
1	101	No power	No	No	No	316 (600)	10/21/74	15:16:28
1	101	No power	No	No	No	316 (600)	10/21/74	15:22:56
1	101	No power	No	No	No	316 (600)	10/21/74	15:31:14
2	101	Flat	No	No	No	316 (600)	10/22/74	13:53:41
2	102	Flat	Yes	No	No	316 (600)	10/22/74	14:45:13
2	103	15%	No	No	No	321 (610)	10/22/74	15:37:17
2	104	15%	Yes	No	No	321 (610)	10/22/74	16:09:33
2	105	25%	No	No	No	321 (610)	10/22/74	16:53:26
2	106	25%	Yes	No	No	318 (605)	10/22/74	17:37:32
2	107	7.5%	No	No	No	329 (625)	10/23/74	11:14:51
2	108	7.5%	Yes	No	No	321 (610)	10/23/74	11:47:58
3	101	Flat	No	6	No	340 (644)	10/23/74	13:53:22
3	102	Flat	Yes	2	No	340 (644)	10/23/74	14:14:13
3	105	7.5%	Yes	4, 5	No	340 (644)	10/23/74	14:54:51
3	106	15%	No	9, 5	No	340 (644)	10/24/74	10:01:29
3	107	25%	No	6	No	340 (644)	10/24/74	10:50:33
3	101	Flat	No	12	No	340 (644)	10/24/74	11:05:17
3	101	Flat	No	12	No	340 (644)	10/24/74	11:11:27

Test	Run	Power (kW/rod)	Rods heated	Skew	Test	Run	Power (kW/rod)	Rods heated	Skew
2	101	5.40	All	Flat	3	101	12.50	All	Flat
2	102	5.40 7.56	All but 10 10	Flat	3	102	12.50	All but 10	Flat
2	103	5.80 5.60 5.40 5.20 5.00	10, 11, 12 3, 4, 9, 13 1, 2, 5, 8, 14 6, 7, 15, 19 16, 17, 18	15%	3	105	17.50 13.00 12.70 12.50 12.30 12.00	10 11, 12 3, 4, 9, 13 1, 2, 5, 8, 14 6, 7, 15, 19 16, 17, 18	7.5%
2	104	7.56 5.80 5.60 5.40 5.20 5.00	10 11, 12 3, 4, 9, 13 1, 2, 5, 8, 14 6, 7, 15, 19 16, 17, 18	15%	3	106	13.43 13.43 12.96 12.50 12.02 11.56	10 11, 12 3, 4, 9, 13 1, 2, 5, 8, 14 6, 7, 15, 19 16, 17, 18	15%
2	105	6.08 5.74 5.40 5.06 4.72	10, 11, 12 3, 4, 9, 13 1, 2, 5, 8, 14 6, 7, 15, 19 16, 17, 18	25%	3	107	14.06 14.06 13.28 11.71 10.93 12.50	10 11, 12 3, 4, 9, 13 6, 7, 15, 19 16, 17, 18 1, 2, 5, 8, 14	25%
2	106	7.56 6.08 5.74 5.40 5.06 4.72	10 11, 12 3, 4, 9, 13 1, 2, 5, 8, 14 6, 7, 15, 19 16, 17, 18	25%					
2	107	5.60 5.50 5.40 5.30 5.20	10, 11, 12 3, 4, 9, 13 1, 2, 5, 8, 14 6, 7, 15, 19 16, 17, 18	7.5%					
2	108	7.56 5.60 5.50 5.40 5.30 5.20	10 11, 12 3, 4, 9, 13 1, 2, 5, 8, 14 6, 7, 15, 19 16, 17, 18	7.5%					

Table 2.2. Continuation of test series 7 (FFM bundle 5D): flow-coastdown tests from an initial test-section flow of 155 liters/min (41 gpm), January 1975 - Gas Injection Series

Test No.	Run No.	Initial temperature [°C (°F)]	Nominal power (kW/rod)	Rods heated	Gas injection	Run performed		Time boiling (sec)
						Date	Time	
2G	101	316 (600)	5.40	All	No	1/22/75	14:04:41	
3G	101	340 (644)	12.50	All	No	1/23/75	9:40:20	5
4G	101	316 (600)	5.40	All	Yes	1/22/75	14:09:50	
4G	101 (repeat)	316 (600)	5.40	All	Yes	1/22/75	15:09:29	
5G	101	340 (644)	12.50	All	Yes	1/23/75	10:00:13	20

Table 2.3. Comparison of test conditions for analysis of bundle 5D

Time	Test No.	Run No.	Conditions	Date
13:53:41	2	101	Flat without gas	10/22/74
14:04:42	2G	101	Flat without gas	1/22/75
14:04:42	2G	101	Flat without gas	1/22/75
14:09:51	4G	101	Flat with gas	1/22/75
15:09:29	4G	101	Flat with gas	1/22/75
13:53:41	2	101	Flat	10/22/74
14:45:13	2	102	Flat overpowered rod 10	10/22/74
15:37:17	2	103	15% skew	10/22/74
16:09:33	2	104	15% skew overpowered rod 10	10/22/74
16:53:26	2	105	25% skew	10/22/74
17:37:22	2	106	25% skew overpowered rod 10	10/22/74
11:14:51	2	107	7.5% skew	10/23/74
11:47:58	2	108	7.5% skew overpowered rod 10	10/23/74
13:53:41	2	101	Flat	10/22/74
11:14:51	2	107	7.5% skew	10/23/74
15:37:17	2	103	15% skew	10/22/74
16:53:26	2	105	25% skew	10/22/74
14:45:13	2	102	Flat overpowered rod 10	10/22/74
11:47:58	2	108	7.5% skew overpowered rod 10	10/23/74
16:09:33	2	104	15% skew overpowered rod 10	10/22/74
17:37:22	2	106	25% skew overpowered rod 10	10/22/74

around each of six heaters. These thermocouples are shown in Fig. 2.9 as dark dots within the large circles that represent the heaters.

Of the October tests, two were major ones — tests 2 and 3. This discussion will deal with the results from test 2, and the results from test 3 will be presented in a later report. As may be seen from Table 2.1, test 2 was performed with four different power distributions — flat, 7.5% skew, 15% skew, and 25% skew. Tests were performed at each of these power distributions with and without rod 10 being overpowered by 40% of the average power. From this series of tests, the effects of

power skews and the effects of the overpowered pin at these power skews may be seen.

The test 2 power distributions from Table 2.1 are illustrated as power regions on the cross section of the bundle in Fig. 2.10. The unshaded rods are powered at the average power of the bundle; the checked rods are powered at one-half the value of the skew above the average power to produce the top position of the skew; the vertically striped rods are powered at one-half the value of the skew below the average power to produce the bottom portion of the skew; and the horizontally

ORNL-DWG 76-8037

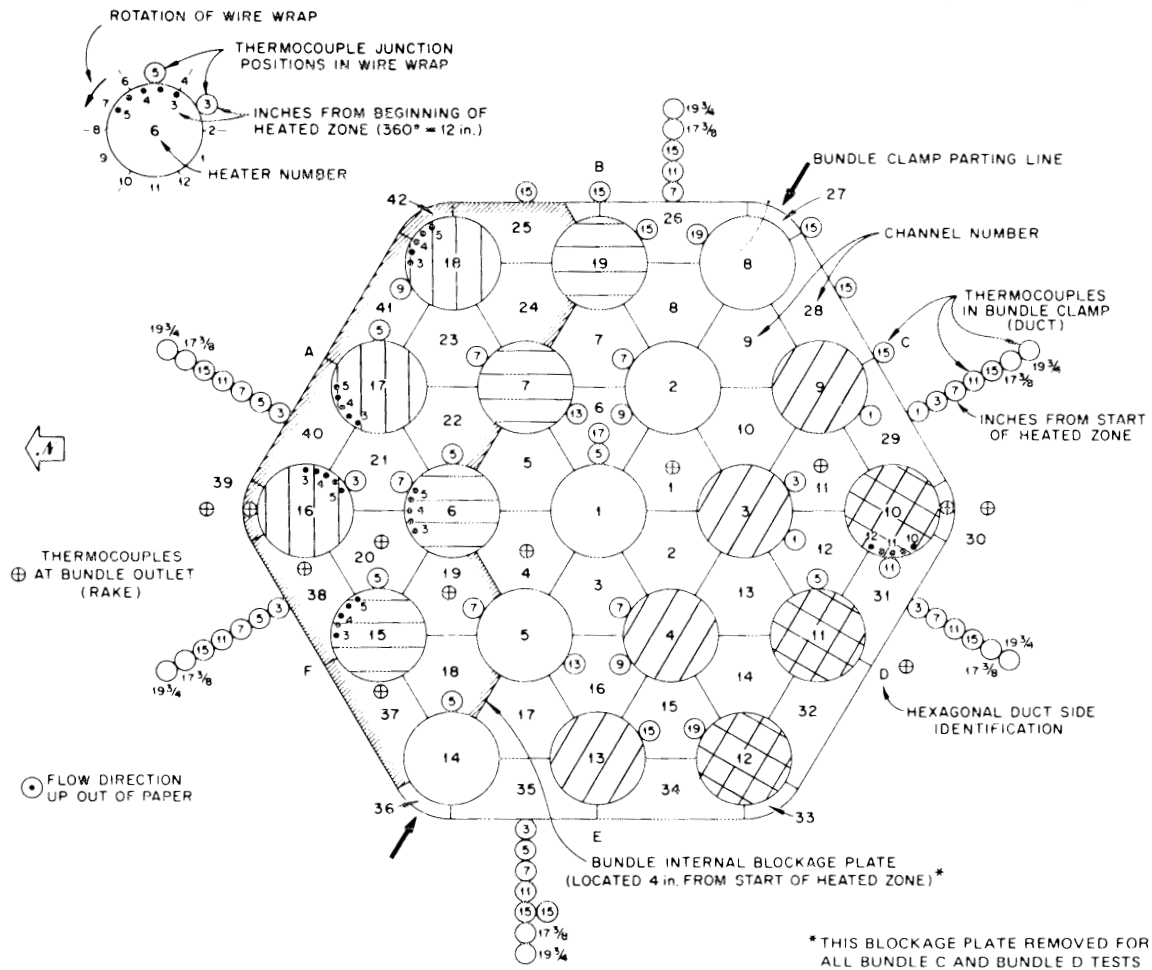


Fig. 2.10. Test 2 power distribution regions (as bundle 5D, the blockage plate was not in the bundle) (1 in. = 25.4 mm).

and diagonally striped rods are, respectively, powered at one-fourth the value of the skew below and above the average power to smooth out the skew.

The responses of duct wall thermocouples were the first to be analyzed. The temperature responses of the thermocouples located at low axial levels indicated that these thermocouples detected the effects of power skews. The responses of the thermocouples located in the under-powered area of the power skew showed decreasing rates of temperature increases and decreasing maximum temperatures as the skew was increased. The responses of duct wall A thermocouples at the 76-mm (3-in.), 127-mm (5-in.), and 178-mm (7-in.) levels illustrate this behavior. Figure 2.11 presents their responses during a test with a flat power distribution, and Fig. 2.12 presents their responses during a test with a 25% power skew. The opposite effects, increasing rates of temperature increases and increasing maximum temperatures, were found in the responses of thermocouples located in the overpowered areas. The responses of duct wall D thermocouples at the 76-mm (3-in.), 178-mm (7-in.), and 381-mm (15-in.) levels illustrate this behavior. Figure 2.13 presents their responses during a test with a flat power distribution, and Fig. 2.14 presents their responses during a test with a 25% power skew. The responses of thermocouples located in the average-powered areas of the skew were essentially unchanged by increasing skew. The responses of duct wall E thermocouples at the 76-mm (3-in.), 127-mm (5-in.), and 178-mm (7-in.) levels illustrate this behavior. Figures 2.15 and 2.16, respectively, present their responses during tests with a flat power distribution and a 25% power skew.

The duct wall thermocouple responses changed dramatically around the 381-mm (15-in.) axial level. Above this axial level, the thermocouple responses no longer continually increased to a maximum temperature, but showed temperature increases and decreases that formed peaks and valleys. The pattern of temperature fluctuation at these levels was somewhat random from wall to wall, but once the pattern became established along a wall, it remained the same with only slight changes throughout the rest of the axial length. The increasing amounts of power skew had some effect on this behavior; increasing the amount of skew would tend either

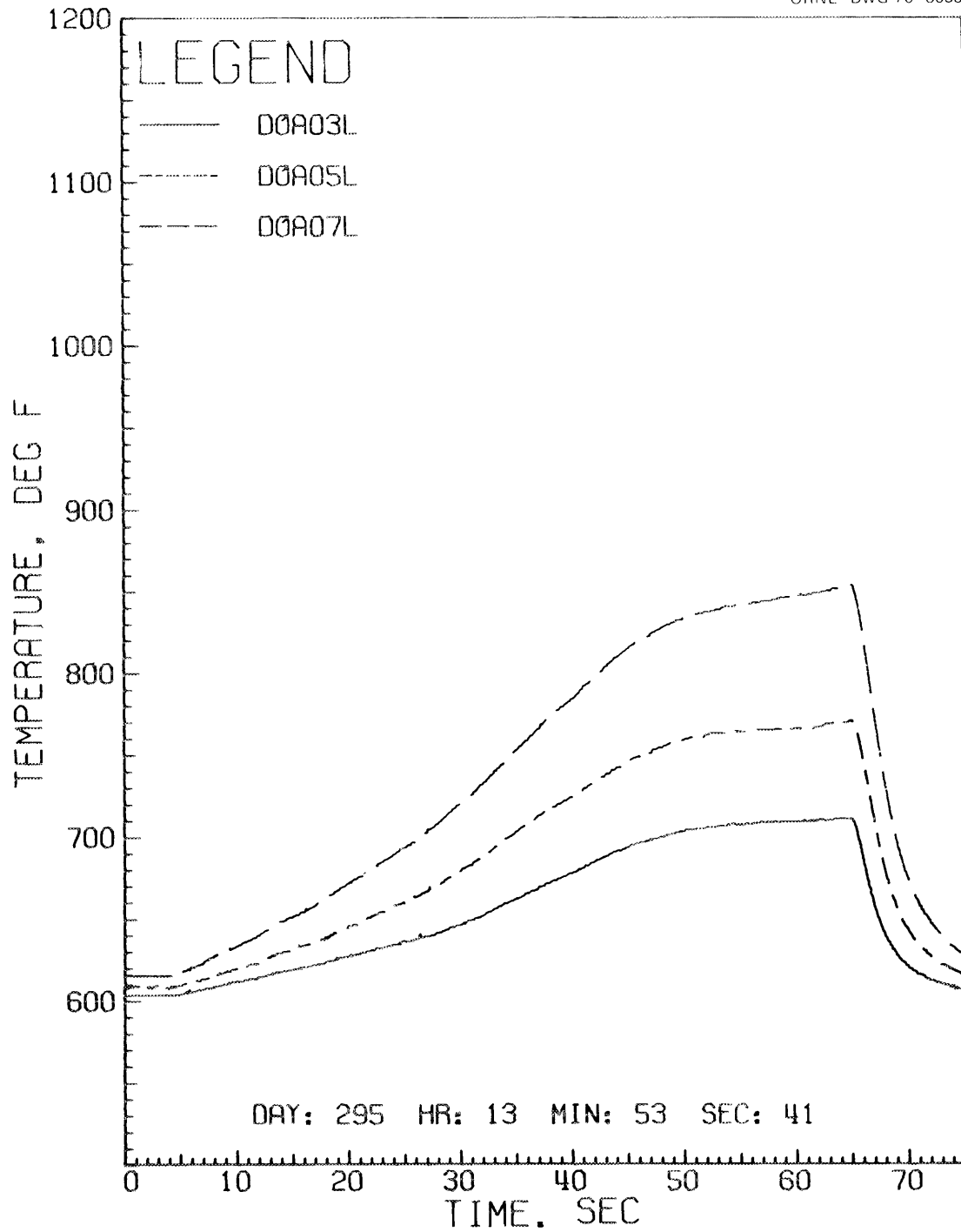


Fig. 2.11. Temperature responses of thermocouples located on duct wall A at the 76-mm (3-in.), 127-mm (5-in.), and 178-mm (7-in.) axial levels, DOA03L, DOA05L, and DOA07L, respectively, for test 2 with a flat power distribution.

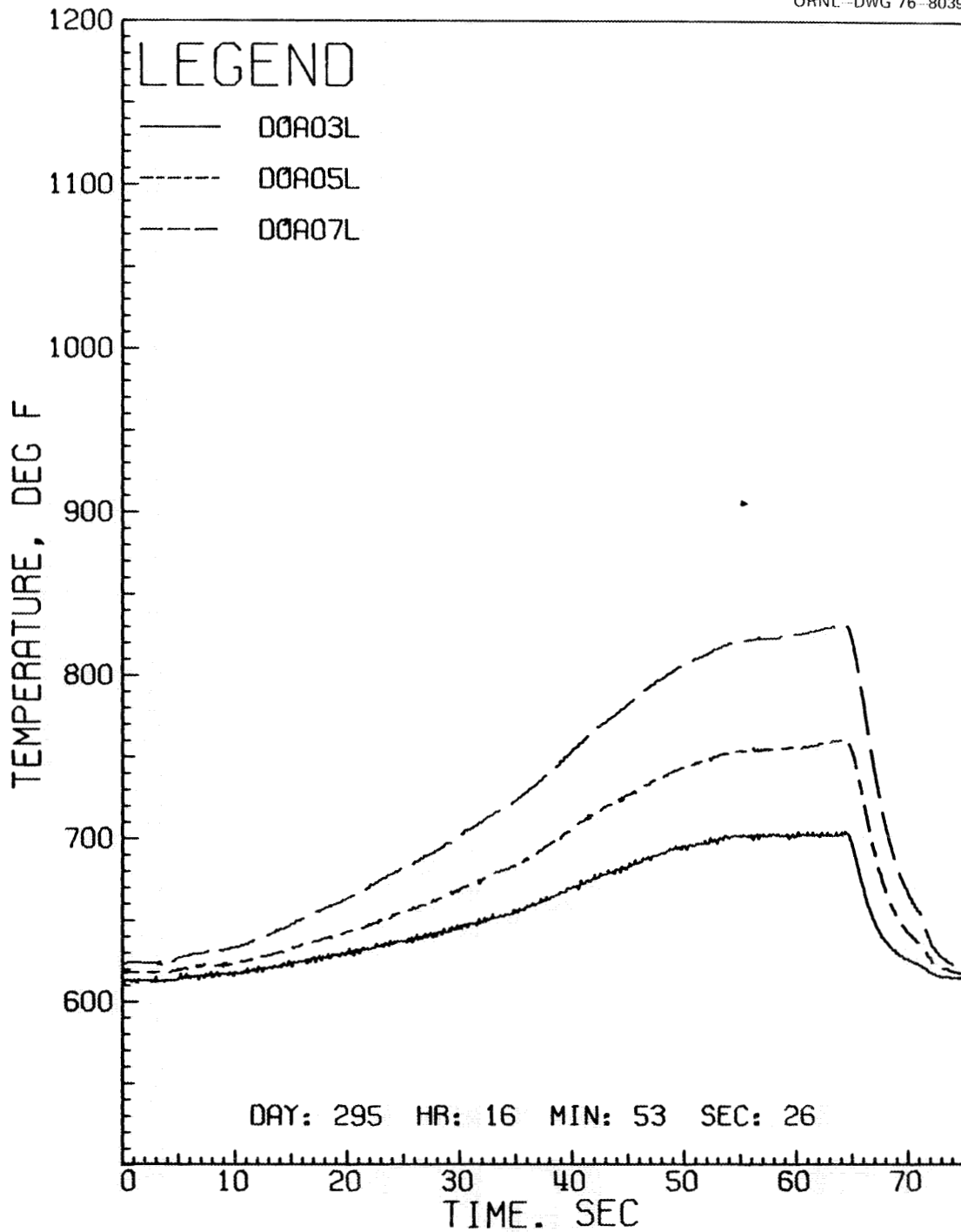


Fig. 2.12. Temperature responses of thermocouples located on duct wall A at the 76-mm (3-in.), 127-mm (5-in.), and 178-mm (7-in.) axial levels, D0A03L, D0A05L, and D0A07L, respectively, for test 2 with a 25% power skew.

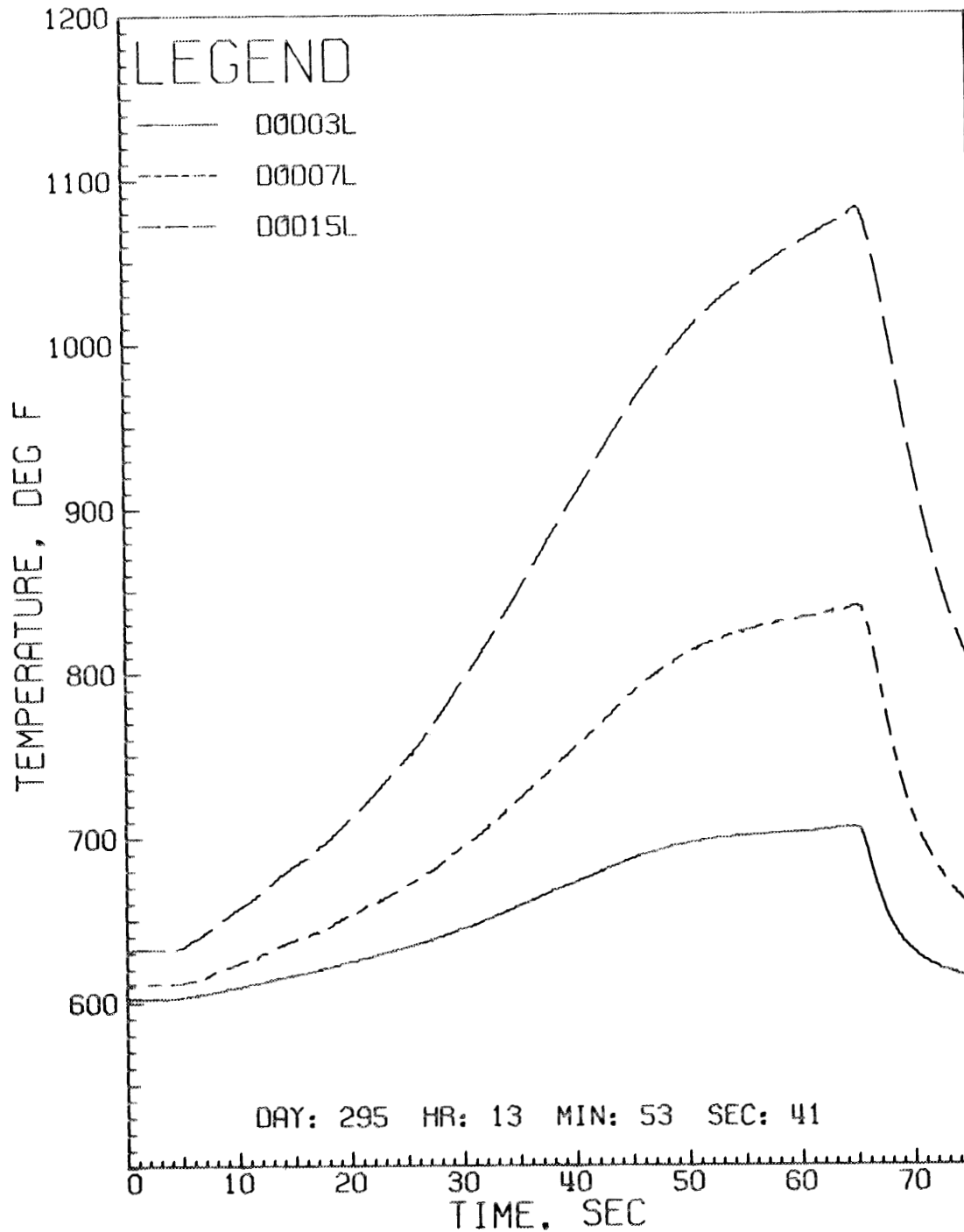


Fig. 2.13. Temperature responses of thermocouples located on duct wall D at the 76-mm (3-in.), 178-mm (7-in.), and 381-mm (15-in.) axial levels, DOD03L, DOD07L, and DOD15L respectively, for test 2 with a flat power distribution.

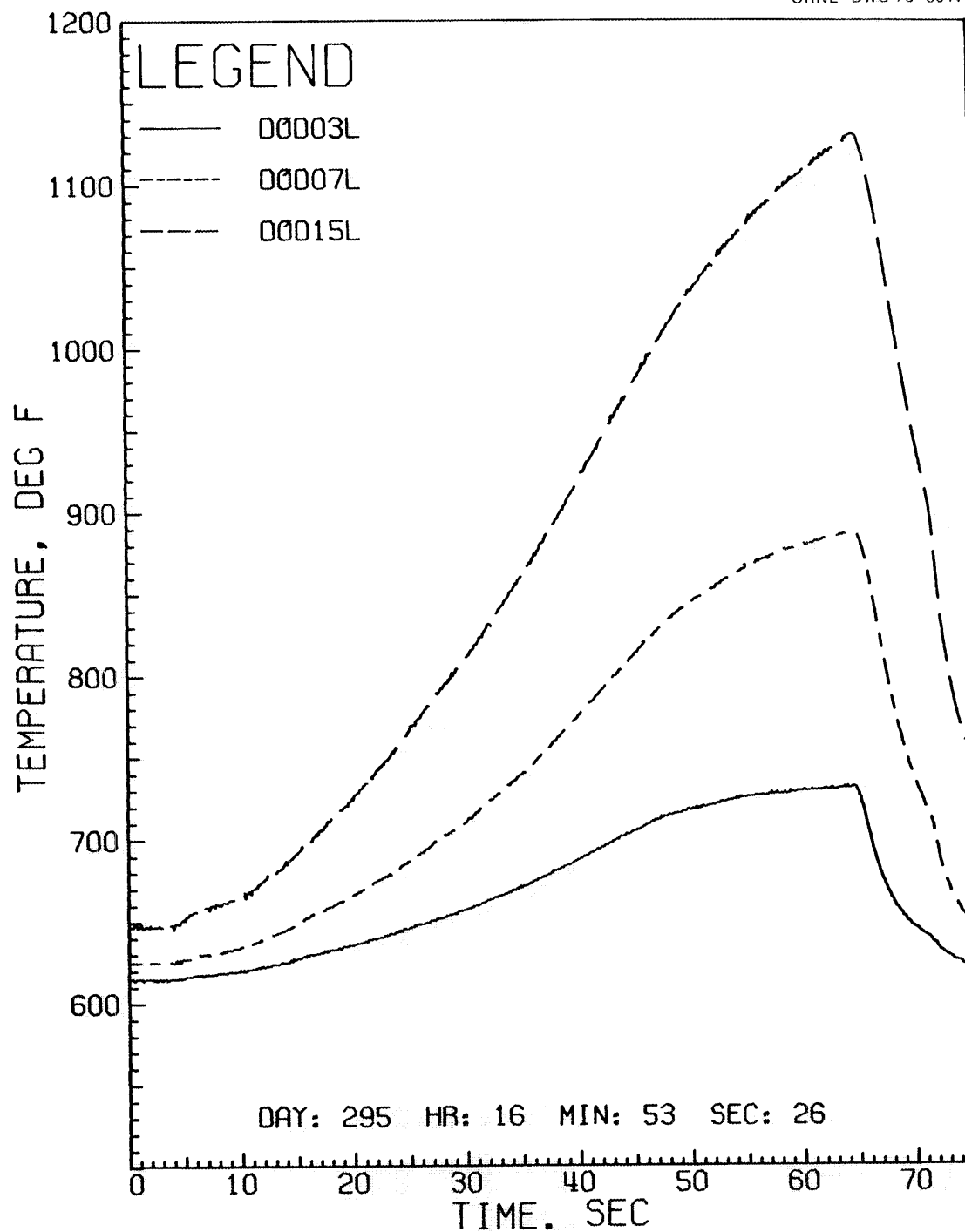


Fig. 2.14. Temperature responses of thermocouples located on duct wall D at the 76-mm (3-in.), 178-mm (7-in.), and 381-mm (15-in.) axial levels, DOD03L, DOD07L, and DOD15L respectively, for test 2 with a 25% power skew.

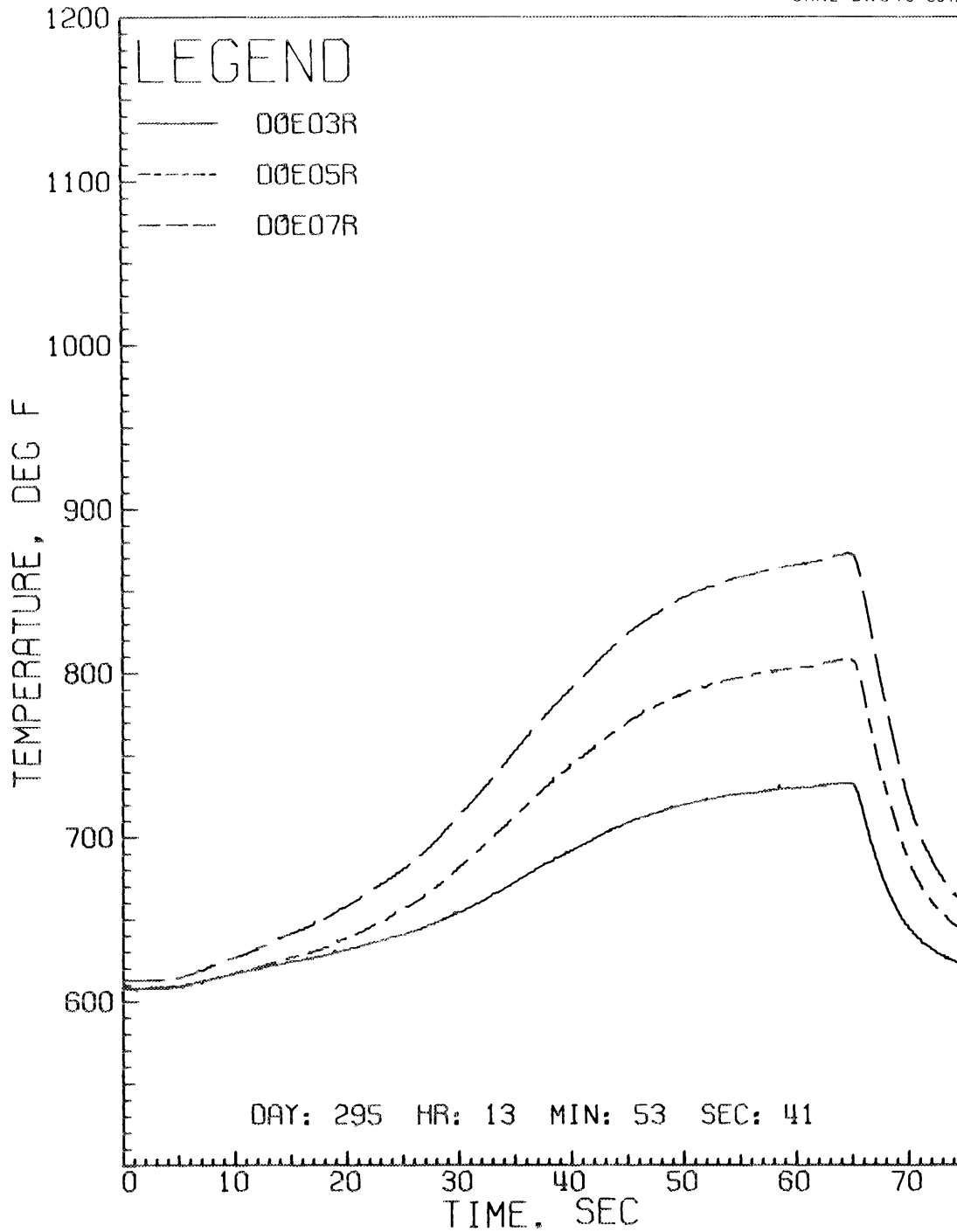


Fig. 2.15. Temperature responses of thermocouples located on duct wall E at the 76-mm (3-in.), 127-mm (5-in.), and 178-mm (7-in.) axial levels, DOE03R, DOE05R, and DOE07R, respectively, for test 2 with a flat power distribution.

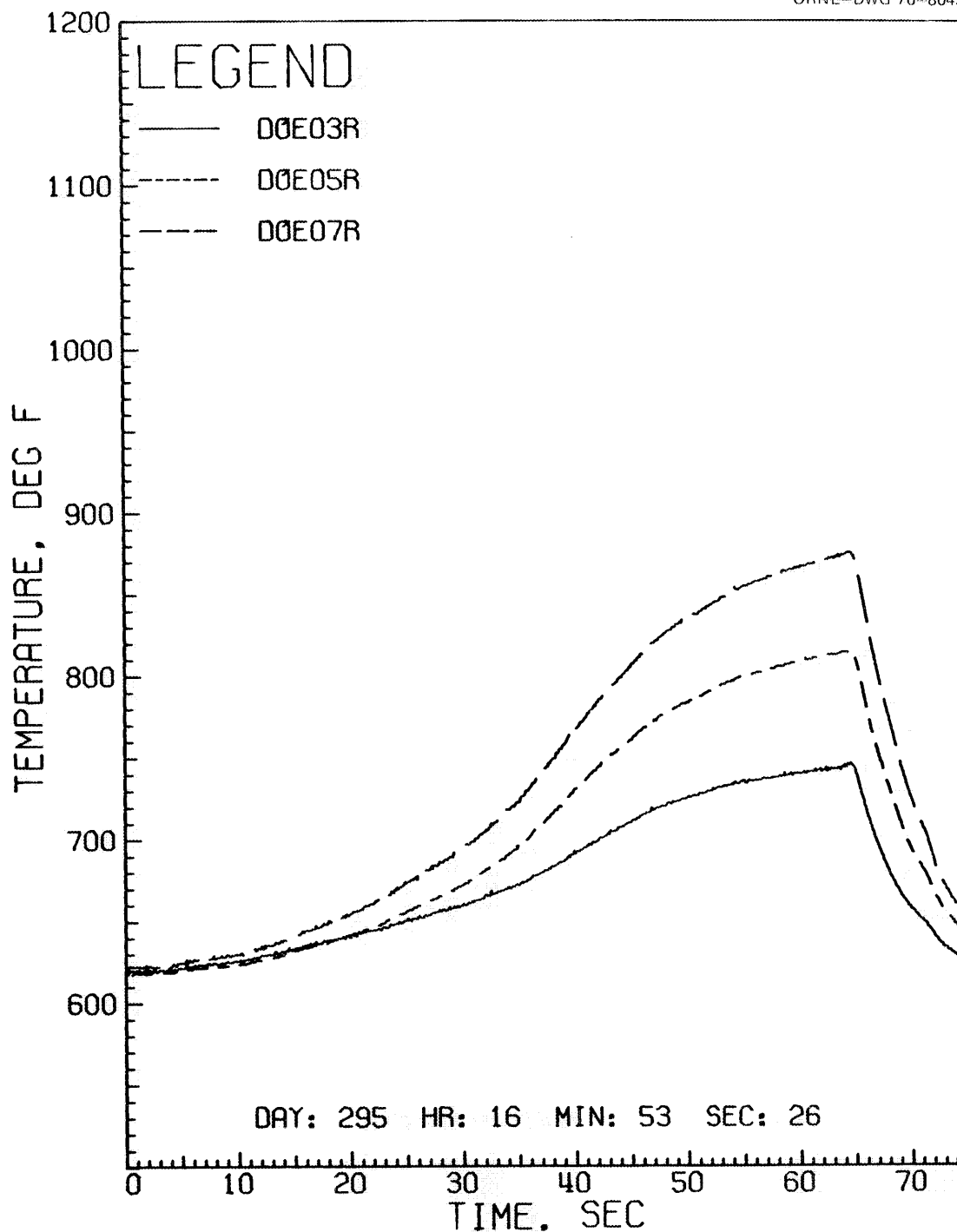


Fig. 2.16. Temperature responses of thermocouples located on duct wall E at the 76-mm (3-in.), 127-mm (5-in.), and 178-mm (7-in.) axial levels, DOE03R, DOE05R, and DOE07R, respectively, for test 2 with a 25% power skew.

to accent a particular peak of the response or to smooth out the entire response. It is interesting that these two opposing effects could both be caused by increasing the amount of skew. Figures 2.17 and 2.18, respectively, present the responses of three thermocouples located on duct wall C at the 381-mm (15-in.) level during tests with a flat power distribution and a 25% power skew. These responses show a peak in the response being accented by increasing power skew.

The overpowering of rod 10, which was located in the region that was overpowered the most during the power skews, caused the responses of the nearby duct wall thermocouples to show increases in rate of temperature increase and in maximum temperature above that of their responses during tests without rod 10 overpowered. Figures 2.19 and 2.20, respectively, present the responses of the thermocouples on duct wall D at the 76-mm (3-in.), 178-mm (7-in.), and 381-mm (15-in.) levels for tests with rod 10 overpowered at a flat power distribution and a 25% power skew. The effects of overpowering rod 10 may be seen by comparing Fig. 2.13 with 2.19 and Fig. 2.14 with 2.20.

The feasibility of determining the effects of power skew and overpowered pin by comparing only the maximum temperatures of all duct wall thermocouples at each axial level was investigated. It was found that the effects of a power skew on these temperatures was enough to indicate the presence of a power skew and also which power skew was the greater. No correlation was made between the observed temperature changes and the amount of power skew present. The overpowering of rod 10 failed to affect these temperatures consistently enough to allow an accurate determination of the presence of the overpowered pin.

In general, without rod 10 overpowered, the duct wall thermocouples located near the average-power region had temperature response fluctuations of $\sim \pm 2$ to $\pm 7\%$ between tests with the flat power distribution and tests with the various power skews. Thermocouples located in the most overpowered region showed temperature increases of ~ 12 to 25% between these tests, and thermocouples located in the most underpowered region showed temperature decreases of ~ 15 to 20% between these tests. The overpowering of rod 10 produced temperature increases of $\sim 5\%$ for a flat

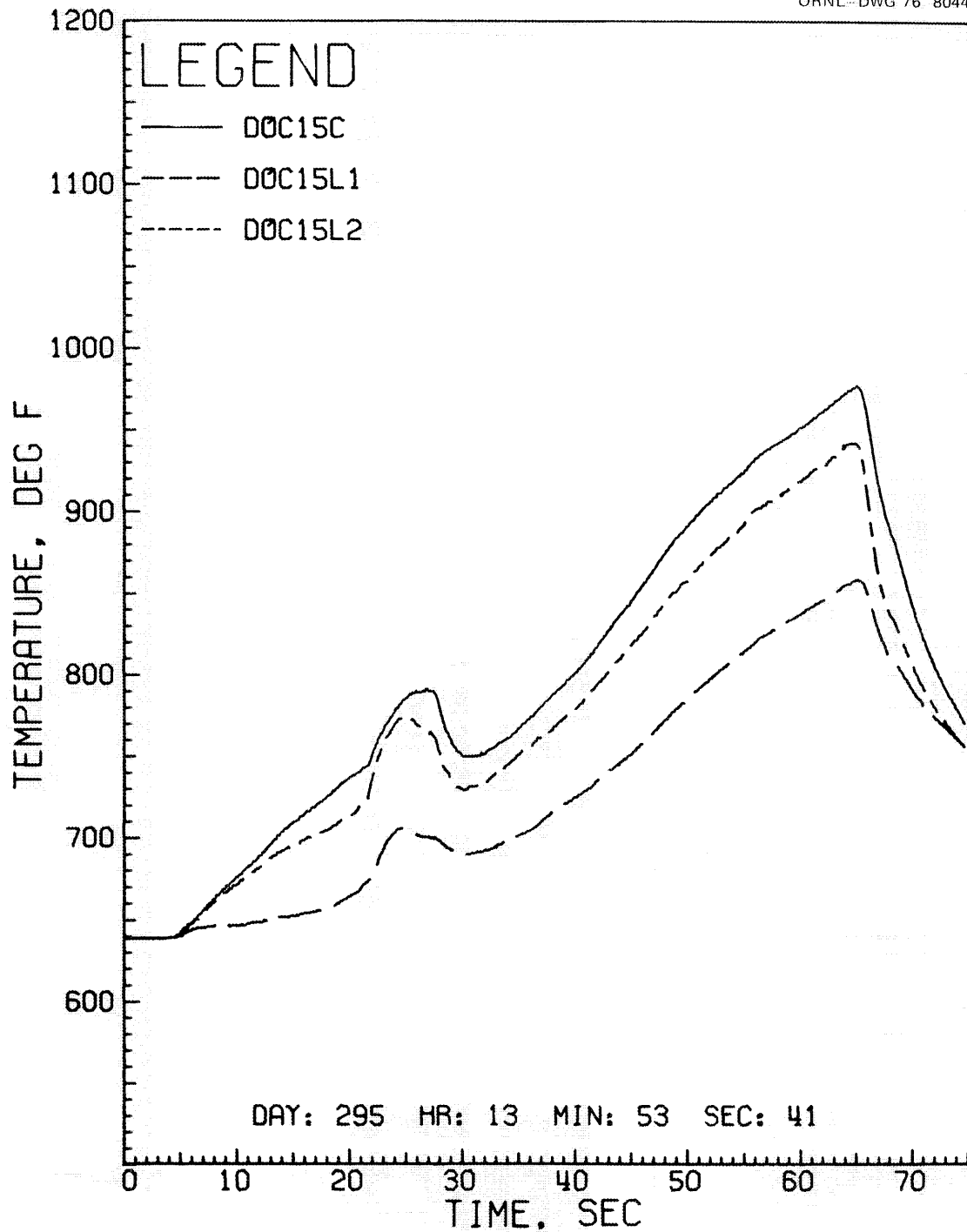


Fig. 2.17. Temperature responses of thermocouples located on duct wall C at the 381-mm (15-in.) axial level, DOC15C, DOC15L1, and DOC15L2, for test 2 with a flat power distribution.

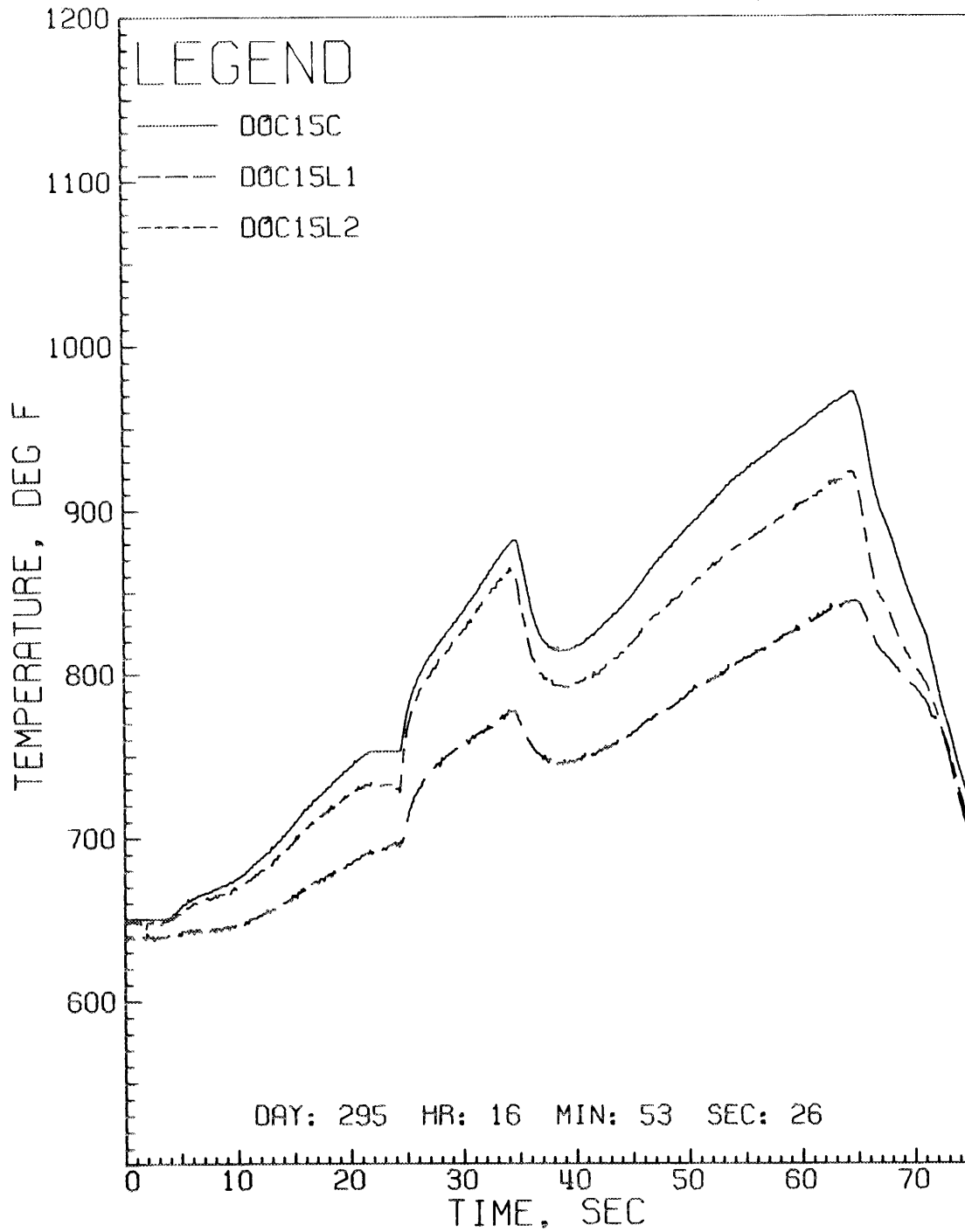


Fig. 2.18. Temperature responses of thermocouples located on duct wall C at the 381-mm (15-in.) axial level, DOC15C, DOC15L1, and DOC15L2, for test 2 with a 25% power skew.

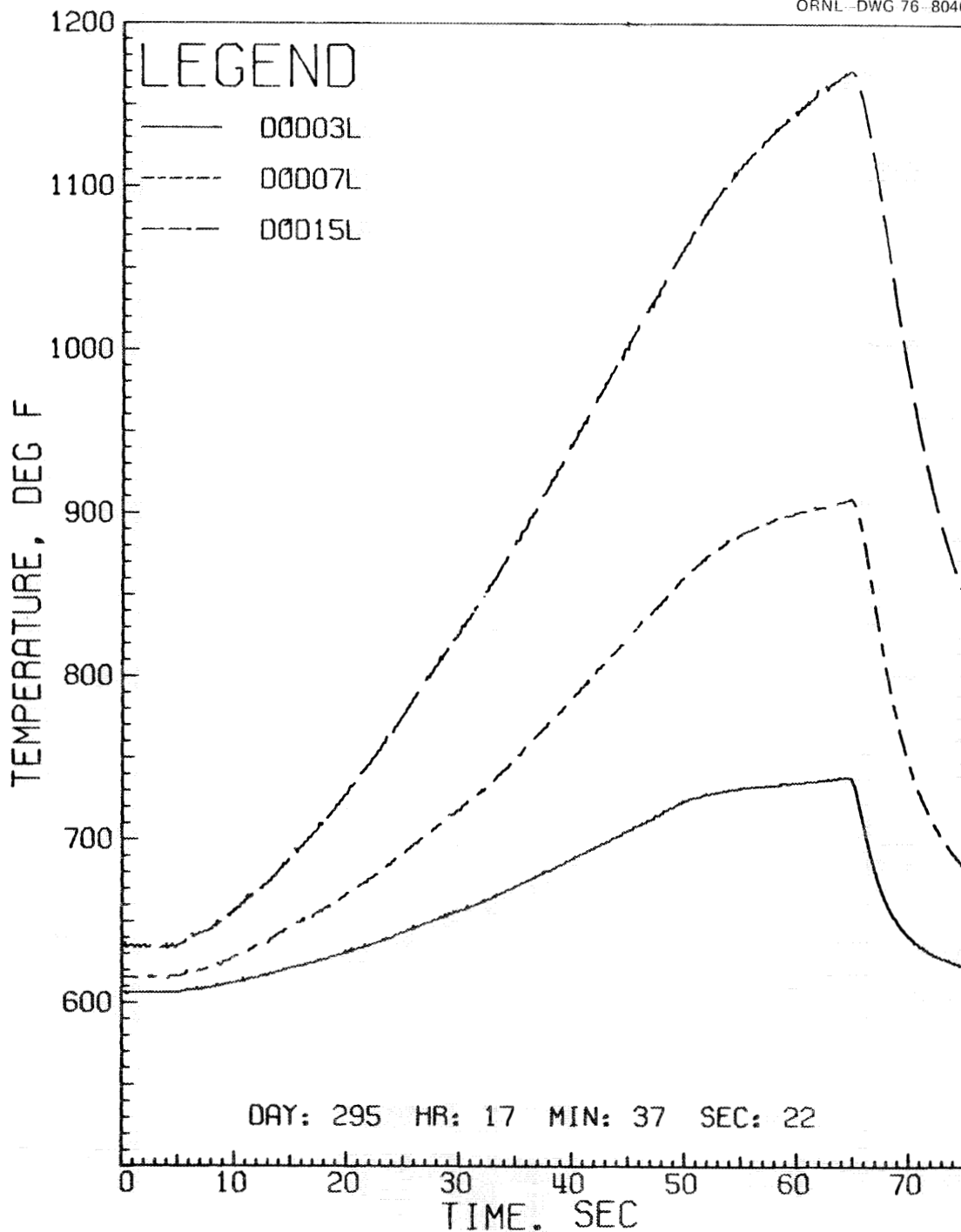


Fig. 2.19. Temperature responses of thermocouples located on duct wall D at the 76-mm (3-in.), 178-mm (7-in.), and 381-mm (15-in.) axial levels, DOD03L, DOD07L, and DOD15L respectively, for test 2 with a flat power distribution plus rod 10 overpowered.

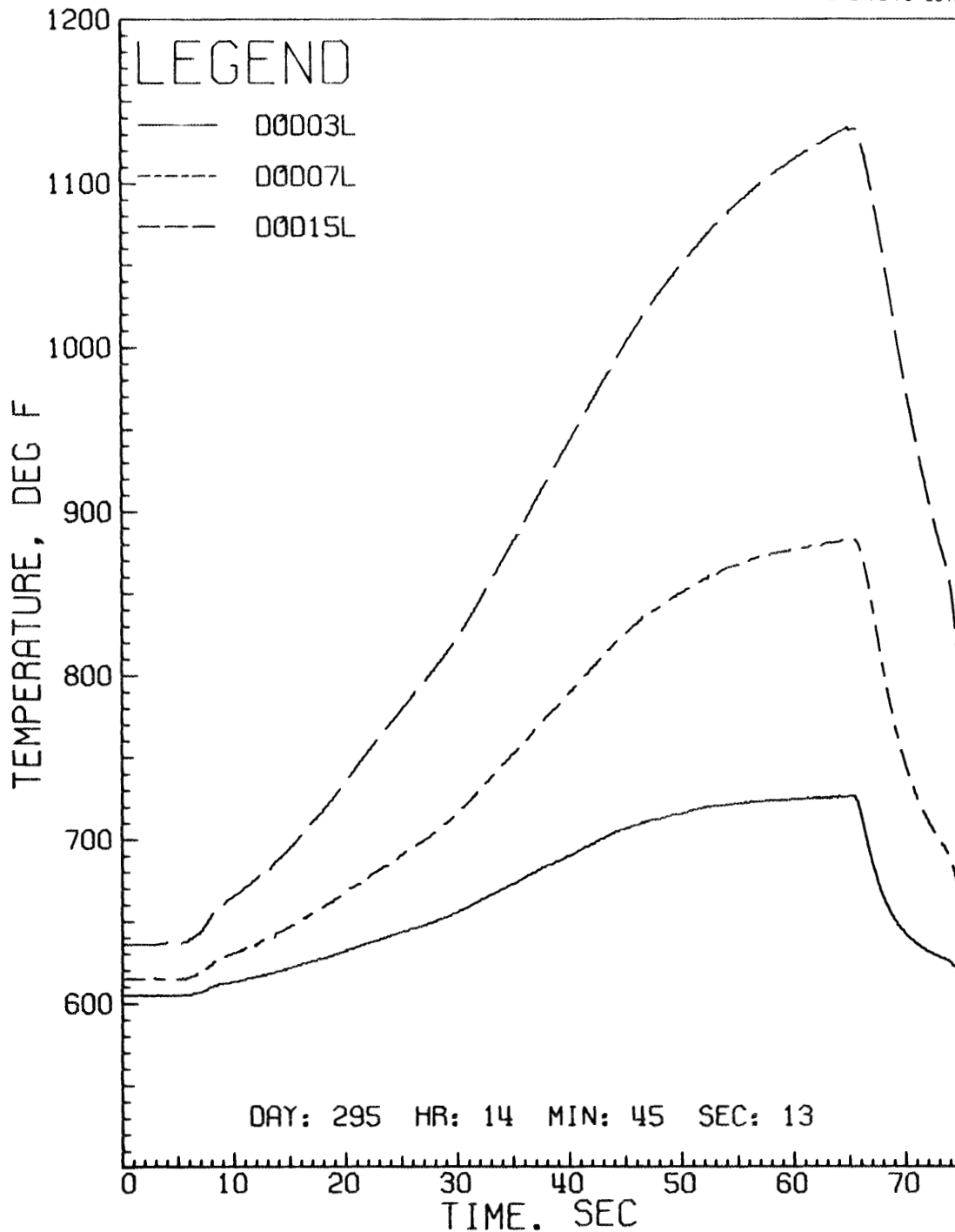


Fig. 2.20. Temperature responses of thermocouples located on duct wall D at the 76-mm (3-in.), 178-mm (7-in.), and 381-mm (15-in.) axial levels, DOD03L, DOD07L, and DOD15L respectively, for test 2 with a 25% power skew plus rod 10 overpowered.

distribution and $\sim 3.5\%$ for a 25% power skew in the responses of duct wall thermocouples that were located close to the overpowered rod.

The wire-wrap thermocouple responses were also affected by the power skews and overpowered rod. The responses of these thermocouples continually increased to a maximum throughout the entire axial length. The effect of the power skews and overpowered rod on these thermocouple responses depended upon their location. The responses of thermocouples located near the average-power region showed little change; those located in the overpowered region showed increased temperatures and increasing rates of temperature increase, while those located in the underpowered region showed decreased temperatures and decreasing rates of temperature increase as the skew was increased. These three types of behavior are illustrated in the following figures, which present the response of wire-wrap thermocouples located in each of the three different power regions. Figures 2.21 and 2.22, respectively, present the responses of the wire-wrap thermocouples located on rod 10 at the 279-mm (11-in.) level (TC 1011), on rod 3 at the 76-mm (3-in.) level (TC 0303), and on rod 15 at the 127-mm (5-in.) level (TC 1505) during tests with a flat power distribution and a 25% power skew. The overpowered pin also affected these thermocouple responses by causing increased temperatures and increased rates of temperature increase in the responses of thermocouples located near the overpowered pin. Figures 2.23 and 2.24 present the responses of these same thermocouples in tests with rod 10 overpowered at a flat power distribution and a 25% power skew. A comparison of Fig. 2.21 with 2.23 and Fig. 2.22 with 2.24 illustrates the effects of overpowering rod 10.

The wire-wrap thermocouples located in the most underpowered region showed temperature decreases of ~ 3 to 5% at the 178-mm (7-in.) level and $\sim 2.5\%$ at the 127-mm (5-in.) level. Thermocouples located close to the average-power region but still in the underpowered region showed temperature decreases of ~ 2 to 3% at the 178-mm (7-in.) level and ~ 1 to 1.5% at the 127-mm (5-in.) level. The responses of thermocouples located slightly into the overpowered region showed slight temperature increases [0.5% at the 178-mm (7-in.) level], while those located in the most overpowered region showed a temperature increase of $\sim 3\%$ at the 127-mm (5-in.)

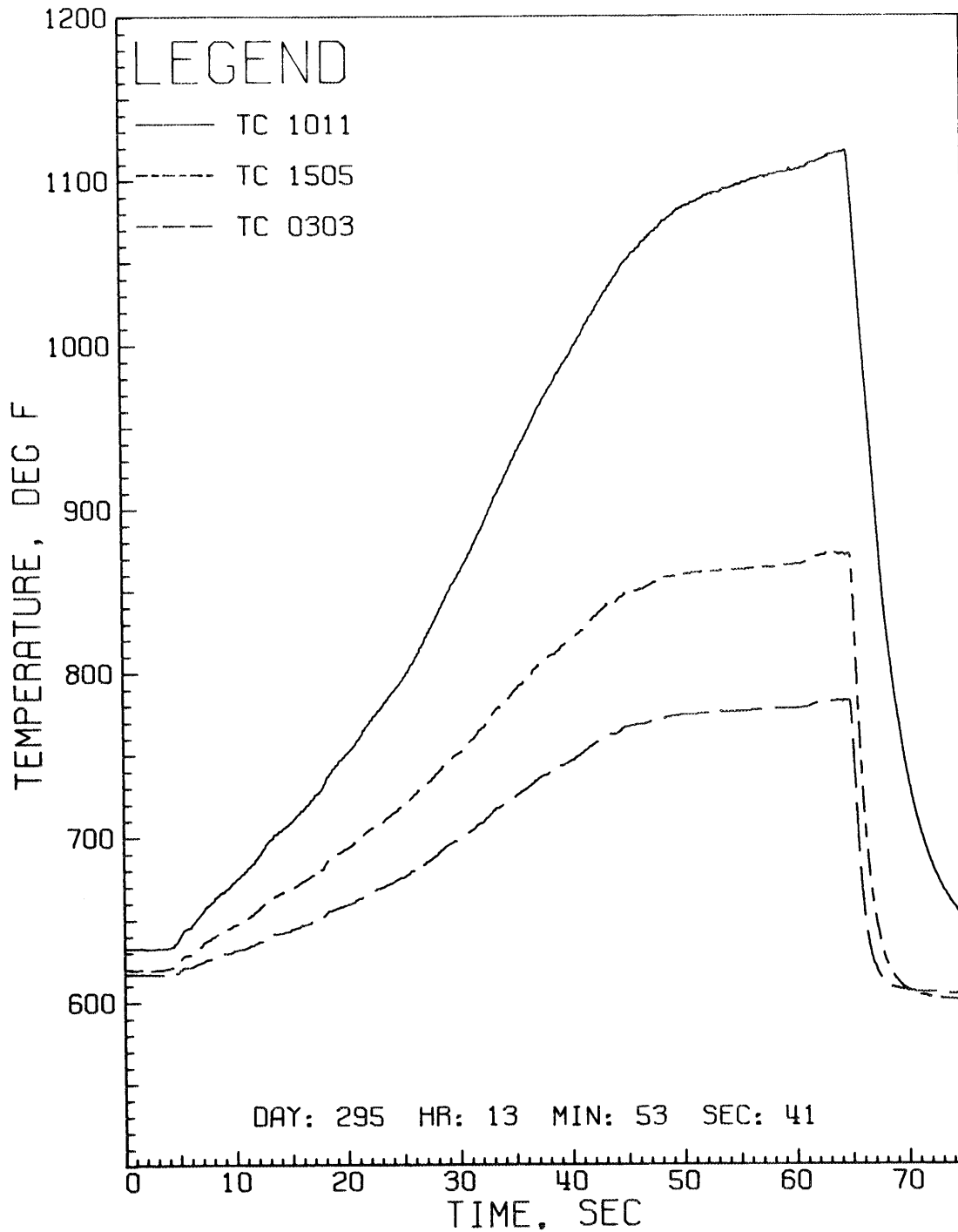


Fig. 2.21. Temperature responses of wire-wrap thermocouples located on rod 10 at the 279-mm (11-in.) level, TC1011, on rod 3 at the 76-mm (3-in.) level, TC0303, and on rod 15 at the 127-mm (5-in.) level, TC1505, for test 2 with a flat power distribution.

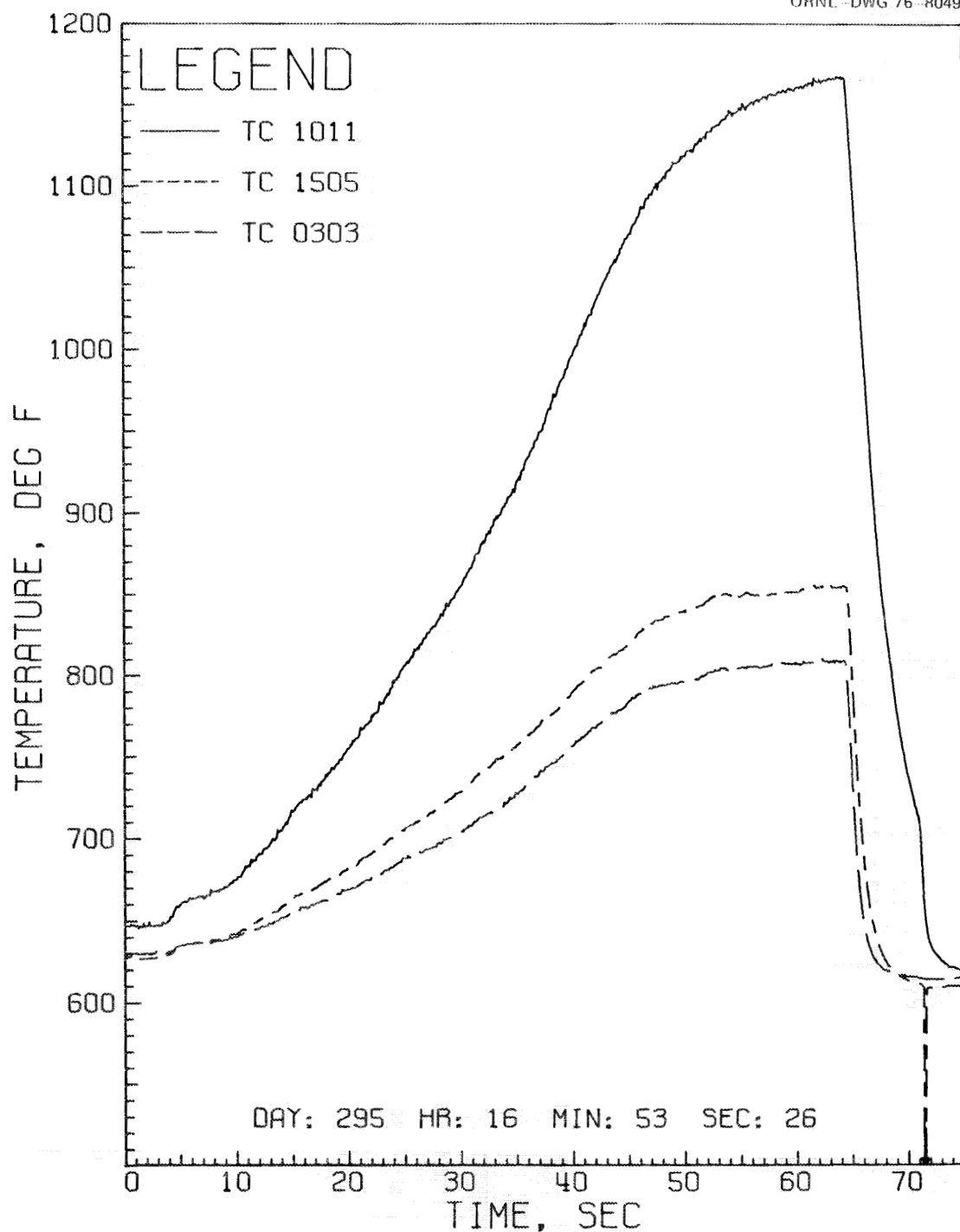


Fig. 2.22. Temperature responses of wire-wrap thermocouples located on rod 10 at the 279-mm (11-in.) level, TC1011, on rod 3 at the 76-mm (3-in.) level, TC0303, and on rod 15 at the 127-mm (5-in.) level, TC1505, for test 2 with a 25% power skew.

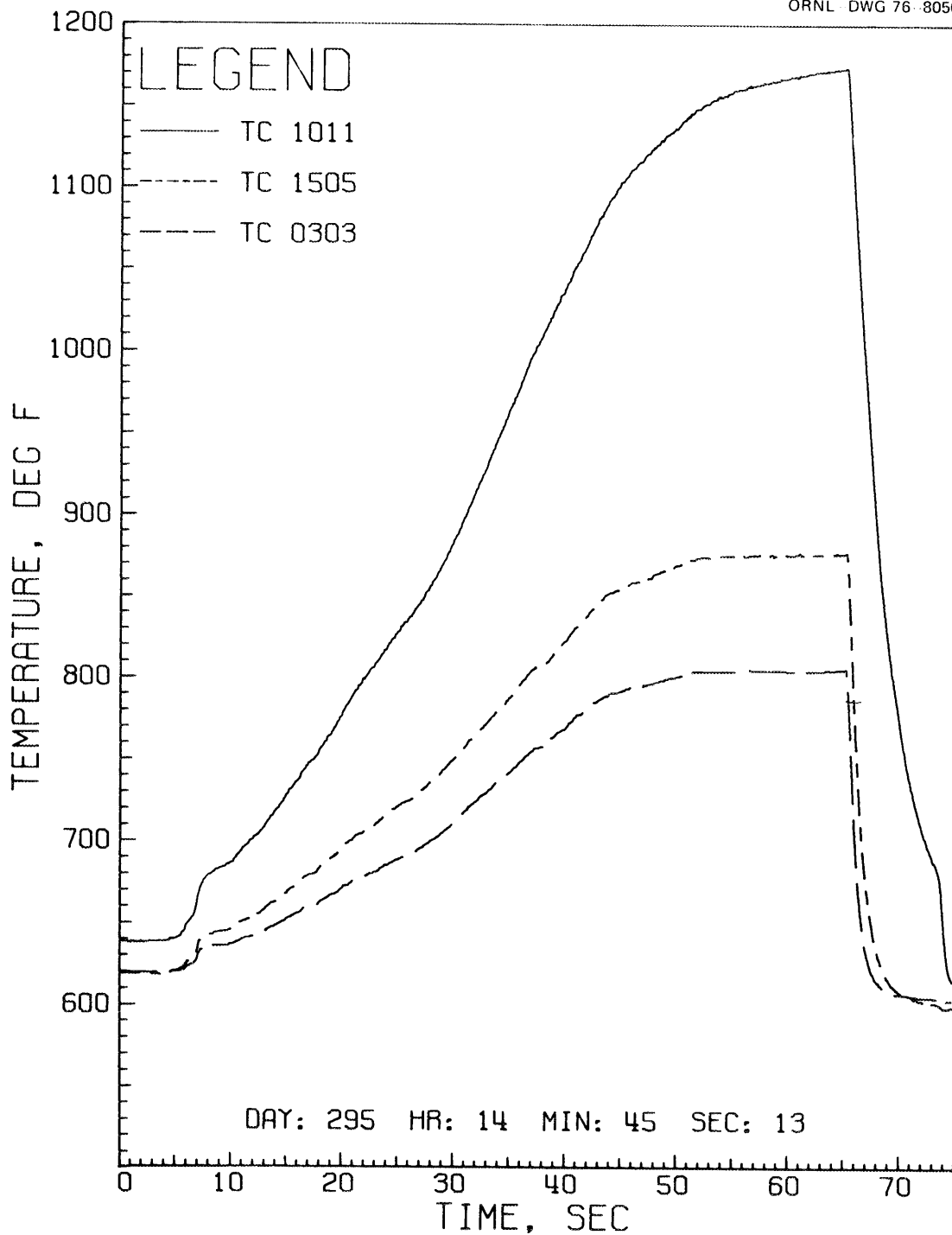


Fig. 2.23. Temperature responses of wire-wrap thermocouples located on rod 10 at the 279-mm (11-in.) level, TC1011, on rod 3 at the 76-mm (3-in.) level, TC0303, and on rod 15 at the 127-mm (5-in.) level, TC1505, for test 2 with a flat power distribution plus rod 10 overpowered.

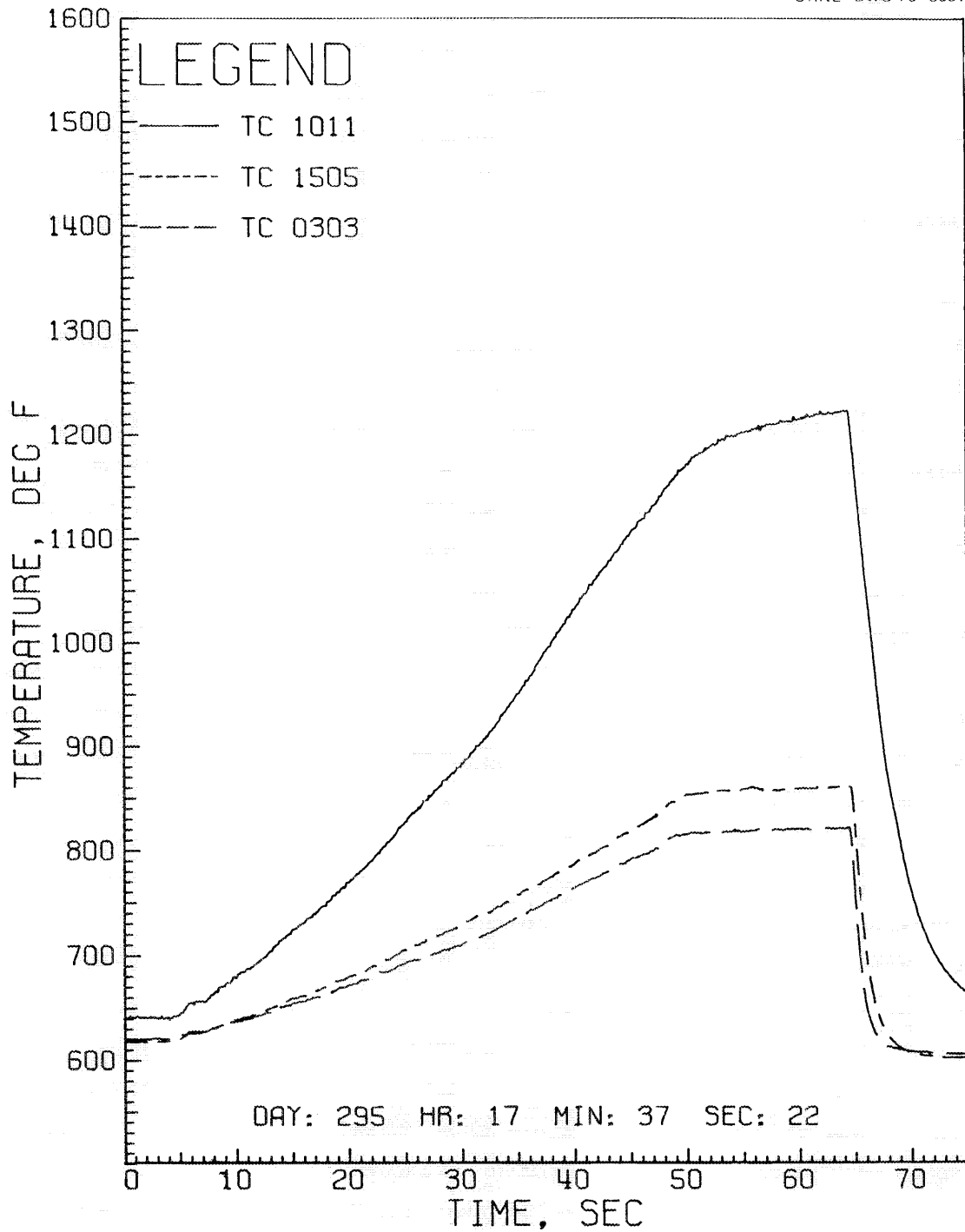


Fig. 2.24. Temperature responses of wire-wrap thermocouples located on rod 10 at the 279-mm (11-in.) level, TC1011, on rod 3 at the 76-mm (3-in.) level, TC0303, and on rod 15 at the 127-mm (5-in.) level, TC1505, for test 2 with a 25% power skew plus rod 10 overpowered.

level and $\sim 3.5\%$ at the 279-mm (11-in.) level. These thermocouple responses were obtained in tests with flat power distributions and tests with a 25% power skew. When rod 10 was overpowered in a test with a flat power distribution, the change in the temperature response of all thermocouples, except those located close to the overpowered pin, was $\sim 1\%$ or less. The responses of thermocouples located in a region close to the overpowered pin showed temperature increases of $\sim 4.5\%$ at the 127-mm (5-in.) and 76-mm (3-in.) levels. When rod 10 was overpowered in a test with a 25% skew, the responses of some thermocouples located far from the overpowered pin showed temperature increases up to $\sim 2.5\%$, while the responses of thermocouples located near the overheated pin showed increases of only $\sim 3.5\%$. With such a small difference in temperature increase, it is difficult to distinguish the presence of an overpowered pin at large power skews. This difficulty may be due to the overpowered pin being located in the region of greatest overpower during the power skews.

The heater internal thermocouples were expected to show the most pronounced effects of power skews and an overpowered pin, and indeed they did. The temperature responses of the heater internal thermocouples in rods located in the most overpowered region clearly showed progressive increases in temperature and in rate of temperature increase as the skew was increased. Similarly, the temperature responses of thermocouples in rods located in the underpowered regions clearly showed progressive decreases in temperature and in rate of temperature increase as the skew was increased. Rod 10 is located in the most overpowered region during a power skew, and rod 6 is located in an intermediately underpowered region during a power skew. Figures 2.25 and 2.26, respectively, present the temperature responses of the heater internal thermocouples located in these rods during tests with a flat power distribution and a 25% power skew in order to illustrate this behavior. Generally, the temperatures of the thermocouples located in the most overpowered region increased $\sim 2\%$ for the 15% skew and $\sim 4\%$ for the 25% skew at the 279-mm (11-in.) level. The temperatures of the thermocouples located in the underpowered region decreased ~ 1 to 2% for the 15% skew and ~ 2 to 4% for the 25% skew at the 76-mm (3-in.) and 102-mm (4-in.) levels.

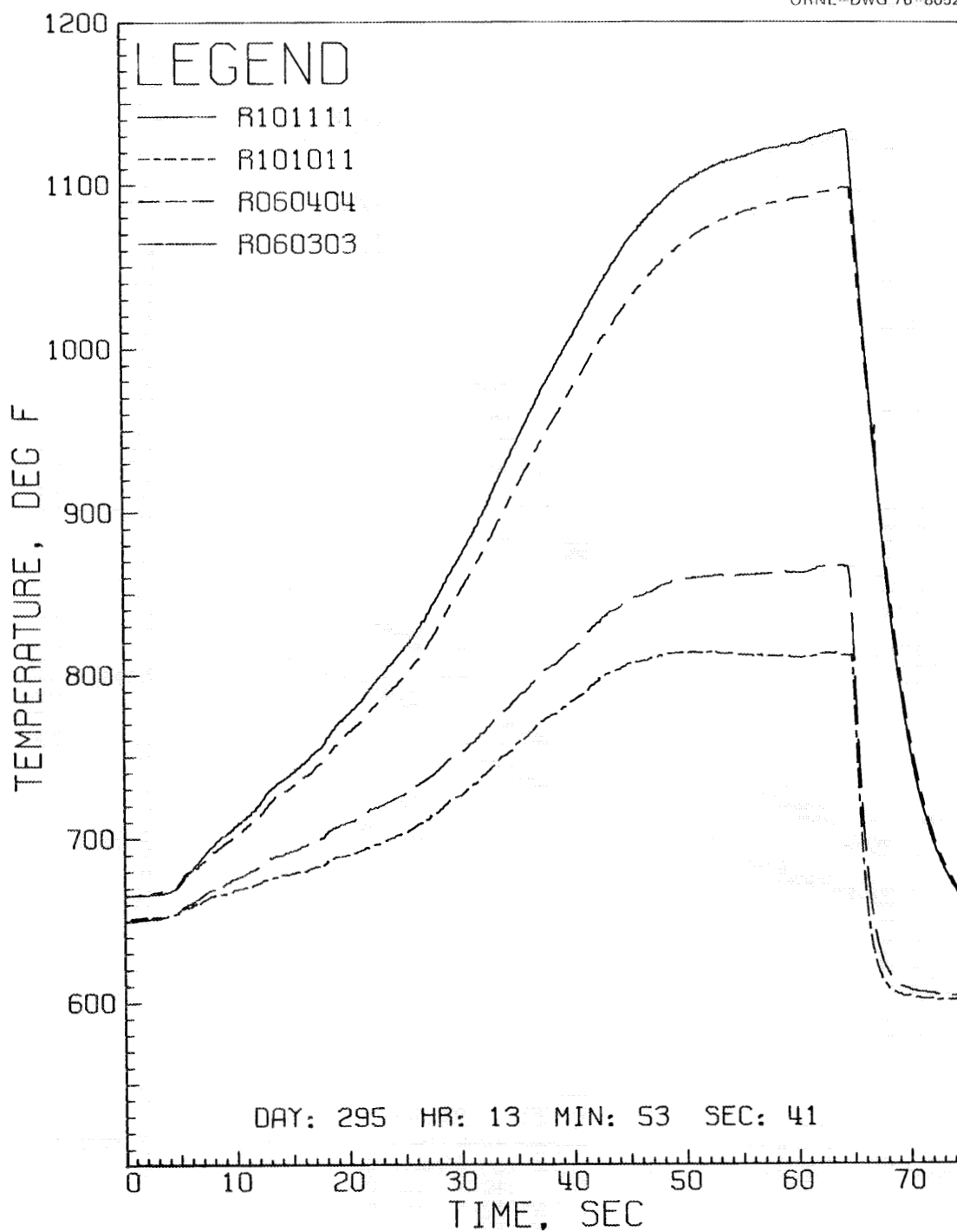


Fig. 2.25. Temperature responses of internal heater thermocouples located in rod 10 at the 254- to 279-mm (10- to 11-in.) levels, R101011 and R101111, and in rod 6 at the 76-mm (3-in.) level, R060303, and the 102-mm (4-in.) level, R060404, for test 2 with a flat power distribution.

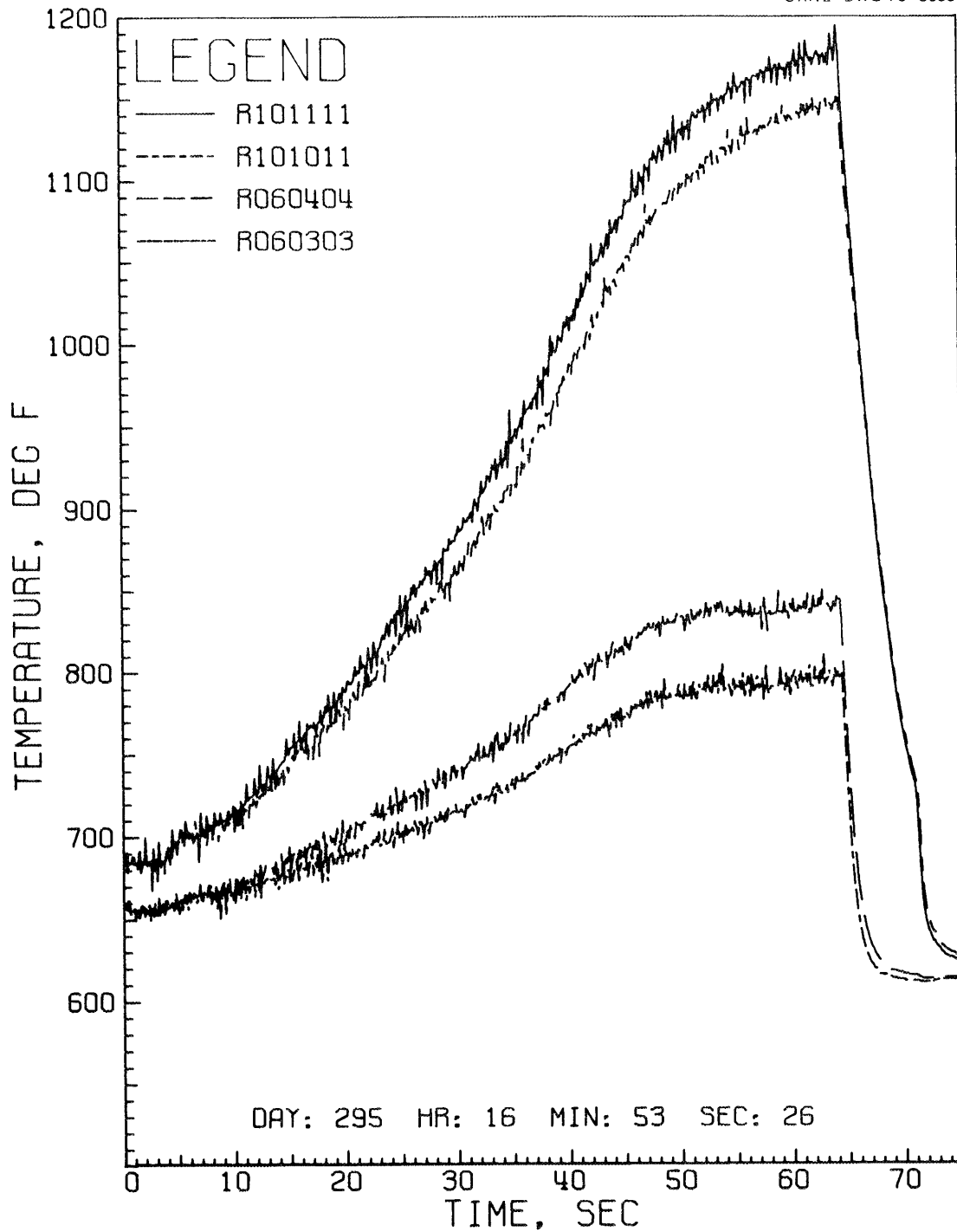


Fig. 2.26. Temperature responses of internal heater thermocouples located in rod 10 at the 254- to 279-mm (10- to 11-in.) levels, R101011 and R101111, and in rod 6 at the 76-mm (3-in.) level, R060303, and the 102-mm (4-in.) level, R060404, for test 2 with a 25% power skew.

The overpowering of rod 10 was indicated by the increases in temperature and in rate of temperature increase in the temperature responses of thermocouples located near the overheated pin. Almost all the heater internal thermocouple responses showed increased temperatures when rod 10 was overpowered, but the responses of thermocouples located near the overpowered rod clearly and consistently showed greater changes than all others. Figures 2.27 and 2.28 present the temperature responses of the same heater internal thermocouples for tests with rod 10 overpowered at a flat power distribution and a 25% power skew. A comparison of Fig. 2.25 with 2.27 and Fig. 2.26 with 2.28 illustrates the effects of overpowering rod 10 as observed in heater internal thermocouple responses. During tests at a flat power distribution, the responses of thermocouples located on the overpowered pin showed temperature increases of $\sim 5\%$ between the tests with and without rod 10 overpowered. The responses of other thermocouples showed no appreciable change ($\sim 1\%$) during these tests. During tests at a 25% power skew, the responses of thermocouples on the overpowered rod showed temperature increases of $\sim 10\%$ between tests with and without rod 10 overpowered. The responses of heater internal thermocouples located near the average-power region showed temperature increases of $\sim 2\%$, while the responses of heater internal thermocouples located farther from the overpowered pin showed no appreciable ($< 1\%$) change in temperature.

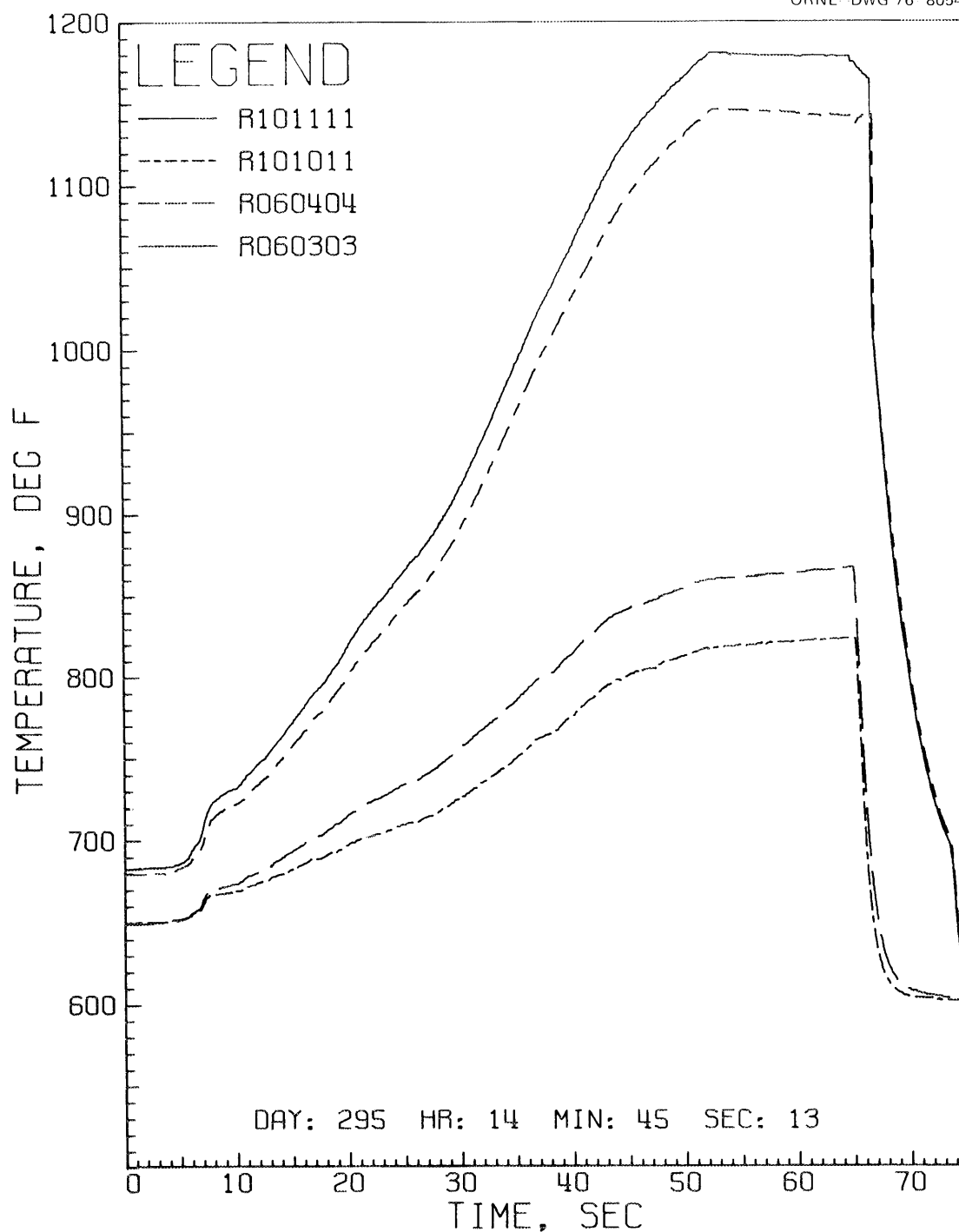


Fig. 2.27. Temperature responses of internal heater thermocouples located in rod 10 at the 254- to 279-mm (10- to 11-in.) levels, R101011 and R101111, and in rod 6 at the 76-mm (3-in.) level, R060303, and 102-mm (4-in.) level, R060404, for test 2 with a flat power distribution plus rod 10 overpowered.

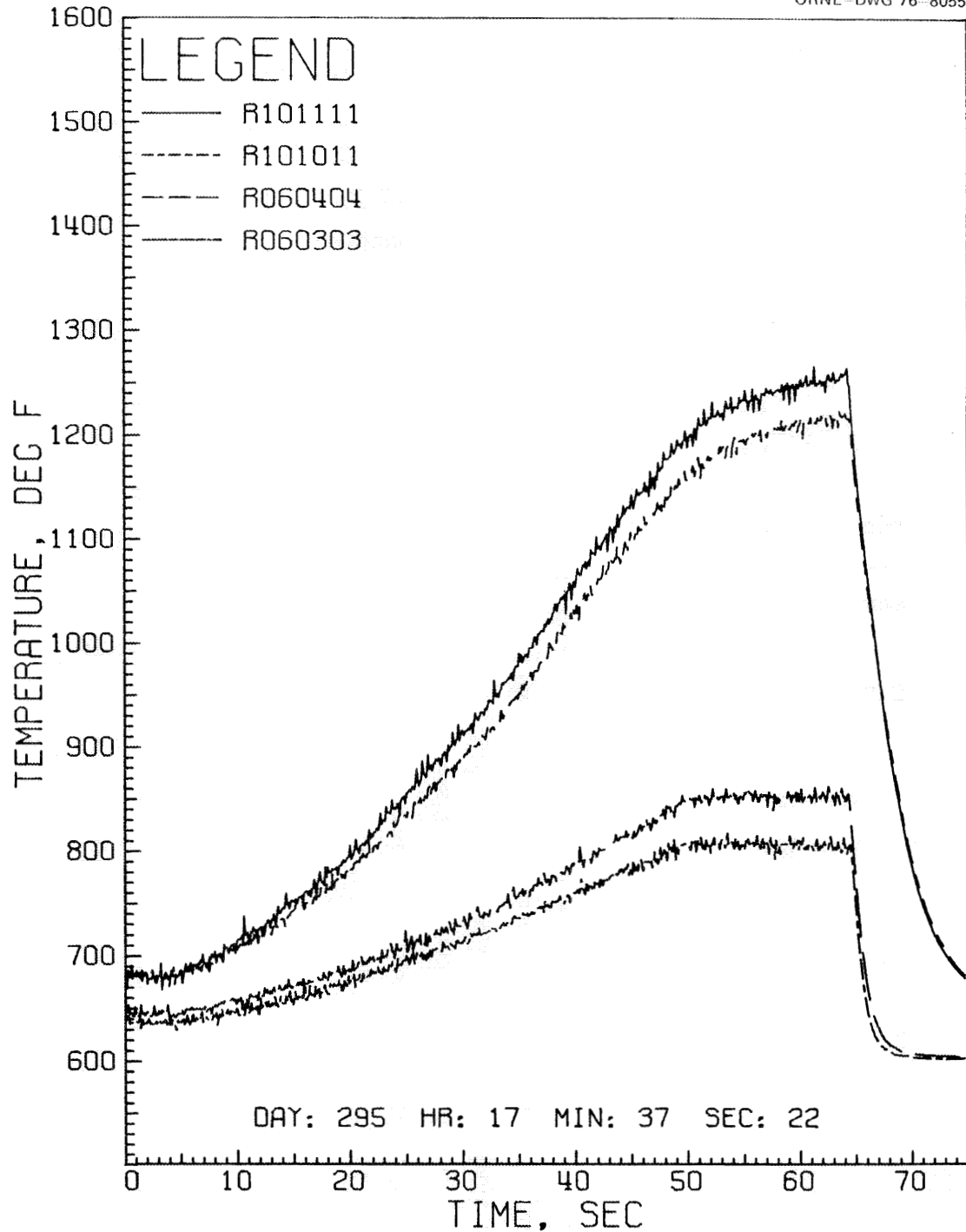


Fig. 2.28. Temperature responses of internal heater thermocouples located in rod 10 at the 254- to 279-mm (10- to 11-in.) levels, R101011 and R101111, and in rod 6 at the 76-mm (3-in.) level, R060303, and 102-mm (4-in.) level, R060404, for test 2 with a 25% power skew plus rod 10 overpowered.

References

1. M. H. Fontana and J. L. Wantland, LMFBR Safety and Core Systems Programs Progr. Rep. July-September 1975, ORNL/TM-5197.
2. R. L. Ludwig, Y-12 Plant Development Div., Union Carbide Nuclear Division, letter to P. A. Gnadt, Oct. 8, 1975; Subject: Examination of Prototype 7A Heater for ORNL Reactor Division.
3. V. Casal, Electrical Heater Rod Development, unpublished KFK report, GfK, Karlsruhe, West Germany, March 1974.
4. D. H. Thompson et al., Test Requirements for Fuel Element Failure Propagation In-Reactor Experiment P1, ANL/RAS 72-9, Rev. 1.
5. M. H. Fontana and J. L. Wantland, LMFBR Safety and Core Systems Programs Progr. Rep. April-June 1974, ORNL/TM-4727.
6. M. H. Fontana, LMFBR Safety and Core Systems Programs Progr. Rep. July-September 1974, ORNL/TM-4776.
7. M. H. Fontana and J. L. Wantland, LMFBR Safety and Core Systems Programs Progr. Rep. October-December 1974, ORNL/TM-4877.
8. M. H. Fontana and J. L. Wantland, LMFBR Safety and Core Systems Programs Progr. Rep. January-March 1975, ORNL/TM-4980.

3. WATER SYSTEM MOCKUP OF THE FFM

Work in this area has been temporarily suspended. Reporting will continue when work is resumed.

4. DETECTION METHODS DEVELOPMENT

W. H. Leavell M. V. Mathis
R. F. Saxe* W. H. Sides

4.1 Temperature Fluctuation Measurement with Stainless
Steel-Sodium Fast-Response Thermocouples

4.1.1 Bundle 6A instrumentation

The use of stainless steel-sodium fast-response thermocouples has been proposed for LMFBR temperature monitoring applications. The response time of these thermocouples is approximately 1 msec, which is faster than that of the Chromel-Alumel thermocouples presently being used in the FFM by a factor of ~ 100 . In order to gain experience in installing and using these thermocouples, we installed seven stainless steel-sodium fast-response thermocouple assemblies in the dummy rod section and exit plenum region of bundle 6A. The locations are shown in Table 4.1. Each assembly contains one stainless steel wire and one Chromel-Alumel thermocouple junction encased in a 1.42-mm-OD (0.056-in.) type 304 stainless steel sheath. The Chromel-Alumel junction is located in the MgO insulation a few mils from the 0.1-mm-thick (0.005-in.) stainless steel cap enclosing the tip of the assembly. The stainless steel wire is welded to the inside of the stainless steel cap. Four assemblies were placed inside the hollow dummy rods, with the tips penetrating the wall of the rods a few mils into the adjacent sodium stream at various axial locations in the unheated zone. These exposed assemblies provide a stainless steel-sodium thermocouple junction. Three of the assemblies were placed in the exit plenum region, two near the sodium exit from the dummy rod unheated zone, and one in a near-stagnant sodium region that will be used as a reference for each of the other six. The temperature fluctuations in the sodium will be measured with these fast-response junctions at higher frequencies than is possible with the insulated-junction Chromel-Alumel thermocouples.

*Consultant from North Carolina State University, Raleigh.

Table 4.1. Location of fast-response thermocouples in bundle 6A

Thermocouple No.	Location (rod number)	Distance from start of heated section [mm (in.)]	Tip orientation (flow channel)
1 (reference)		2.4 (95)	In plenum region near dummy rod support tie rod
2	Dummy rod support tie rod	2.2 (85)	31
3	Dummy rod support tie rod	2.2 (85)	29
4	3	1.6 (64)	10
5	2	1.4 (56)	6
6	3	1.3 (52)	10
7	2	1.1 (44)	6

Because of the low sensitivity of the stainless steel-sodium junction ($<17 \mu\text{V}/^\circ\text{C}$) and the presence of large amounts of 60-Hz power supplying the 19 electrically heated fuel pins, special care was taken in both the design and installation of the fast-response thermocouple assemblies and associated signal conditioning instrumentation to reduce electromagnetic interference and 60-Hz ground loop interference with the temperature signals. Figure 4.1 is a schematic diagram of the instrumentation for noise analysis measurements showing a typical circuit for one assembly. The stainless-steel-sheathed assemblies exit the bundle 6A test section housing through a Conax fitting and are terminated within a junction box shield welded to the test-section instrument nozzle. Special low-noise, twisted-pair, shielded signal cables (Chromel, Alumel, and copper) are routed through a flexible conduit between the junction box and a signal-selection junction box located outside the FFM loop enclosure. Precautions were taken to ensure that the twisted-pair signal cables were connected to the FFM ground only at the test section to prevent interfering ground loops in the system. In the signal-selection junction box, provision was made for independent selection of

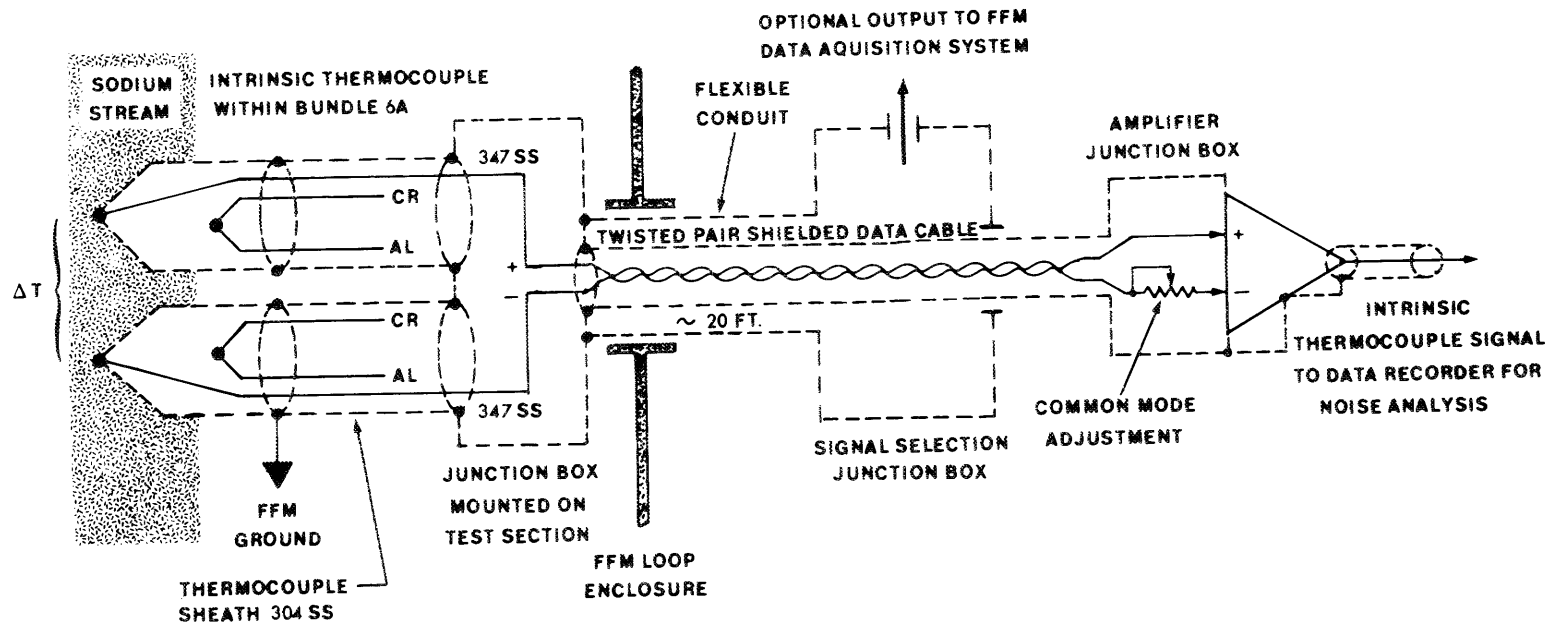


Fig. 4.1. Schematic diagram of fast-response thermocouples installation in bundle 6A. (20 ft = 6.1 m)

each Chromel-Alumel or stainless steel-sodium thermocouple for noise analysis of the signal or for use in the FFM data acquisition system. When noise analysis measurements are made, the thermocouple signals will be disconnected from the FFM data acquisition system and reconnected, using approximately 4 m (12 ft) of low-noise, triaxial, shielded cable, to the input of a high-gain, low-noise amplifier provided with adjustable common-mode rejection to further minimize interference. The signals will be recorded on a multichannel FM tape recorder during sodium fill in phase I of the FFM bundle 6A test program and at several steady-state loop conditions during phase II.

4.1.2 Single-pin test loop measurements

In addition to the seven assemblies installed in bundle 6, two similar fast-response thermocouple assemblies were installed in the single-pin heater test loop. One was located in a region of near-stagnant sodium below the test-section sodium inlet and one in the sodium stream near the top of the heater. This arrangement provided for measurement of the temperature difference between the sodium at the top of the heater and in the near-stagnant region using the stainless steel-sodium junctions and of the temperature difference at these same two locations using the Chromel-Alumel thermocouple in each assembly. Similar signal-lead shielding precautions were taken in this installation as were described for the installation in bundle 6A. During December, the signals from these two thermocouple assemblies were recorded on an FM tape recorder during operation of the single-pin heater test loop, and the recorded noise signals are currently being analyzed.

4.1.3 Temperature measurement problems with stainless steel-sodium thermocouples in the FFM

Measurements of temperature differences in bundle 6A or in the single-pin heater test loop using the stainless steel-sodium junctions will not be reliable unless they are calibrated using the Chromel-Alumel thermocouple within the same assembly. This is due to the uncertainty

about (1) the thermoelectric properties of the stainless steel-sodium junction,¹ (2) the long-term stability of these properties, (3) the effects of contamination of the sodium with corrosion products and the changes in the composition of the stainless steel sheath due to corrosion,² and (4) the emf losses due to shunt resistance of the sheath and structure.² The data from two investigators^{1,3} on the thermoelectric properties of the stainless steel-sodium junction indicate, with reasonable agreement, that the junction has a sensitivity of $\sim 17 \pm 2 \mu\text{V}/^\circ\text{C}$. The effect of shunt resistance can be demonstrated as follows.² (See Fig. 4.2.) In the figure, V_{Na} is the emf ($17 \mu\text{V}/^\circ\text{C}$) generated from the temperature difference in the sodium between the measurement junction, T , and the reference junction, T_{R} . The value of this emf measured externally is V . The terms R_{Na} and R_{S} are the resistances of the paths between the two junctions through the sodium and through the sheaths and structure respectively. An electrical current, I , flows in the loop formed by these two paths. From electrical considerations,

$$V_{\text{Na}} - IR_{\text{Na}} - IR_{\text{S}} = 0 \quad (1)$$

and

$$V = V_{\text{Na}} - IR_{\text{Na}} \quad (2)$$

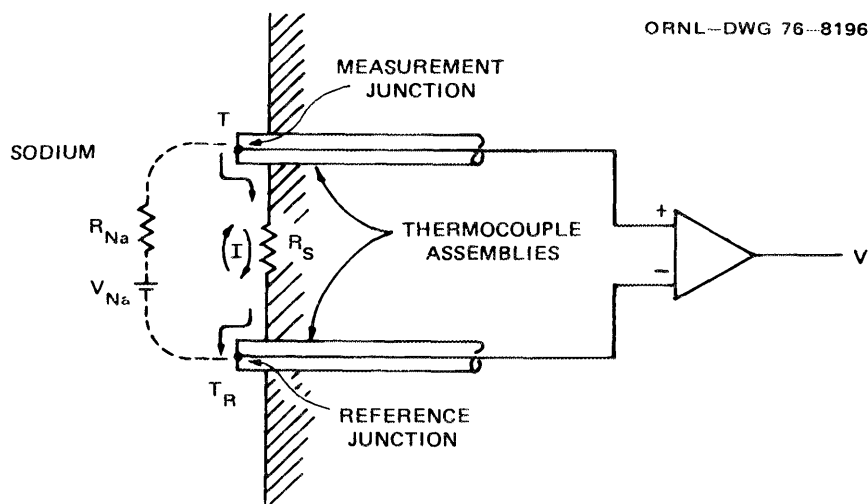


Fig. 4.2. Schematic diagram showing effect of shunt resistance.

Combining yields

$$\frac{V}{V_{Na}} = \frac{R_s}{R_{Na} + R_s} \quad (3)$$

Therefore, the measured emf will be less than the expected emf ($17 \mu\text{V}/^\circ\text{C}$) due to the shunt resistance of the stainless steel structure between junctions. Preliminary measurements in the single-pin heater test loop installation indicated a 40% loss of junction emf at a temperature difference between the locations of the two assemblies of 287°C ; that is, the measured sensitivity was $\sim 10 \mu\text{V}/^\circ\text{C}$ instead of the expected $17 \mu\text{V}/^\circ\text{C}$. For a 40% reduction in expected emf, $R_s = 1.5R_{Na}$. In order for this error to be less than the uncertainty in the expected value ($\pm 2 \mu\text{V}/^\circ\text{C}$), the shunt resistance must be greater than the sodium resistance by a factor of 7.5. The effect of the shunt losses will be important in the bundle 6A installation, since the shunt resistance from the thermocouple assembly tip to ground through the stainless steel sheath is similar to that in the single-pin loop and will be variable from one assembly to another.

References

1. J. Kuwabara, "A New Thermometry for Liquid Sodium," IEEE Trans. Nucl. Sci. 19, 899 (1972).
2. T. G. Kollie, private communication.
3. E. Combillard, J. Huetz, and N. Lions, "Experience with a Thermocouple Working with Zero Time Constant," pp. 286-88 in Proc. Am. Nucl. Soc. Top. Meet.: Irradiat. Exp. Fast React. Sept. 10-12, 1973.

5. FFM FACILITY OPERATIONS

P. A. Gnad	R. E. MacPherson
J. W. Koger*	D. G. Linz†
R. H. Thornton	R. L. Ludwig*

5.1 Test Facility Operation

The test facility has been shut down since May 1975 for major modifications to increase the bundle power supply to 2 MW. The new test-section housing and bundle 6 have been installed in the facility, and operational checkout has been started.

5.2 Test Bundles

5.2.1 Bundle 6

Bundle 6 is designed as a loss-of-pump test in support of the ANL SLSF program. The test section is described in Ref. 1. The bundle is designed to operate for short periods of time at 980°C (1800°F). Table 5.1 presents a summary of the instrumentation designed into the bundle, and Figs. 5.1 and 5.2 show the locations of the thermocouples in the bundle.

Assembly of the bundle has been completed, and it is now installed in the facility. Figures 5.3 to 5.14 show the bundle at various stages of completion.

5.2.2 Bundle 7

Bundle 7, a 19-rod bundle, is also to be used in support of the ANL SLSF test program. Bundle 7 tests are intended to simulate the effect of a LOPI incident on LMFBR fuel. The bundle design is very similar to bundle 6A except for thermocouple locations. The design of the bundle is described in Ref. 2.

*Metallurgy Department of the Y-12 Plant Development Division of Union Carbide Nuclear Division.

†On loan from RDD Components Development Branch (Washington).

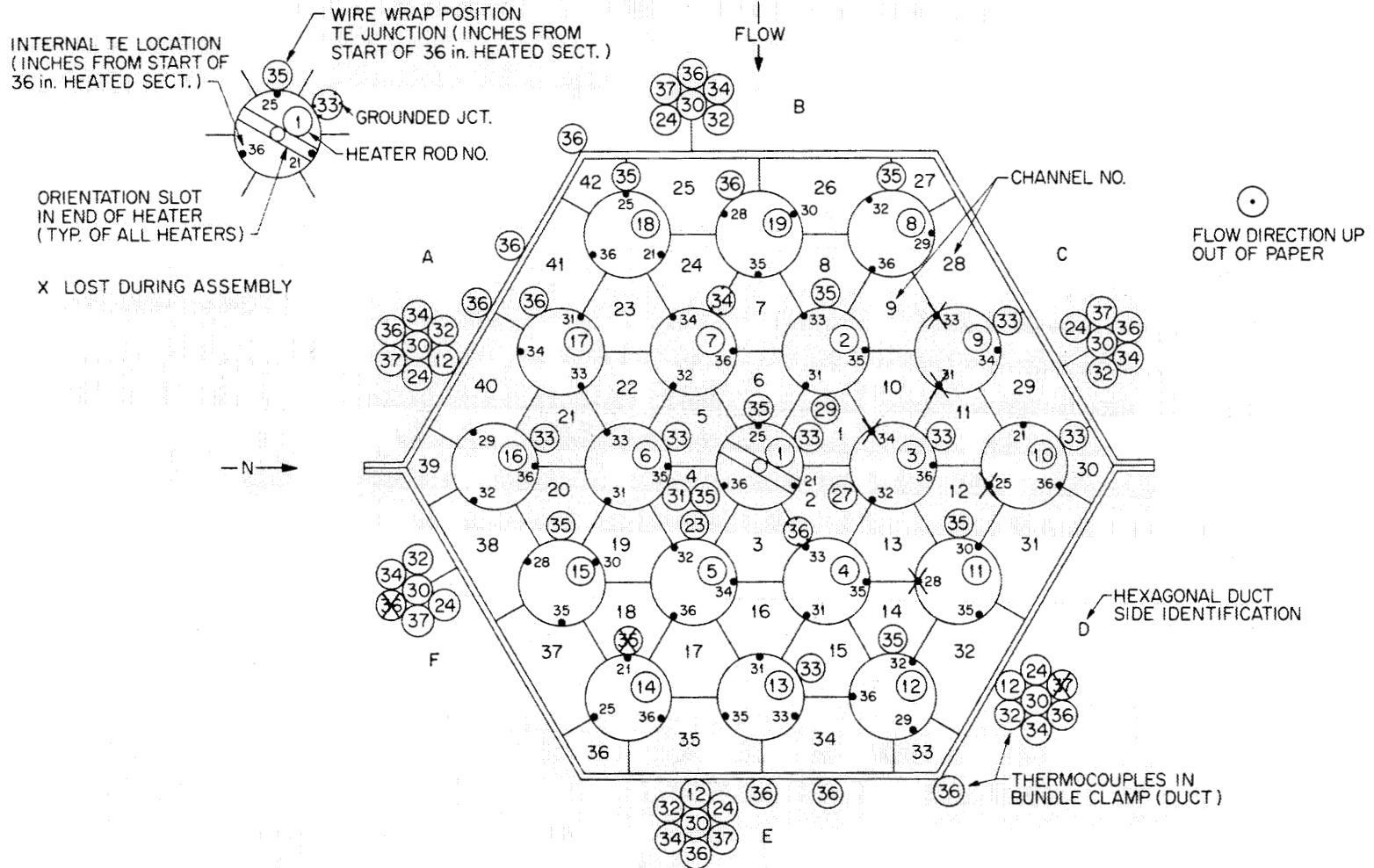


Fig. 5.1. LMFBR-FFM bundle 6A heater rod bundle instrumentation.
(1 in. = 25.4 mm)

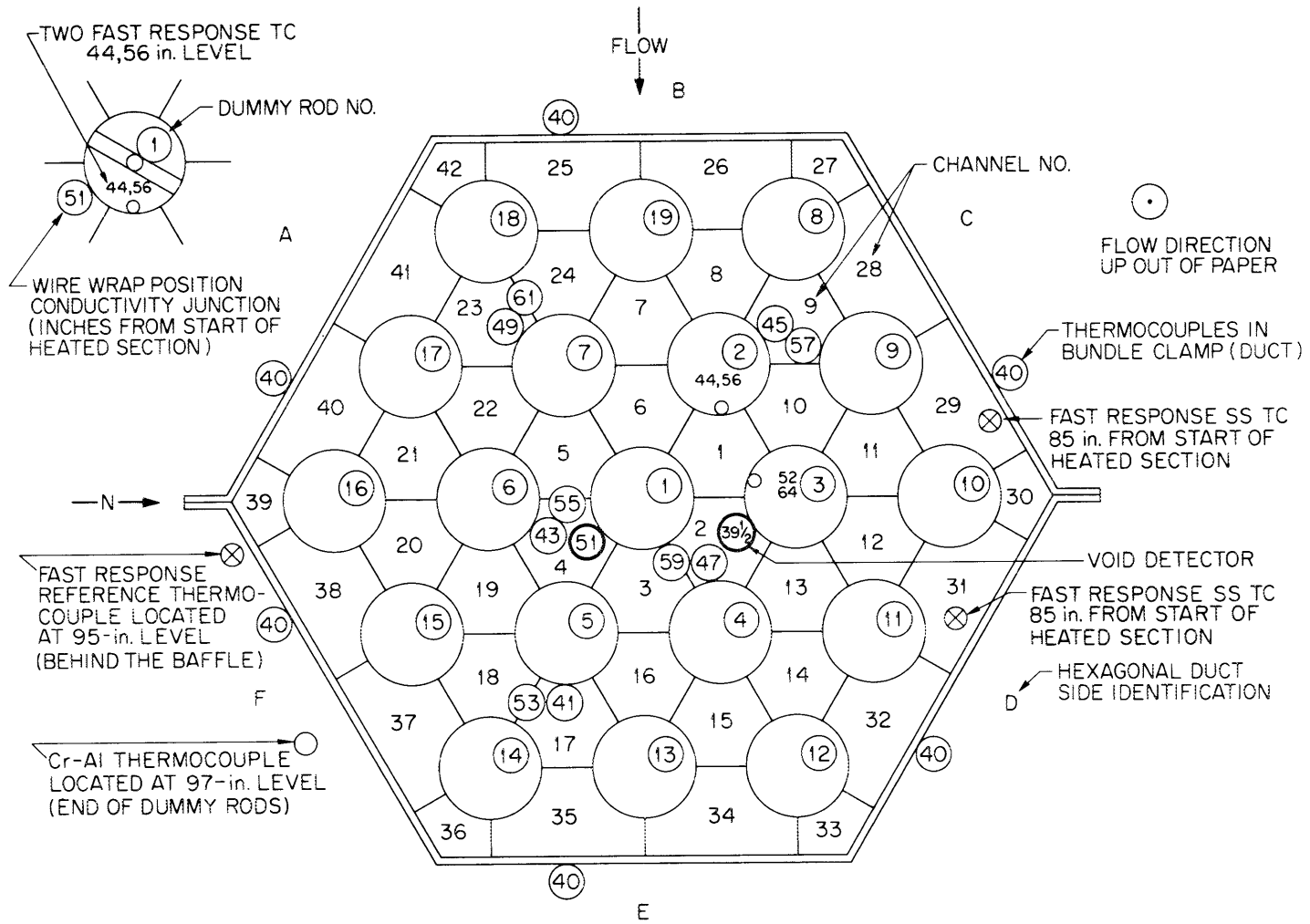


Fig. 5.2. LMFBR bundle 6A dummy rod bundle instrumentation. (1 in. = 25.4 mm)

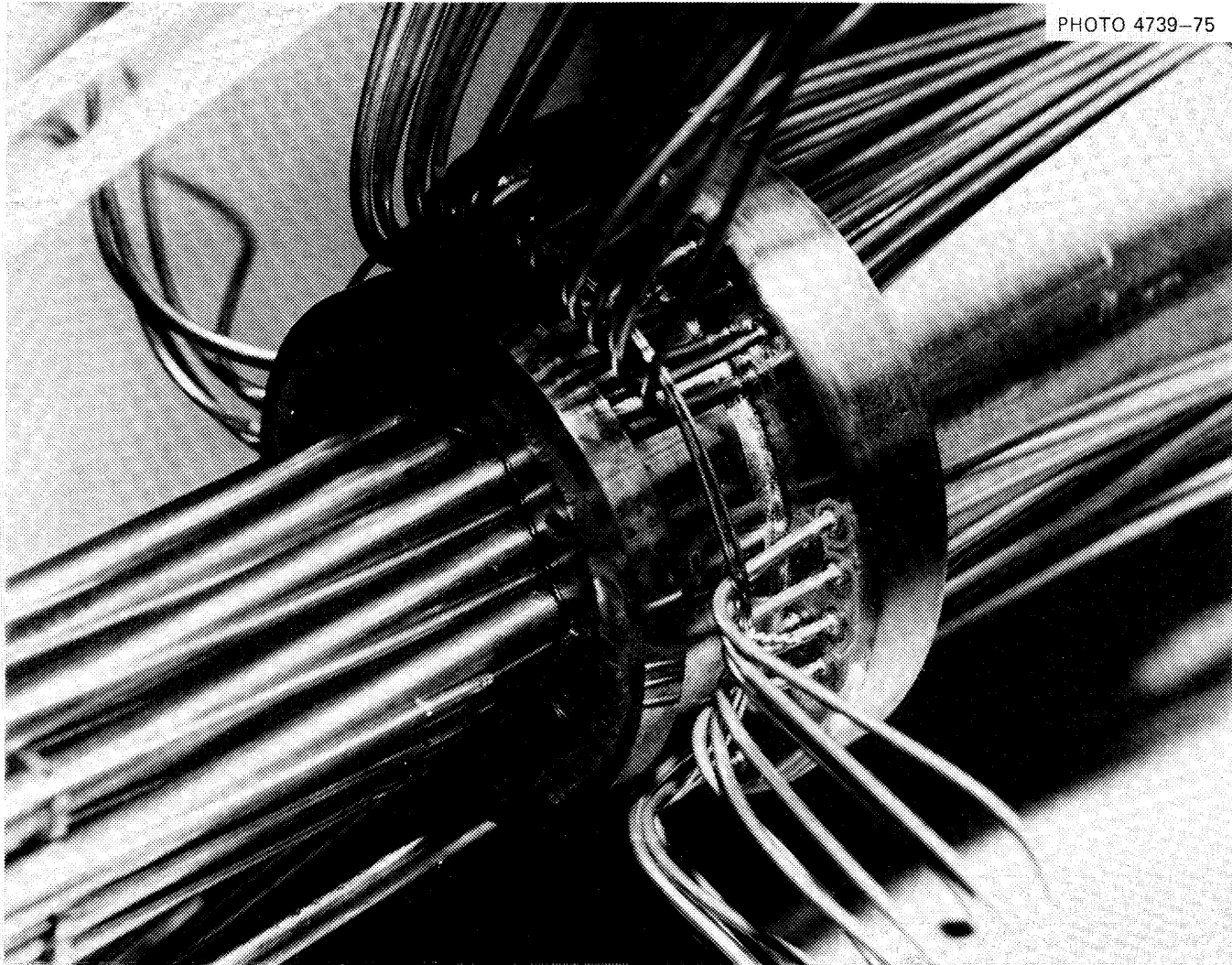


Fig. 5.3. LMFBR-FFM bundle 6. Photographic details of duct wall thermocouples to bulkhead braze joints and assembly weld of bulkhead to sodium duct wall.

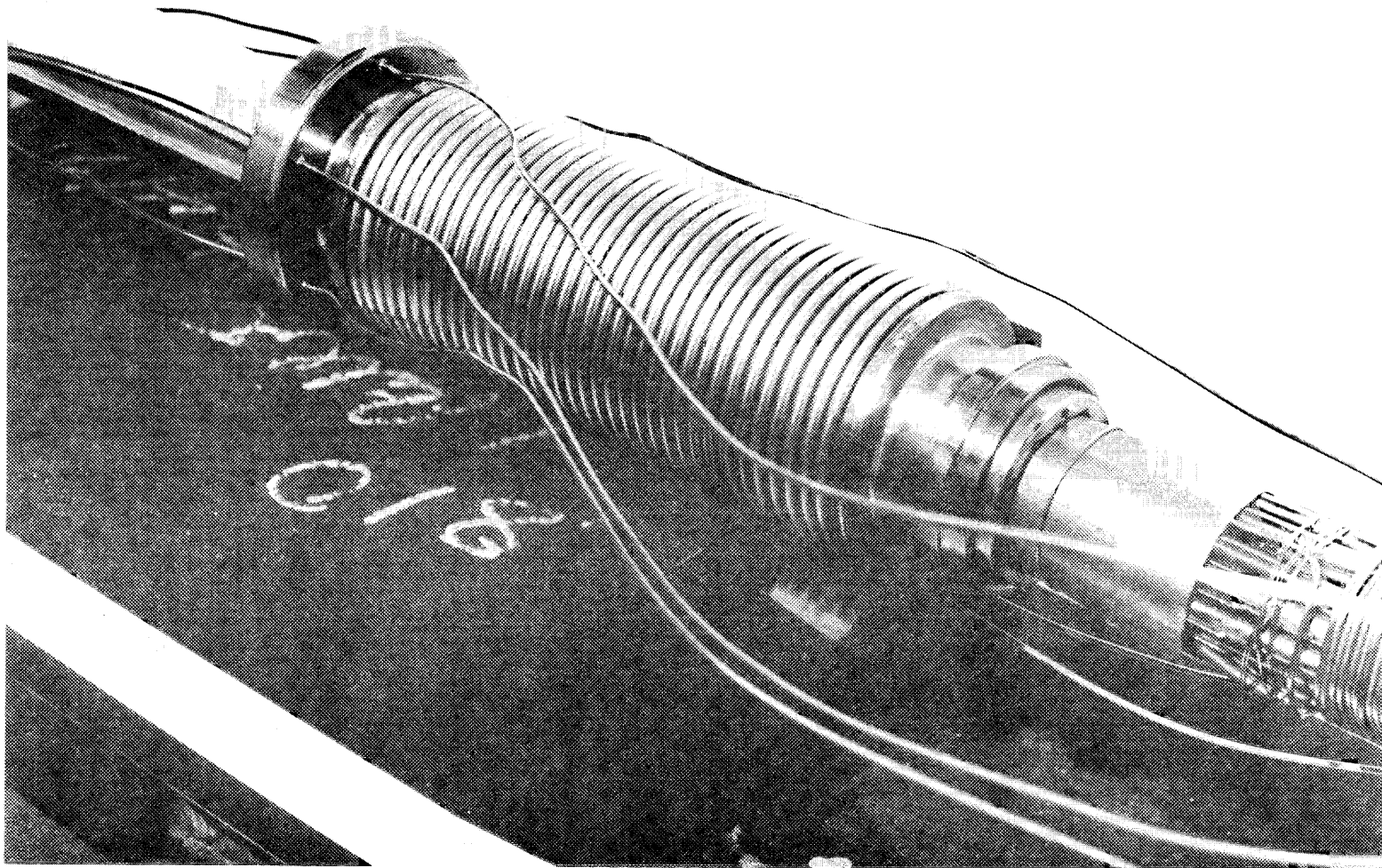


Fig. 5.4. LMFBR-FFM bundle 6 showing the bellows subassembly prior to welding and duct wall thermocouple penetrations and braze joints.

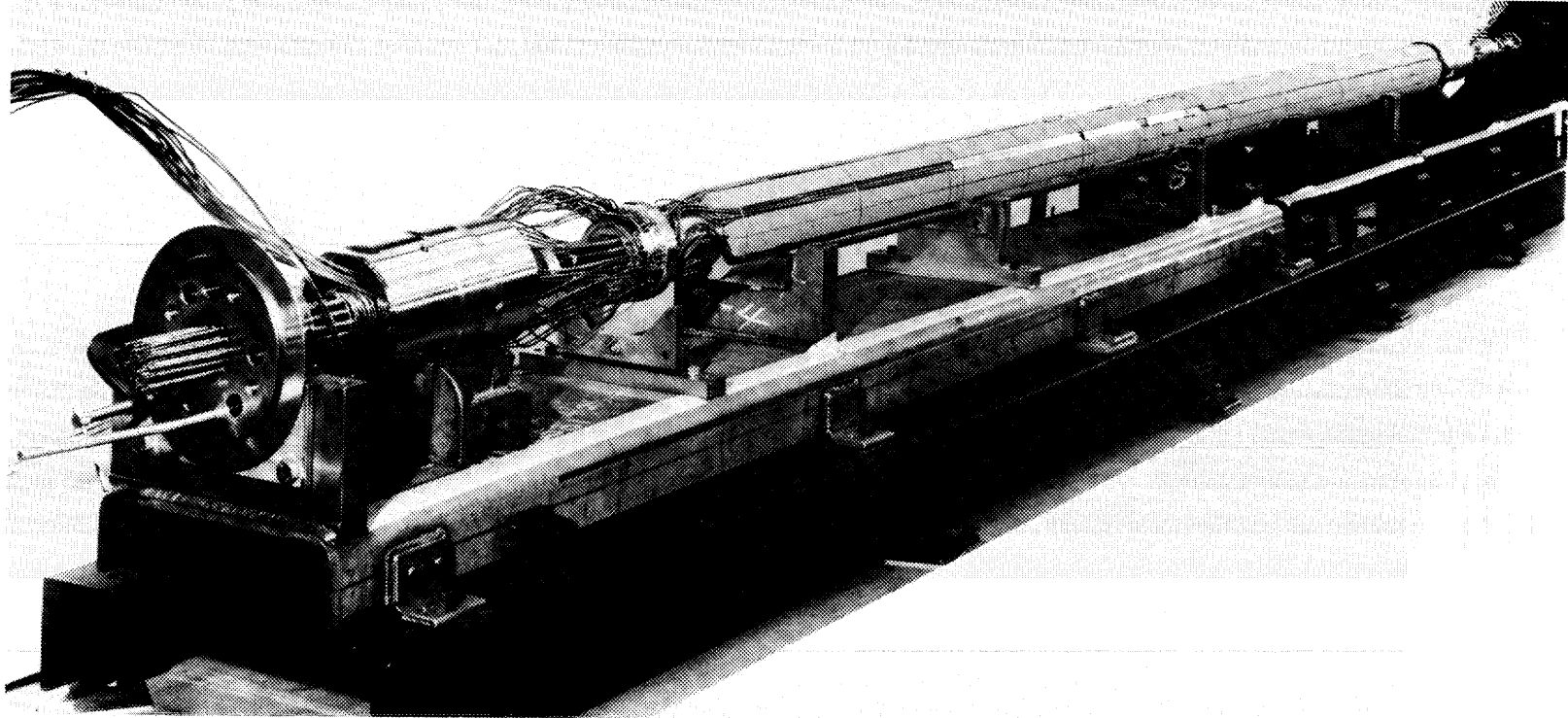


Fig. 5.5. LMFBR-FFM bundle 6. Overall view of assembled Marimet insulation and duct wall thermocouples.

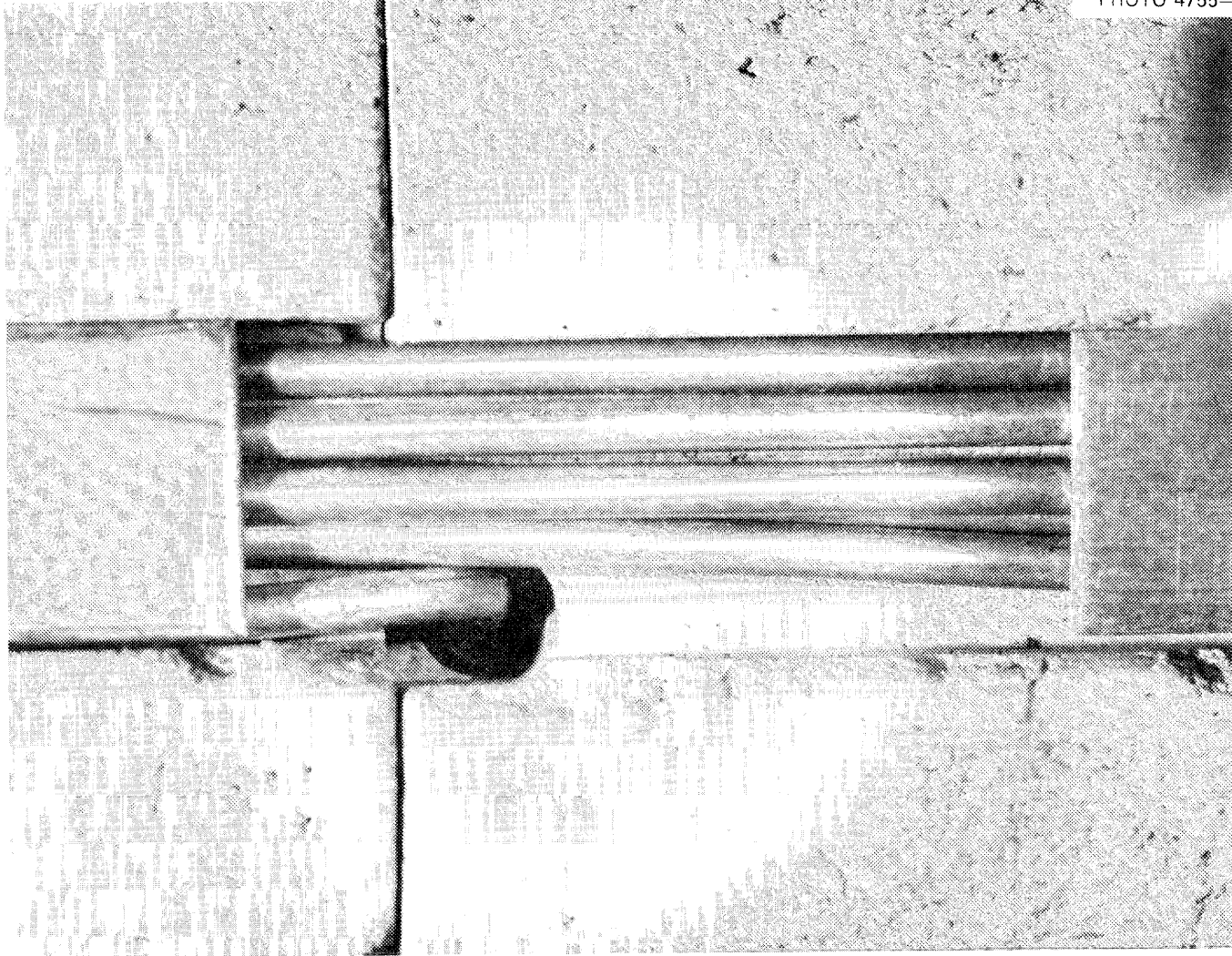


Fig. 5.6. LMFBR-FFM bundle 6. Magnified view of duct wall thermocouple after final installation.

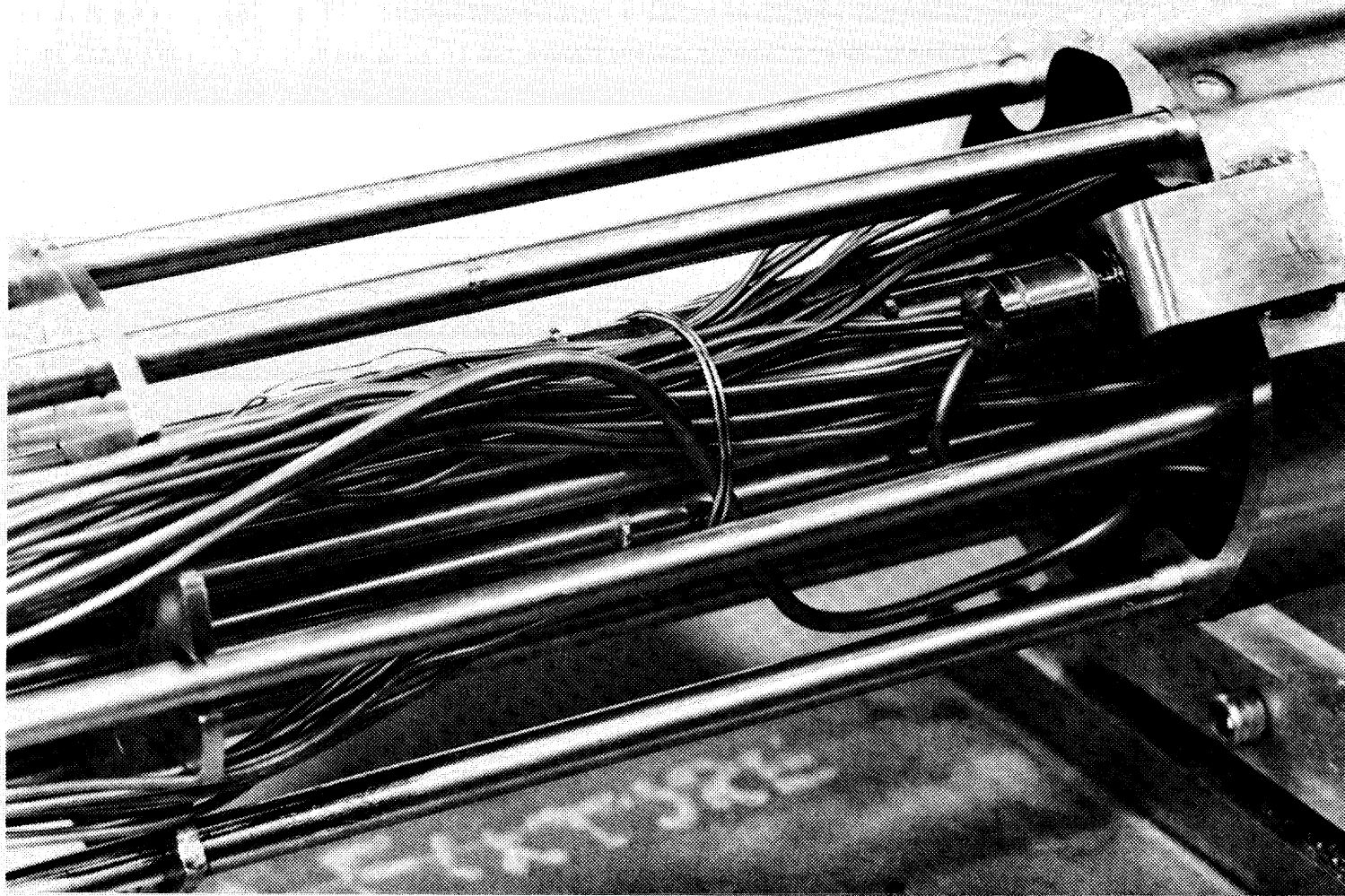


Fig. 5.7. LMFBR-FFM bundle 6 showing inlet pressure transducer attached to bundle subassembly.



Fig. 5.8. LMFBR-FFM bundle 6 showing inlet acoustic sensor attached to bundle subassembly.

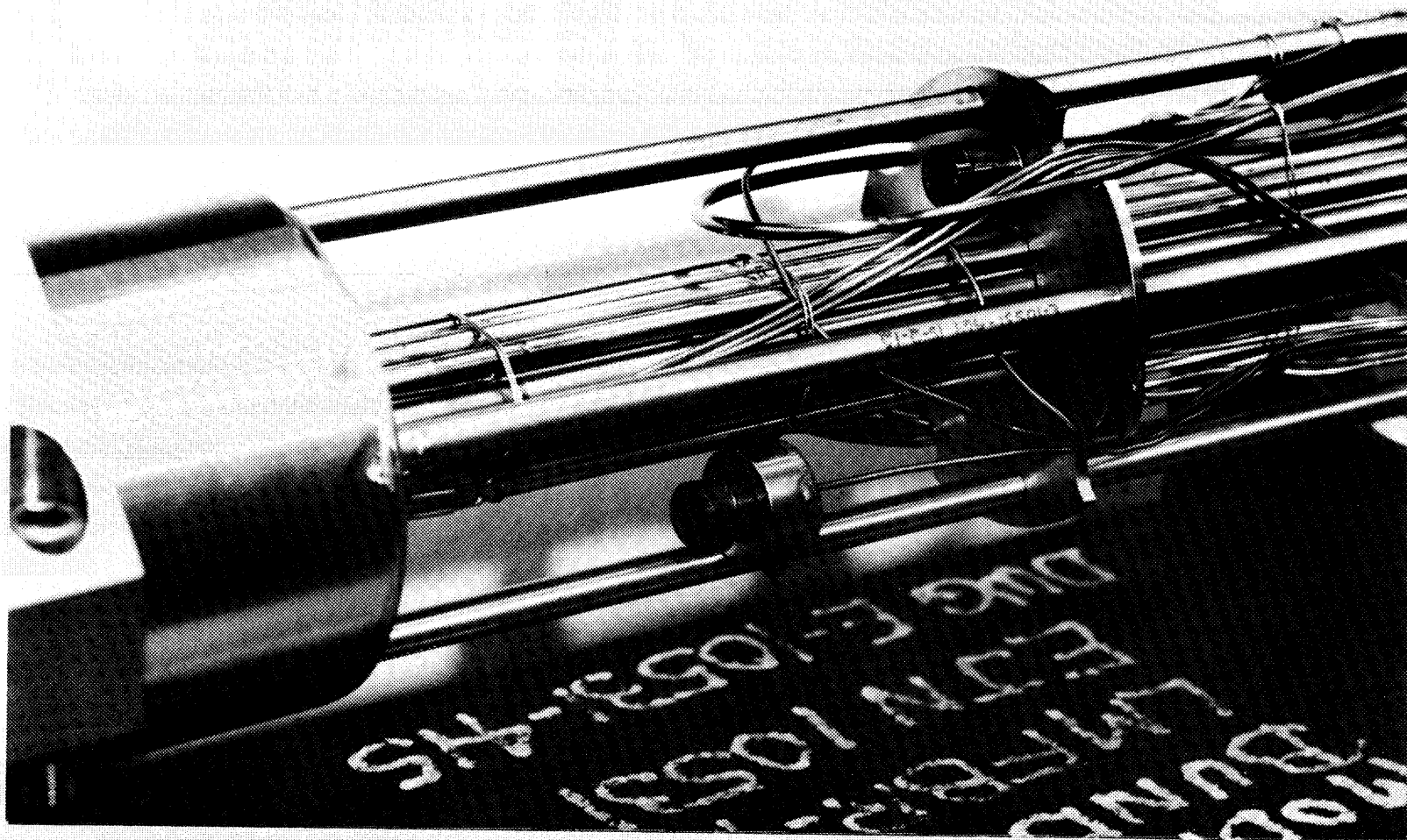


Fig. 5.9. LMFBR-FFM bundle 6. View of ANC pressure sensor (lower sensor) and pressure transducer attached to downstream end of the bundle subassembly.

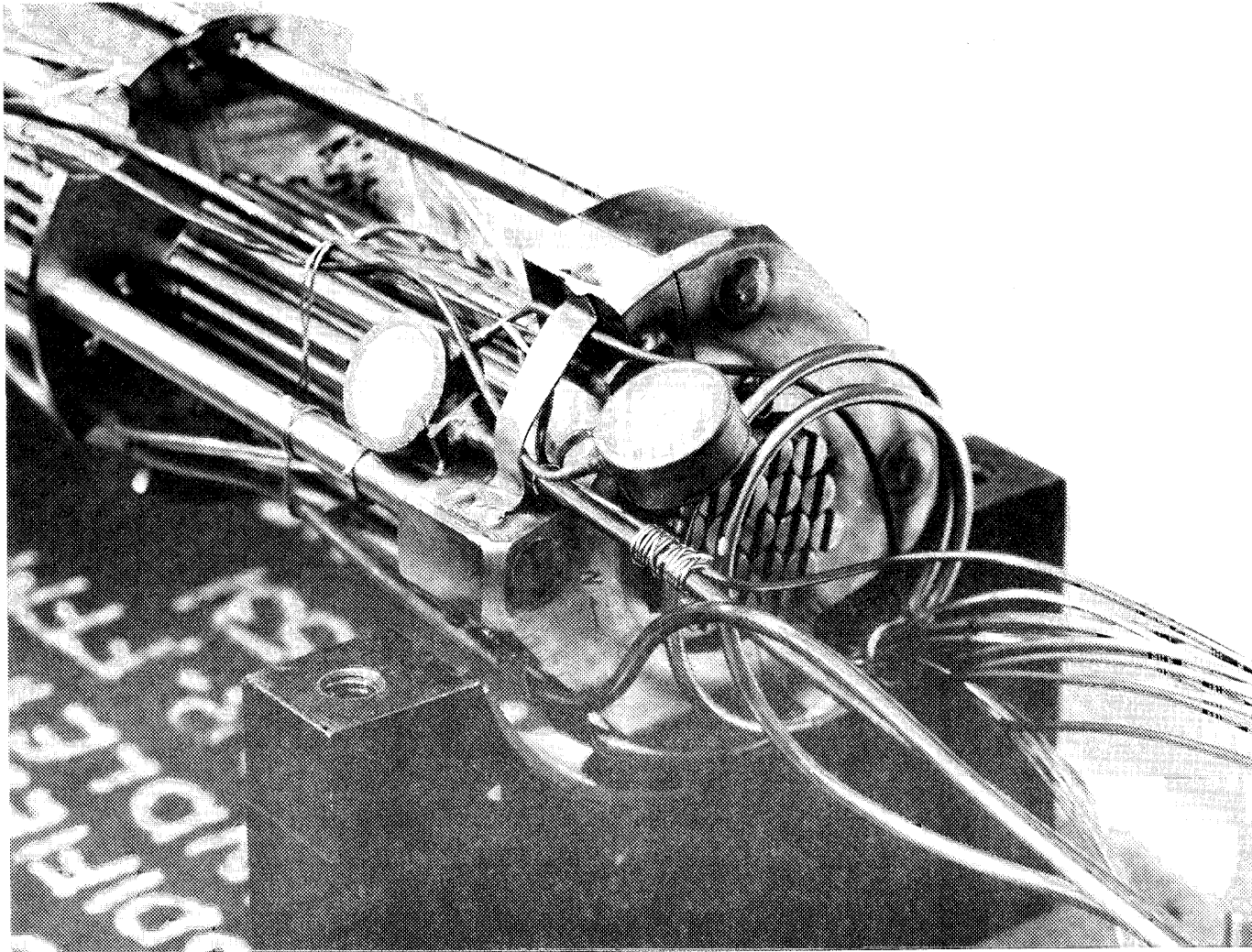


Fig. 5.10. LMFBR-FFM bundle 6. View of acoustic sensors attached to downstream end of the bundle subassembly.

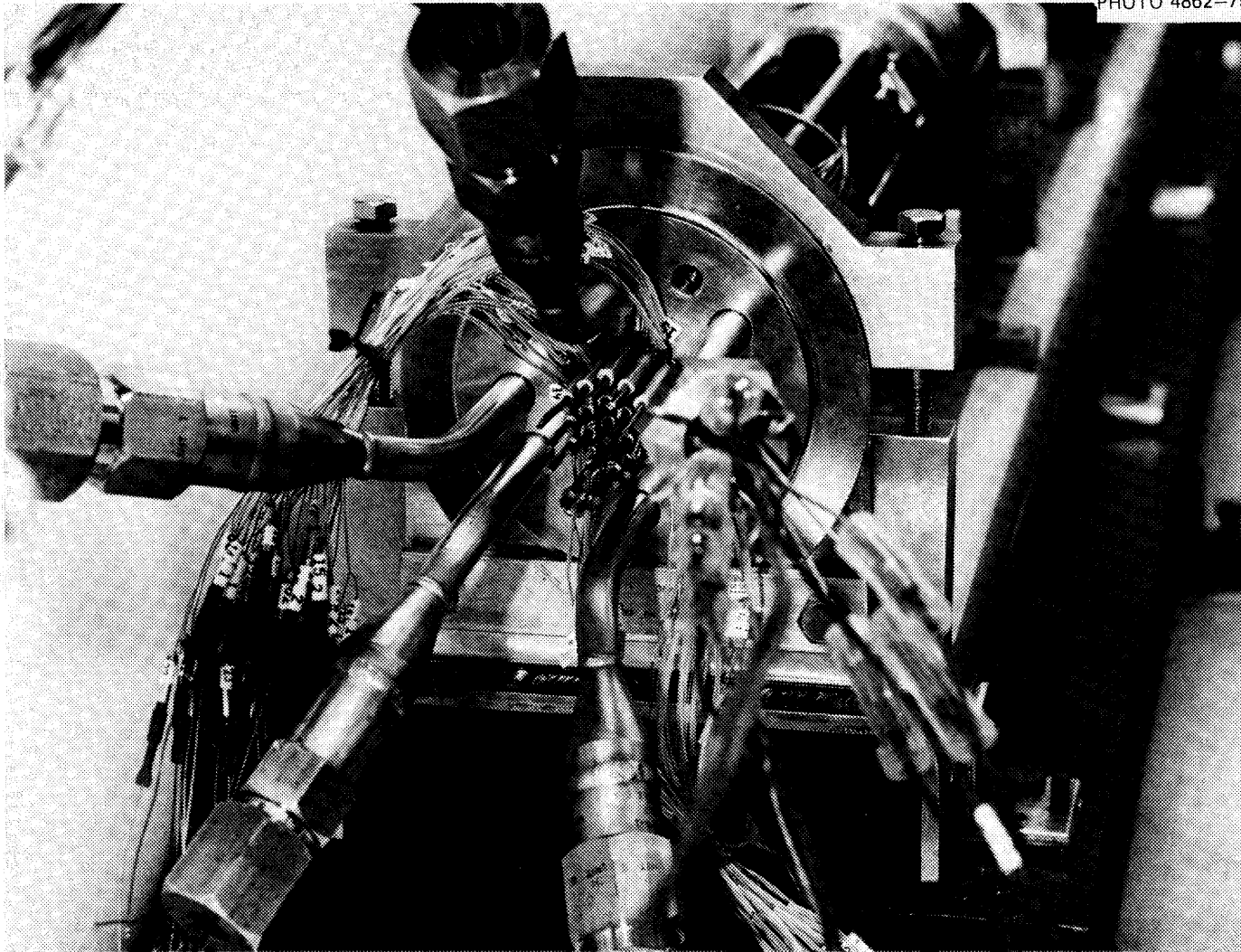


Fig. 5.11. LMFBR-FFM bundle 6. View of heater leads, internal heater thermocouples, and Conax fittings penetrating the heater tube sheet.

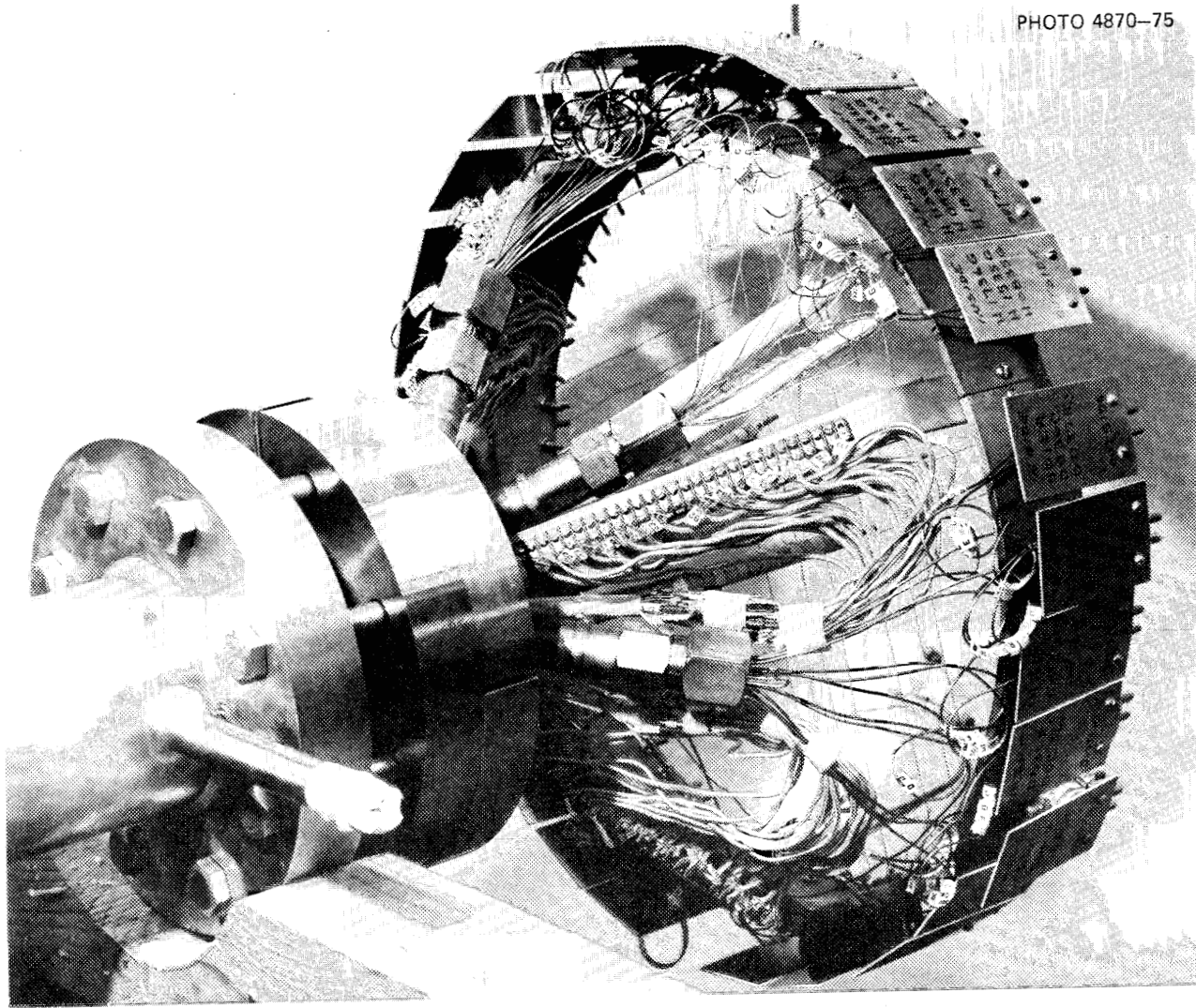


Fig. 5.12. LMFBR-FFM bundle 6. View of tube sheet and instrumentation support ring and penetrations.

PHOTO 4871-75

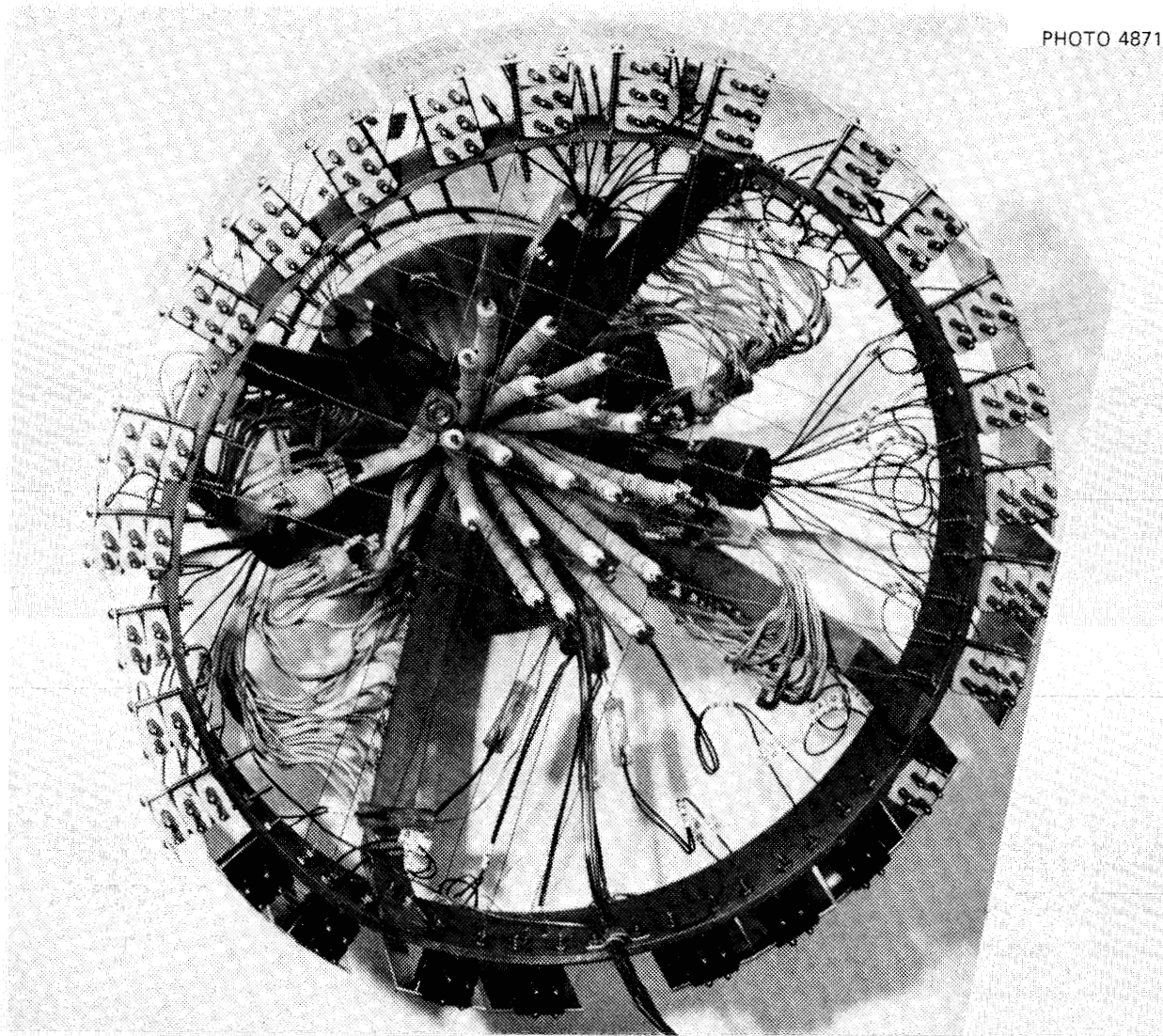


Fig. 5.13. LMFBR-FFM bundle 6. View of tube sheet and instrumentation support ring and penetrations.

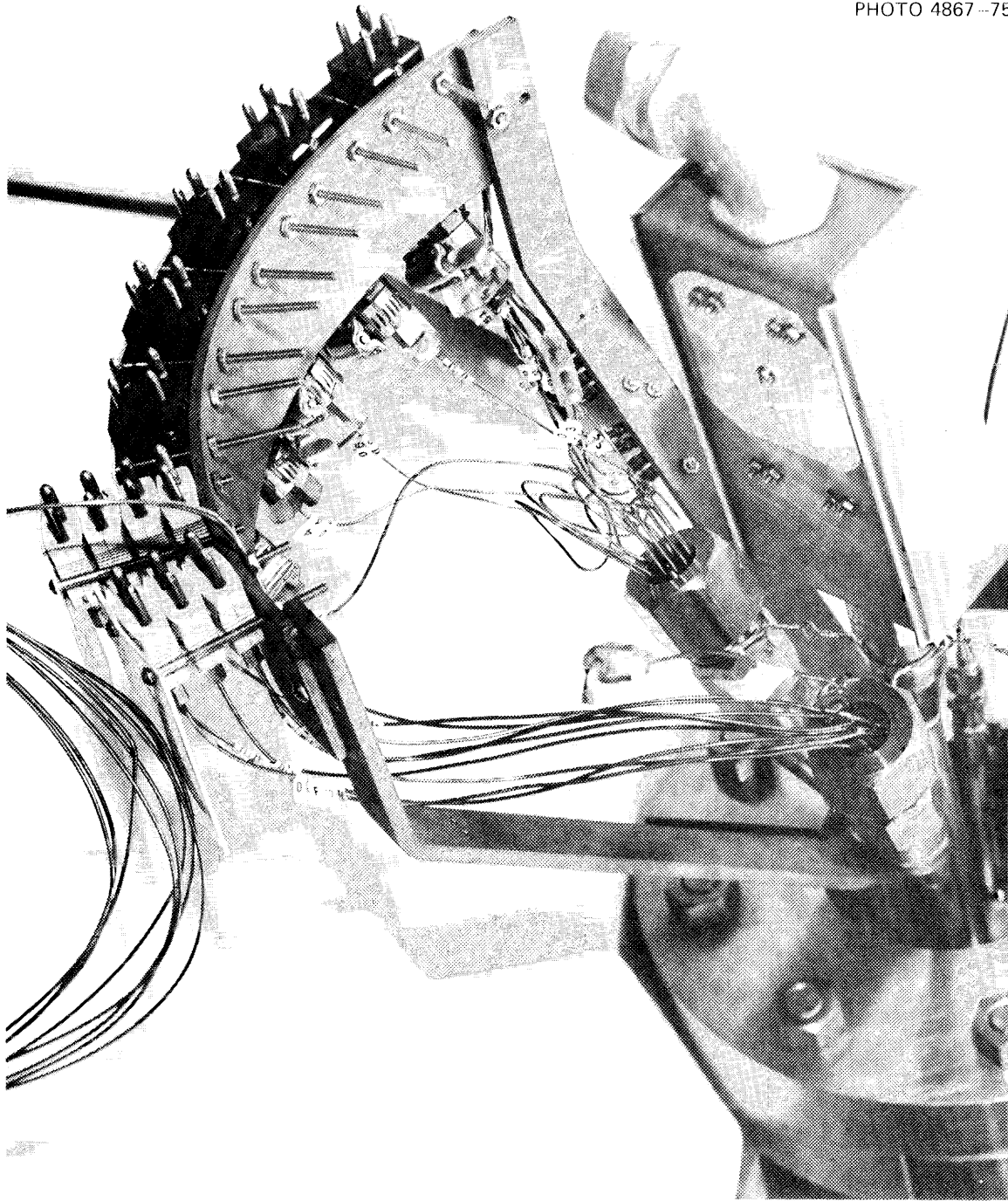


Fig. 5.14. LMFBR-FFM bundle 6. Photograph of upper bundle instrumentation penetrations and support bracket.

Table 5.1. Summary of instrumentation in bundle 6A

Type	Location	Number
Thermocouple	Inside heater sheath	52
	Wire wrap on heaters	25
	Duct wall of heater section	43
	Duct wall of dummy section	6
	Wire wrap on dummy rods	10
Fast-response thermo- couple	In dummy rods	4
	In upper plenum area	3
Void detector	Wire wrap on dummy rods	2
Acoustic sensor	In sodium at test-section inlet	1
	In sodium at test-section outlet	2
Pressure transducers or sensors	In sodium at test-section inlet	1
	In sodium at test-section outlet	2
Total		151

The design layout and details for this bundle have been revised to take advantage of the experience gained during the fabrication of bundle 6. The need for this bundle is being evaluated, however, and a possibility exists that this bundle will be delayed or canceled in order to proceed with the operation of larger bundles.

5.3 Facility Modifications

5.3.1 Bundle power supply and control

The 2.0-MW bundle heater power supply and control system has been installed. The control circuits and the protective "crowbar" circuits have been checked out and are ready for operation. A section of the main control board, which contains the heater zone control cabinets, is shown in Fig. 5.15. A complete description of the power system is given in Ref. 1.

A programmable control system, which was designed to control the FFM bundle power to simulate Fast Test Reactor (FTR) power transients,

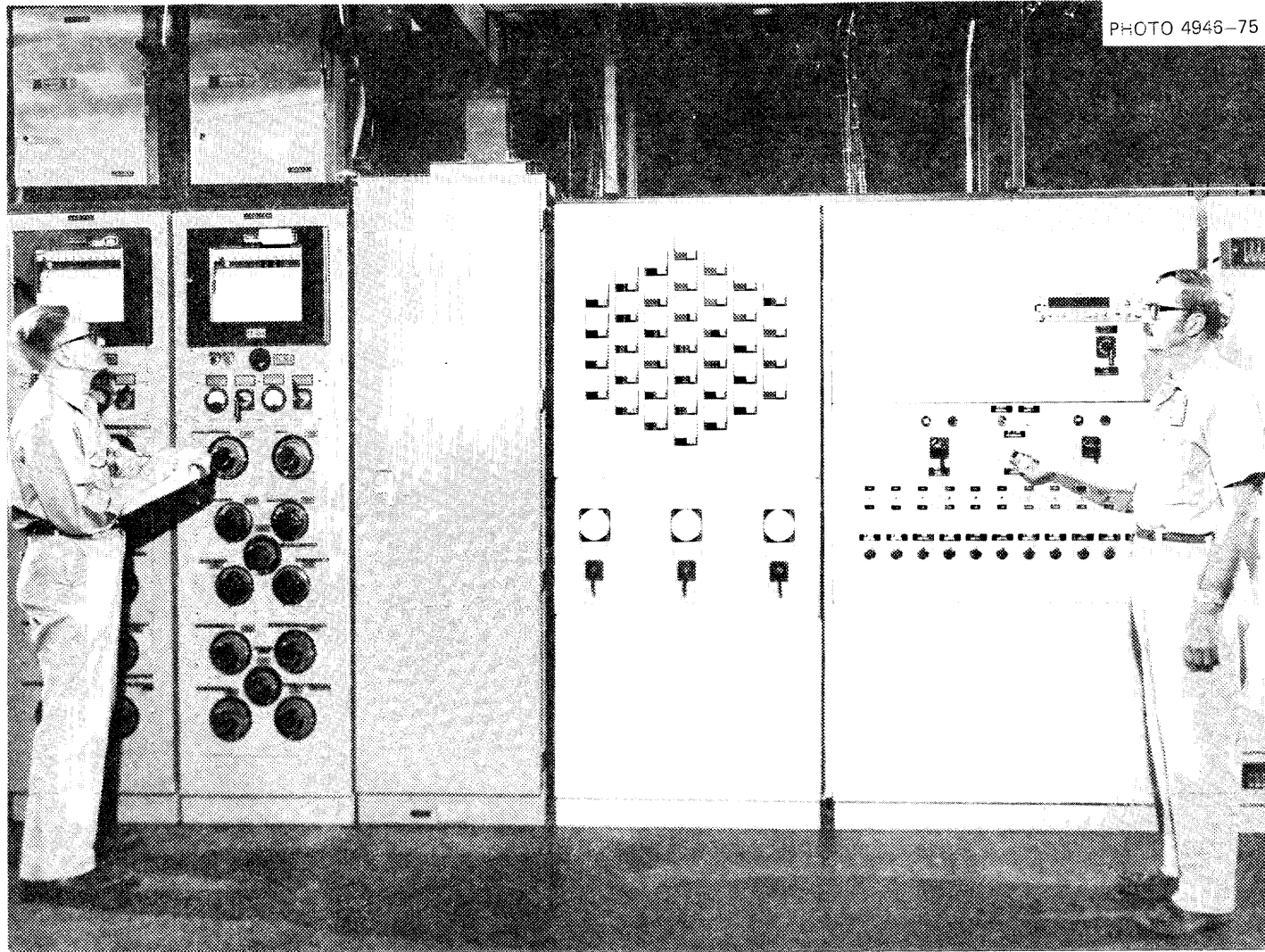


Fig. 5.15. LMFBR FFM. Section of main control area showing the control cabinets for the main bundle heater power.

has been fabricated and installed. A programmable pump control system, which was designed to simulate FTR flow transients in the FFM, has also been installed.

5.3.2 Bundle 6 operation

The piping changes required for bundle 6 operation² have been completed. (The flow diagram for the present system is shown in Fig. 5.16.) All trace heaters and thermocouples have been installed and checked out. Some of the control cabinets and the cabinets housing the trace heater control Variacs and temperature recorders are shown in Fig. 5.17.

Figure 5.18, a photograph of the recent modifications to the FFM, shows the east side of the facility, including the new dump tank, the expansion tank (top), and part of the new test-section housing (extreme left). Figure 5.19 shows the new test section after installation in the facility and after all the electrical and instrument connections have been made.

Figure 5.20 is a close-up view of the bottom of the test section showing the bundle instrument connections. Bundle 6 instrumentation includes grounded and ungrounded thermocouples, fast-response thermocouples, void detectors, acoustic sensors and hydrophones for boiling detection, and high-temperature pressure transmitters. This instrumentation is shown in Figs. 5.1, 5.2, 5.21, and 5.22. Preoperation testing is now under way.

Bundle 6 tests will be followed by an experiment to investigate the temperature distribution in a mixing tee in which hot and cold sodium streams are mixed.¹ The design and thermocouple locations for the mixing tee are shown in Fig. 5.23. Figure 5.24 is a photograph of the mixing tee assembly prior to installation in the facility, and Fig. 5.25 shows the mixing tee installed in the FFM facility.

5.4 Investigation of Failure of Bundle 5D

Bundle 5D failed while undergoing tests during which the sodium coolant boiled.^{3,4} Electrical changes were noted in several heaters,

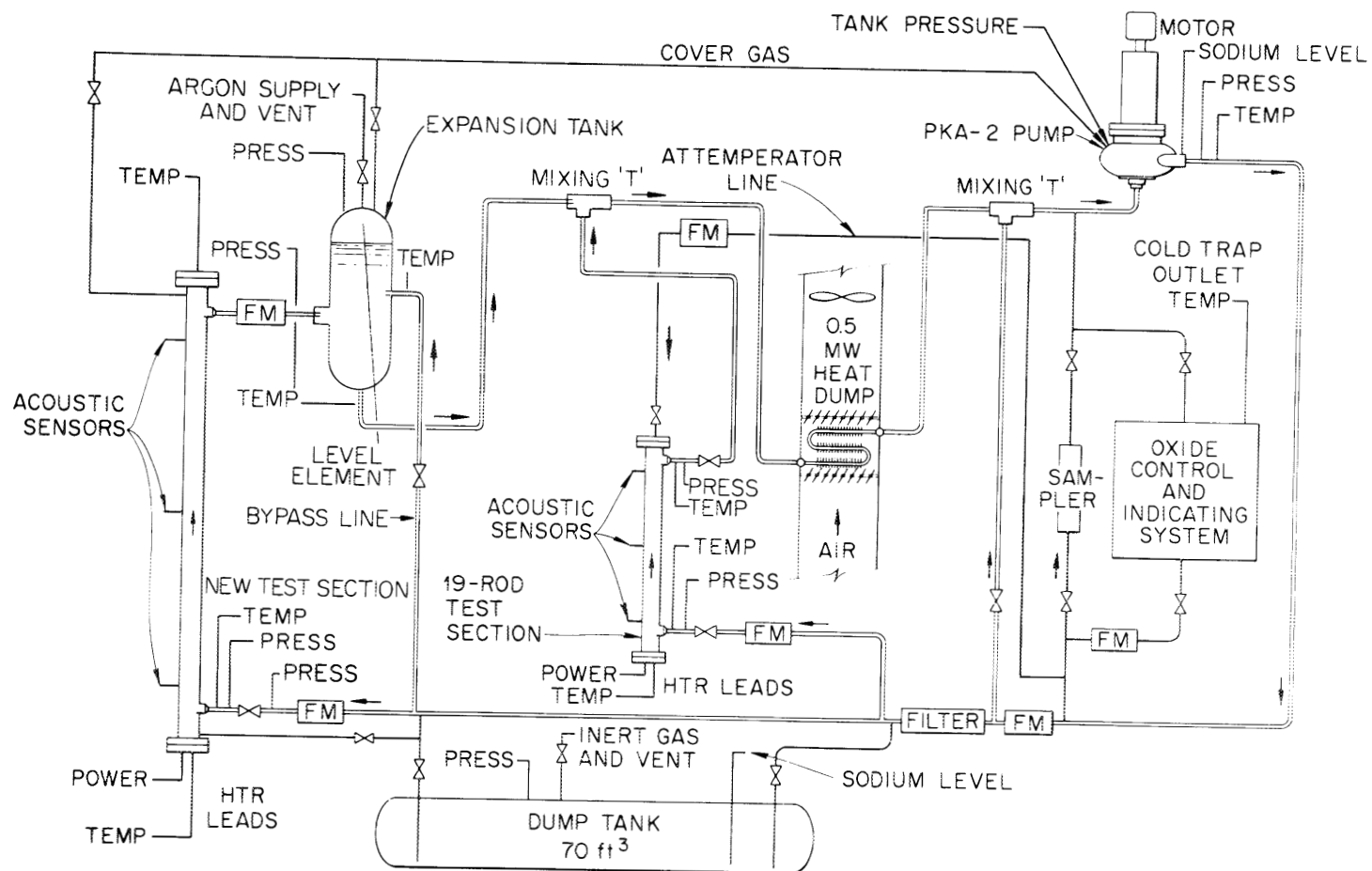


Fig. 5.16. LMFBR-FFM flow diagram.

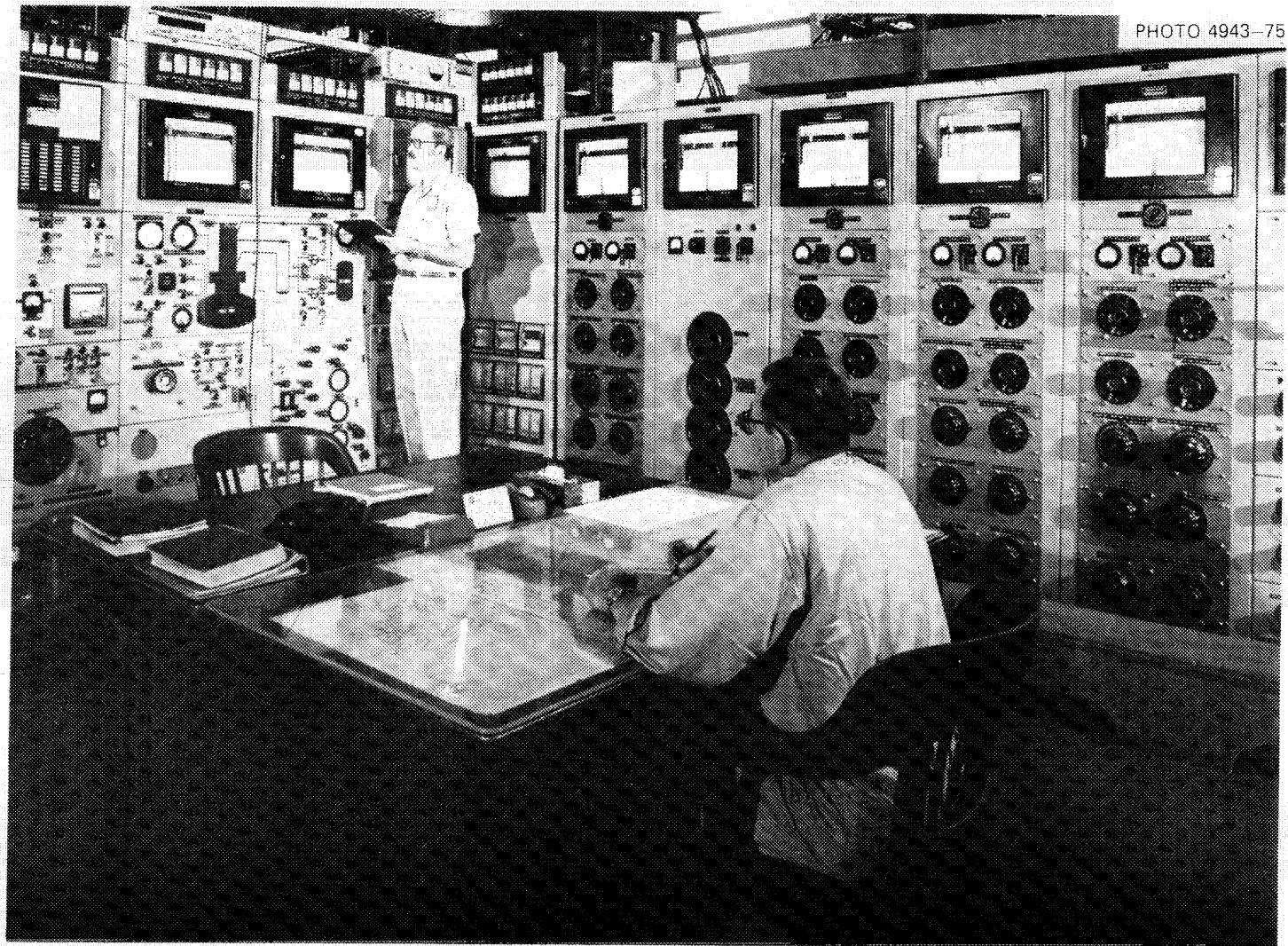


PHOTO 4943-75

Fig. 5.17. LMFBR FFM. Section of main control area showing the control panel for applying heat to the trace heaters and the control panels for the main pump and radiator blower motor.

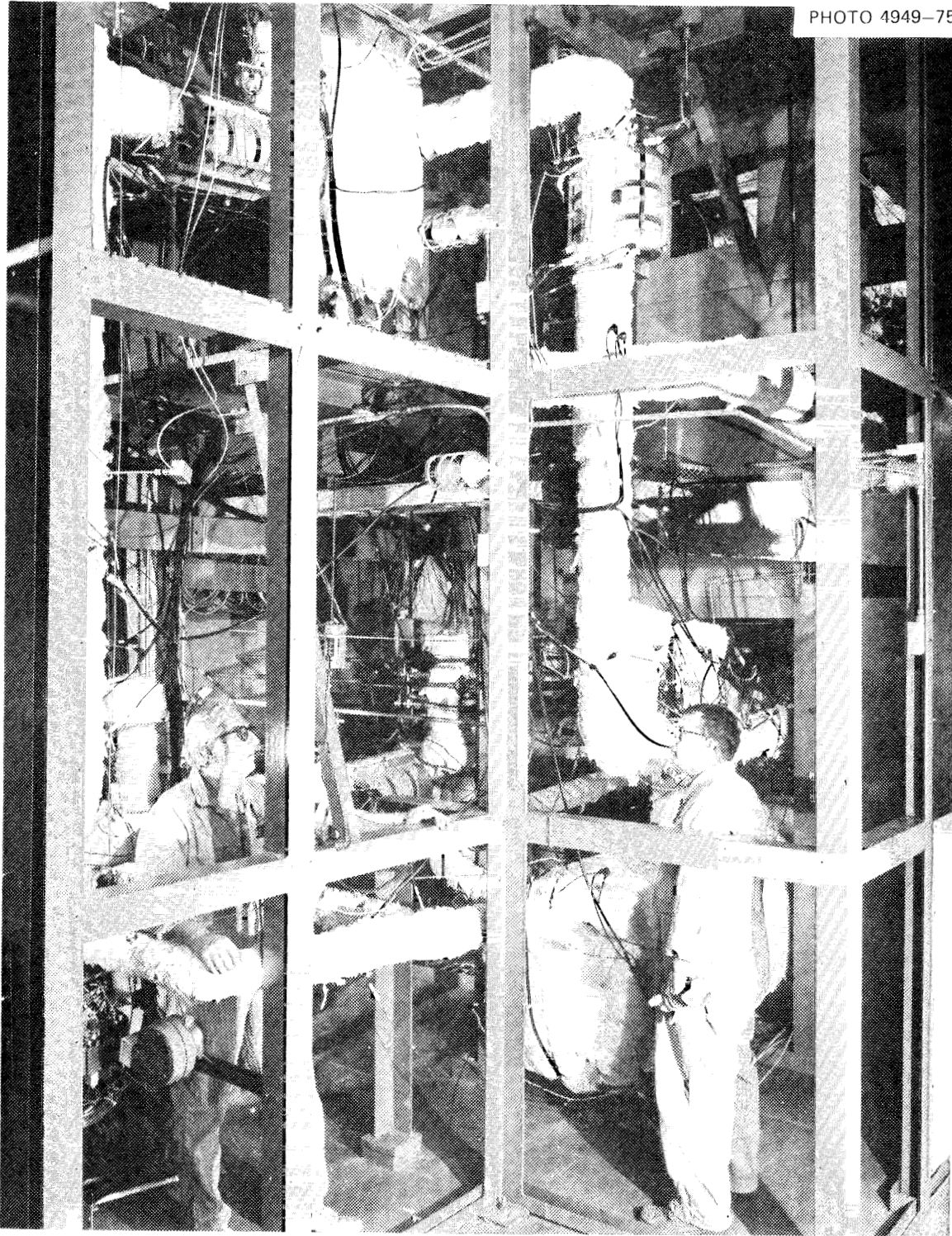


Fig. 5.18. LMFBR FFM. View of new piping added for the boiling experiments.

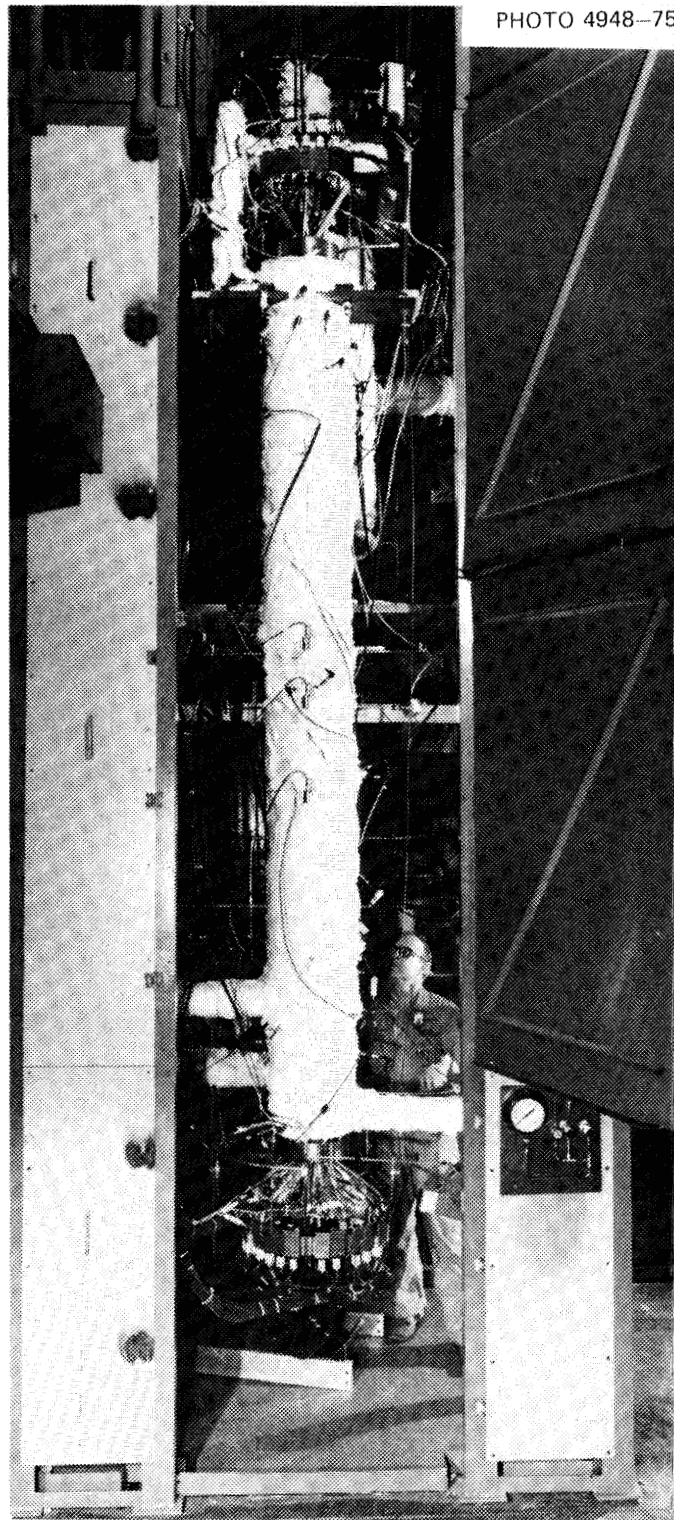


Fig. 5.19. LMFBR FFM. New test-section housing showing bundle 6 heater and instrument connections.

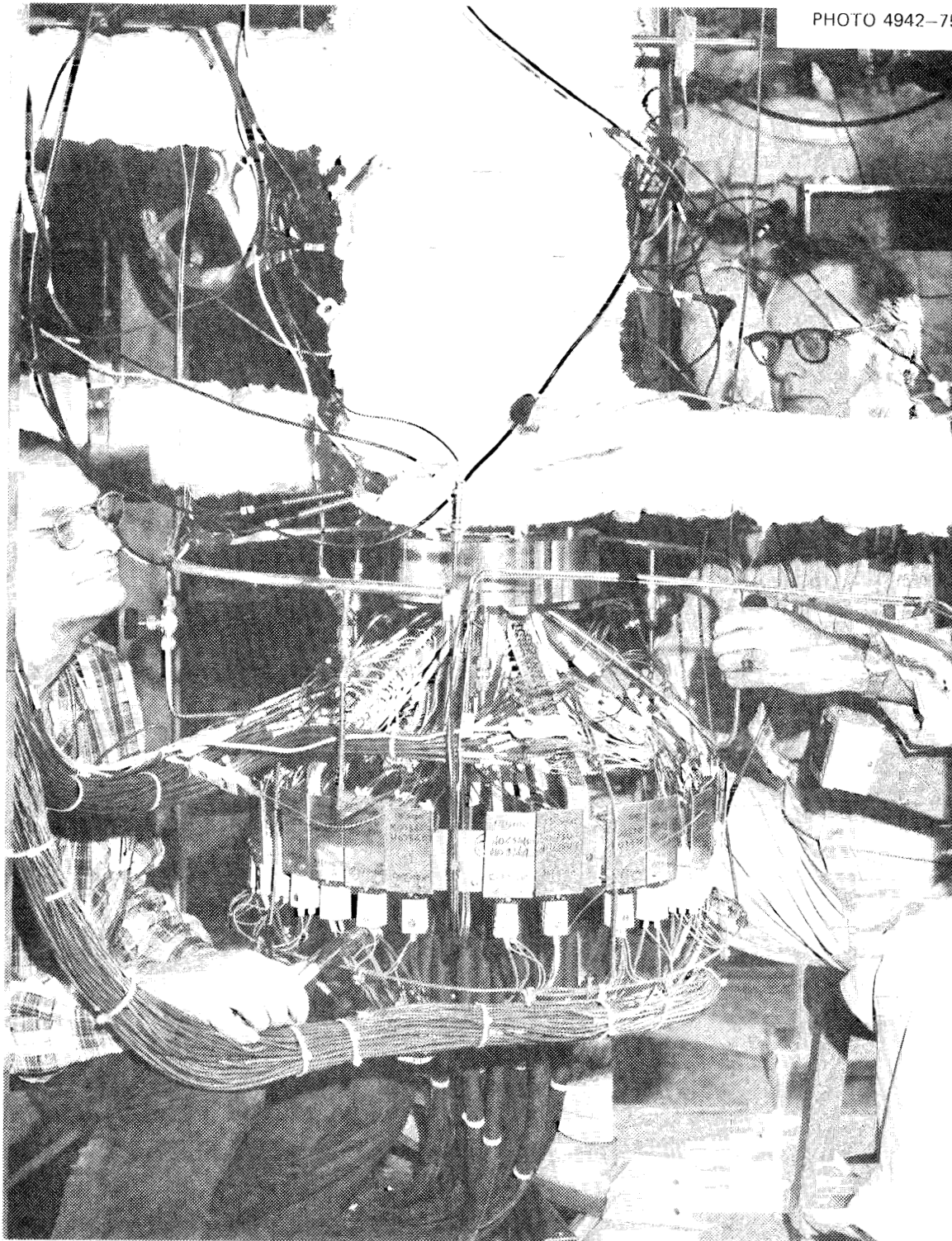


Fig. 5.20. LMFBR-FFM bundle 6A installed in test facility after all instrument and power connections have been made.

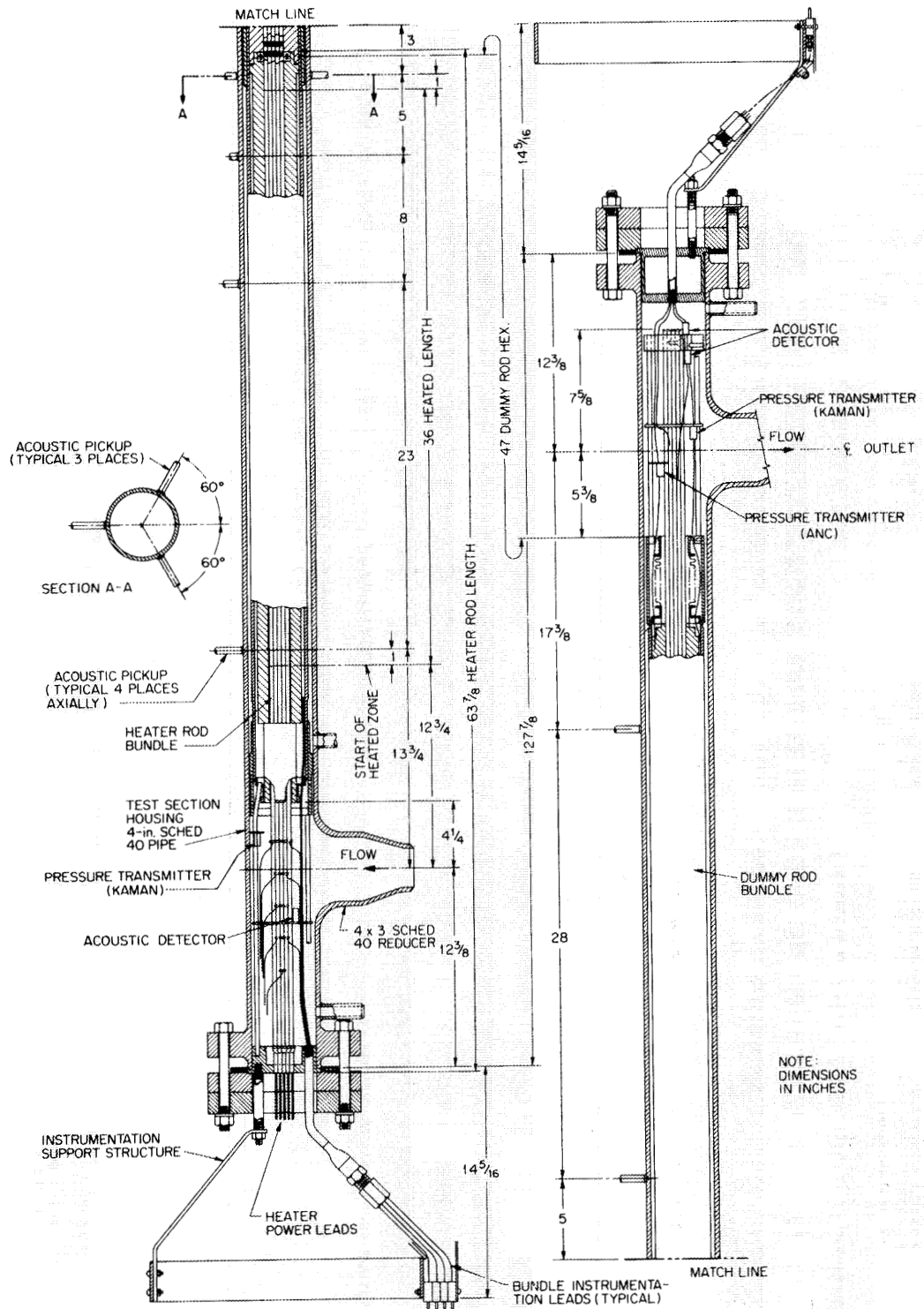


Fig. 5.21. LMFBR-FFM test section bundle 6A assembly. (1 in. = 25.4 mm)

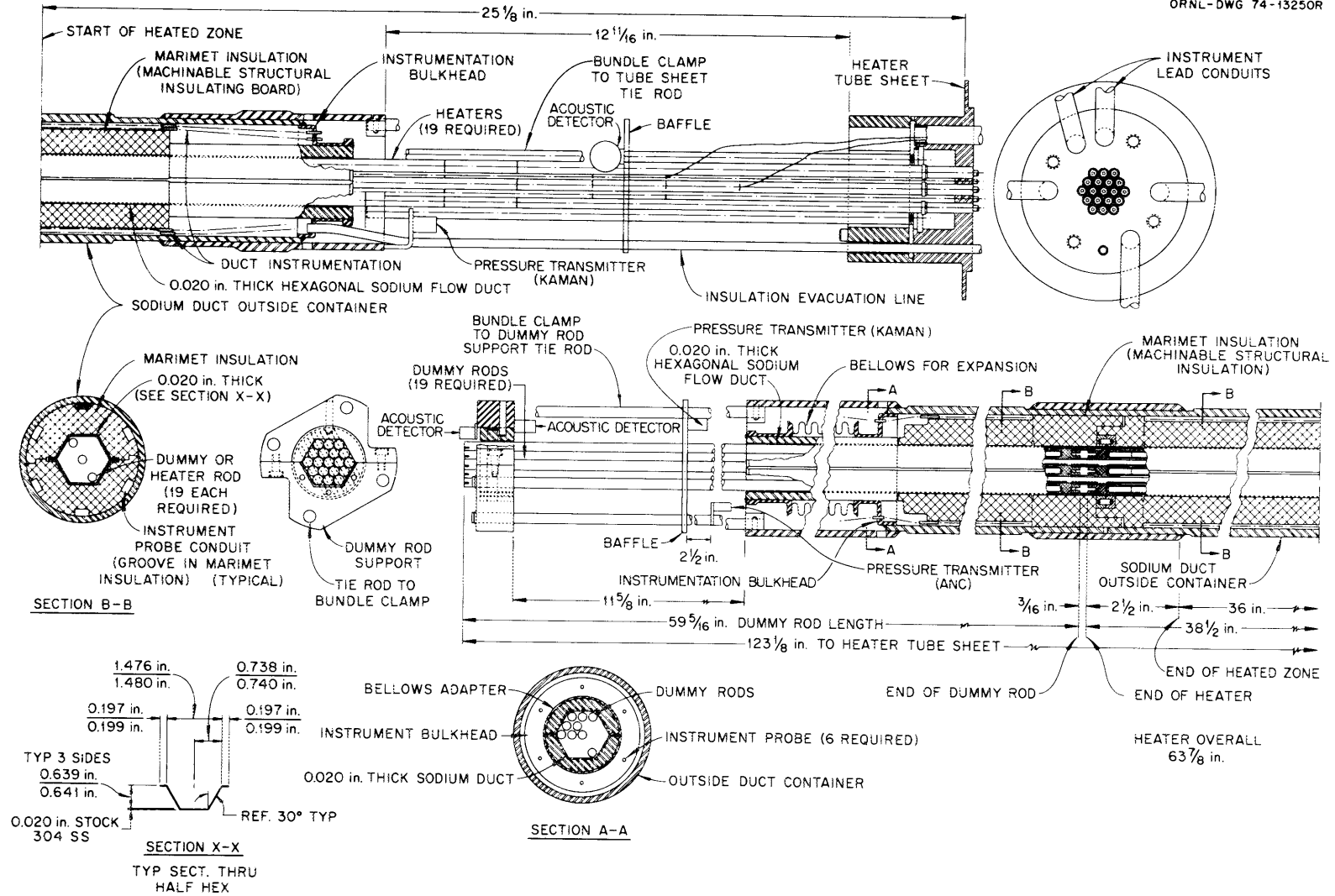


Fig. 5.22. LMFBR-FFM bundle 6A assembly. (1 in. = 25.4 mm)

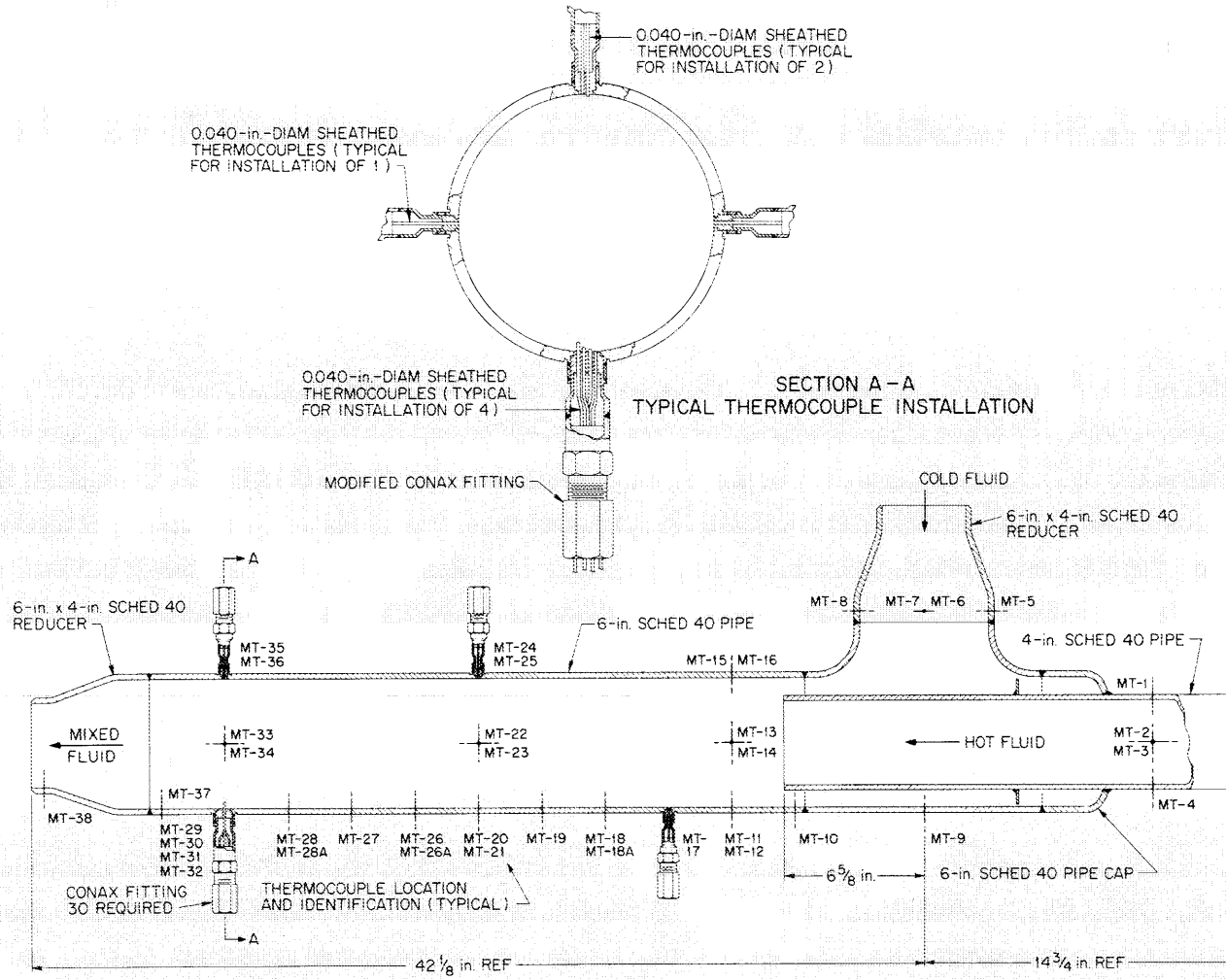


Fig. 5.23. LMFBR FFM. Mixing tee built for Argonne National Laboratory tests. (1 in. = 25.4 mm)



Fig. 5.24. LMFBR FFM. ANL mixing tee assembly after completion of fabrication.



Fig. 5.25. LMFBR FFM. ANL mixing tee assembly after installation in the facility.

and the pressure drop along the flowing sodium increased significantly. To develop an understanding of the cause of the failure, we made a destructive examination of the bundle. Of particular interest was a determination of the points of origin of the heater failures, the underlying cause of the failures, the reason for the increased pressure drop, the location of any heater sheath or internal material freed during the test, and the extent of the rearrangement of the bundle components that occurred during the test.

After the sodium had been removed, the assembly was potted in epoxy and cut into transverse slices to facilitate examination. To maintain identification, lengthwise marks were milled on the outside of the bundle adjacent to sides A and B of the hexagonal cavity. In addition, small transverse grooves were milled at 12.7-mm (1/2-in.) intervals along the length of the 914-mm (36-in.) bundle, and, beginning at the upstream (sodium inlet) end, the spaces between marks were identified by the numbers 1 through 72.

A bandsaw was used to section the potted bundle. The cuts were made so that a number and the milled mark downstream from it appeared on each slice. The surfaces of each slice were prepared for examination by grinding with 60- and 120-mesh silicon carbide abrasive paper on a water-lubricated, high-speed wheel. The ground surfaces were sprayed with lacquer to improve the transparency of the epoxy surface.

Information from the examination is presented in detail in Ref. 3. Visual examination disclosed that heaters 1, 4, 5, and 6 were damaged. In heaters 1, 4, and 5 there was an apparent forceful expulsion of molten Nichrome V heating coil alloy through ruptures in the type 316 stainless steel heater sheaths. Most of the molten alloy froze on the outside of various adjacent heater sheaths; a small quantity spheroidized into globules in the molten sodium and either lodged within the bundle or was swept out. One of these globules proved to be Nichrome V heating element alloy which, after freezing, contained boron in the grain boundaries. Much of the molten alloy formed spheres under the influence of surface tension and remained within the heater tubes. Most of the BN insulation appeared to have remained in place except at the actual rupture sites.

The circumstances surrounding the failure of heater 6 are not as clear, since the entire heater disintegrated over a short section. This failure was also associated with overheating and melting of the heater coil, which, for heater 6, was a high-melting alloy, Kanthal Al. The hot-pressed BN mandrel rods from heater 6 broke into short lengths and lodged in various channels within the bundle. The BN around the outside of the heater coil disintegrated into small granules, except for a few large pieces that lodged within the bundle.

The x-ray mapping capability of a scanning electron microscope was employed to study the distribution of the various alloys throughout the damaged area of the bundle. The alloys of interest were the type 316 stainless steel cladding (heater sheath material) and the Nichrome V and Kanthal Al heater element metals. Maps showing relative iron and nickel concentrations were sufficient to distinguish among the three, assuming that there was no extensive interalloying of the metals. Areas of high nickel and no iron indicated Nichrome V; areas of no nickel and high iron indicated Kanthal Al; and areas of low nickel and high iron indicated type 316 stainless steel. Chromium maps were also made to give experimental assurance. These maps gave increased confidence in the identity of the alloys, but they did not aid in distinguishing among them, since the chromium content of all three alloys is very similar.

The ruptured heaters that contained Nichrome V windings were heaters 1, 4, and 5. All the Nichrome V found in the bundle originated from these heaters. The rupture in heater 5 was the farthest upstream in the slice 57-58 area. A relatively small amount of Nichrome V was expelled from this break. Some of the Nichrome V ran down the sides of the heater under the influence of gravity (upstream with respect to the sodium flow) a distance of 38 mm (1 1/2 in.) to 50 mm (2 in.). Some Nichrome V was observed 76 mm (3 in.) to 102 mm (4 in.) upstream from the rupture spot at slice 54. The metal expelled was attached principally to heaters 1, 3, 4, 5, and 6. Figure 5.26, a nickel x-ray map, reveals that the bridge material between heaters 1 and 5 in slice 57 is a high-nickel metal, which can only be Nichrome V. No penetration or alloying of the sheath by the molten Nichrome V is evident.

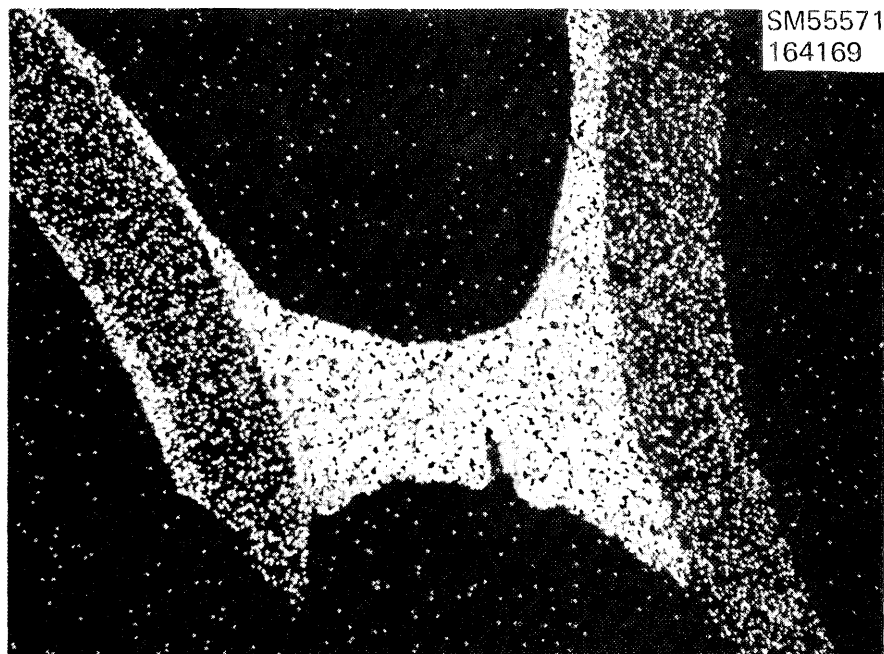


Fig. 5.26. X-ray map of slice 57 showing Nichrome V bridge between heaters 1 and 5.

Close examination of the rupture of heater 5 showed that the sheath was blown open by internal pressure and failed in a highly ductile manner. The nickel x-ray map, Fig. 5.27, more clearly shows one side of the failed sheath and identifies the metal adhering to it and to the sheath of heater 1 as Nichrome V.

In heater 1 the rupture farthest upstream occurred in slice 59. Apparently, little Nichrome V escaped from this rupture, since the hole in the sheath was at least partially blocked by Nichrome, as shown by the nickel and iron x-ray maps in Fig. 5.28. In the figure, the hole in the sheath is filled with Nichrome V. A droplet of stainless steel is attached to the sheath of the heater, and there is a thin layer of Nichrome V between the sheath material and the stainless steel droplet. A broader, thin droplet of either stainless steel or Kanthal Al (or both) is bonded to the sheath, but the nickel map does not clearly reveal the presence or absence of nickel and makes identity uncertain.

Little Nichrome V was in evidence between slices 61 and 65. Most of the Nichrome V present was in thin layers or spots on the sheaths of heaters 1, 4, 5, and 6. The second of the two ruptures in heater 1 was

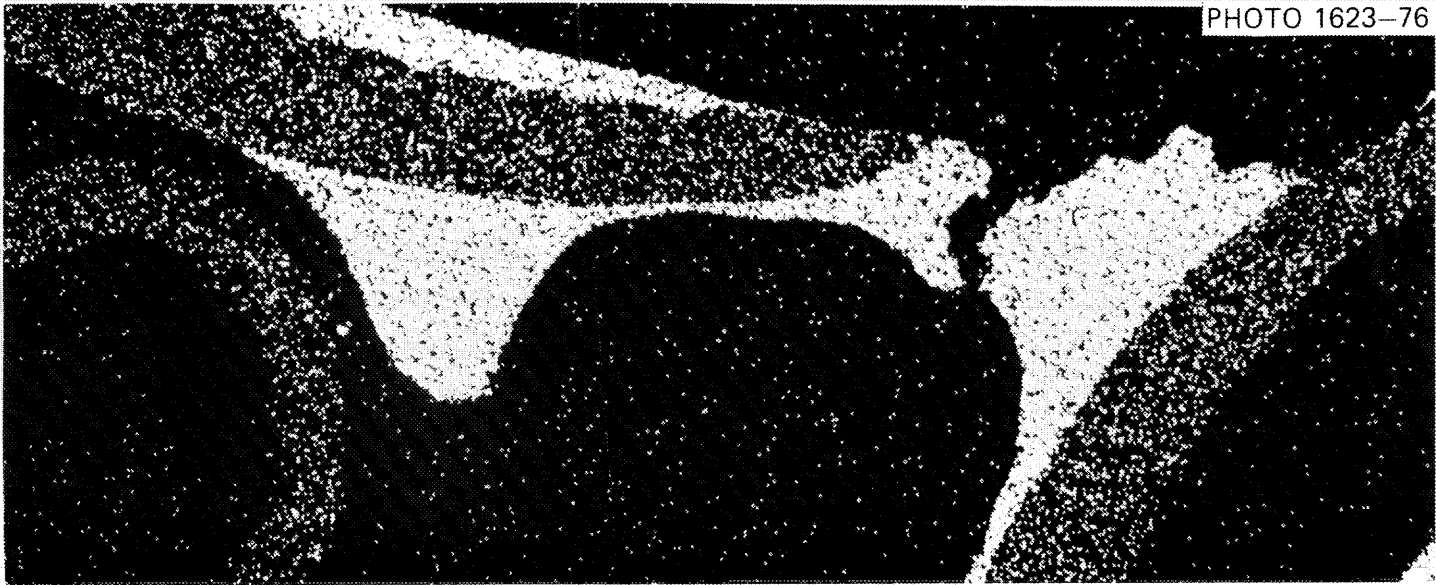
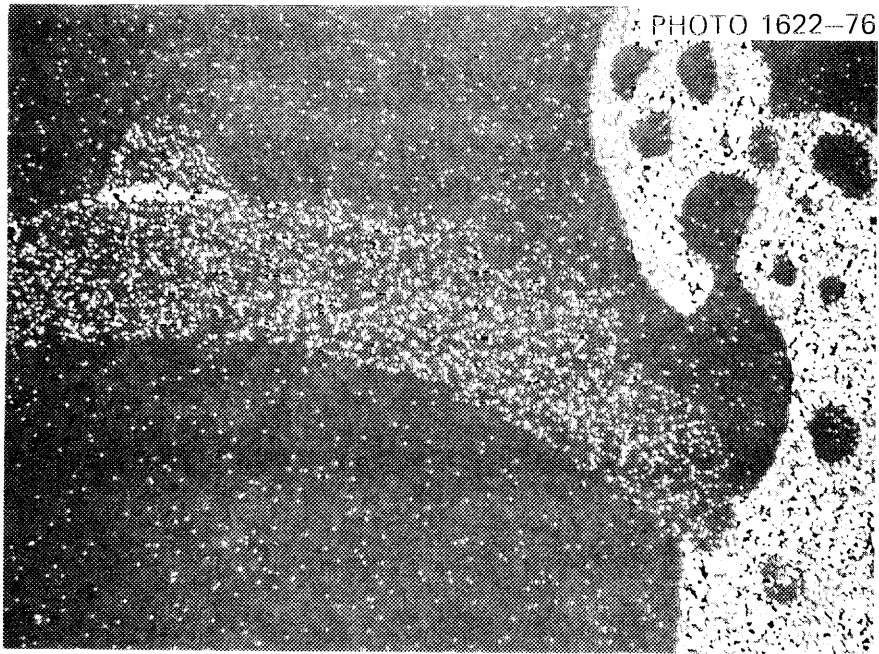
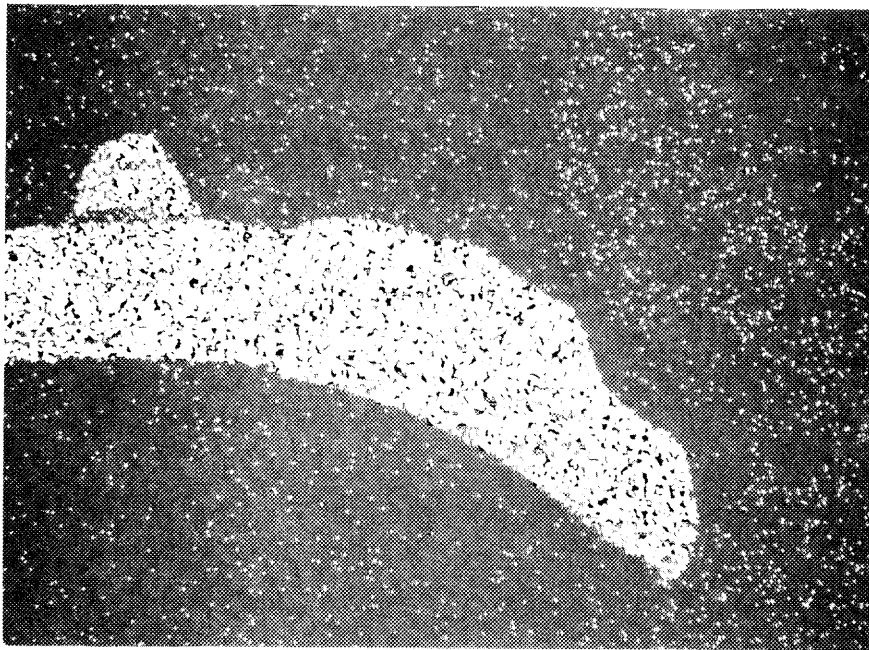


Fig. 5.27. Nickel x-ray map from slice 58-57 showing necked-down heater 5 sheath and Nichrome V from melted heater 5 winding adhering to sheath of heater 1 (right).



(a) NICKEL X-RAY MAP



(b) IRON X-RAY MAP

Fig. 5.28. Nickel and iron x-ray maps of upstream burst of heater 1 as shown on upstream face of slice 60.

in slice 65. Figure 5.29 shows a necked-down part of the sheath from this rupture encased in Nichrome V and adhering to heater 4.

The largest accumulation of Nichrome V was in the vicinity of heaters 12 and 13 in the slice 66 to 67 area and came from the rupture in heater 4. The large quantity of molten Nichrome V ejected through



Fig. 5.29. Nickel x-ray map of area of downstream face of slice 65 showing piece of thinned and necked stainless steel sheath from heater 1 encased in Nichrome V and adhering to heater 4.

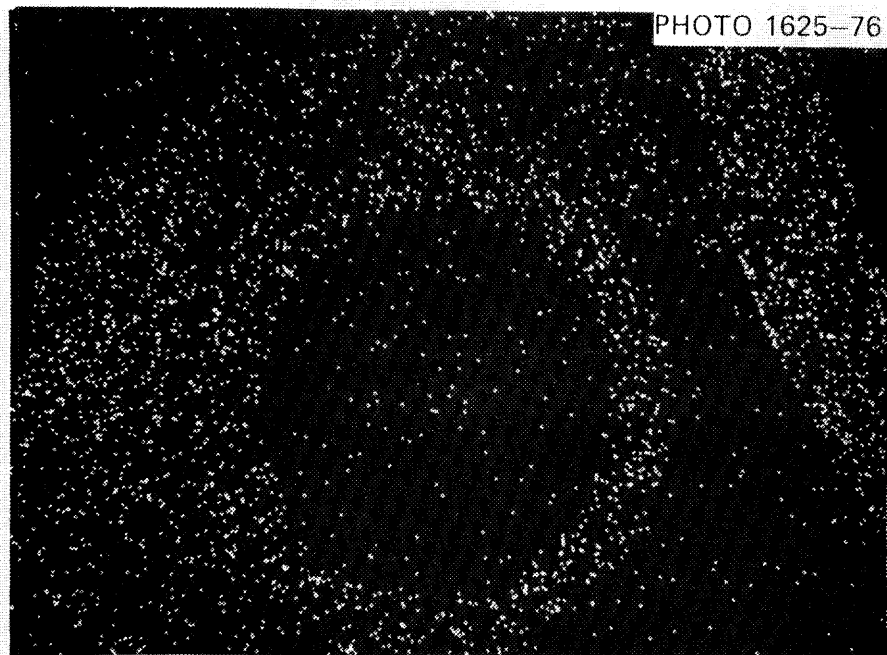
this hole, together with the Nichrome V from heater 1, accounted for the large accumulation in this area of the bundle.

The principal source of stainless steel and the sole source of Kanthal Al was from the burst that occurred in heater 6 between slices 57 and 62. Stainless steel was also freed in the ruptures of heaters 1, 4, and 5 and was deposited on heater 1. These ruptures were small compared to that of heater 6, and the dispersal of stainless steel was probably not very widespread.

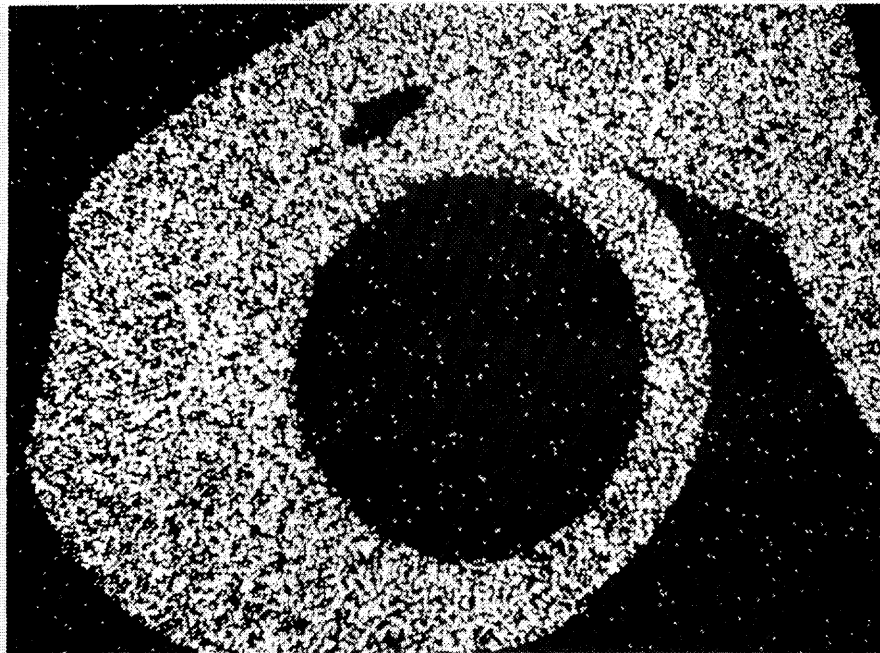
The first damage to heater 6 was observed at slice 57. The BN core was missing at this point, and the Kanthal Al heating element had melted, apparently at the inside diameter of the element. Heater 6 was in a state of complete disintegration. It appeared that pieces of the stainless steel sheath, in a near-molten state, were blown out radially from heater 6 and struck an adjacent heater or wire wrap to which they readily bonded. Figure 5.30 (slice 60) shows this condition as well as an uneven nickel response that suggests the presence of some Kanthal Al mixed with, but not dissolved in, the stainless steel. The presence of Kanthal Al outside of heater 6 is verified by the x-ray maps in Fig. 5.31; the lack of a nickel response identifies the droplets in the maps as Kanthal Al. Figure 5.32 shows x-ray maps of an area on slice 61 in which an apparent stainless steel material has bridged the gap from heater 6 to heater 1. The nickel map indicates a variability in nickel content, with the lowest nickel content being adjacent to heater 1. The shape of the bridging metal reveals that it had been molten when it flowed into position.

Heater 6, at the downstream face of slice 62, illustrates (1) the two types of sheath material transport discovered in the study, (2) the flow of molten metal, and (3) the method and type of deposition of solid pieces. Figure 5.33 shows that the ruptured wall of heater 6 has been thickened by additional stainless steel that probably melted and flowed from another location on the same heater. The nickel x-ray map indicates that the flat projections shown in the map are low in nickel and may be Kanthal Al.

Slices 63, 64, and 65 all showed the thickening of the stainless steel sheath of heater 6, but no areas of thinning were evident in these



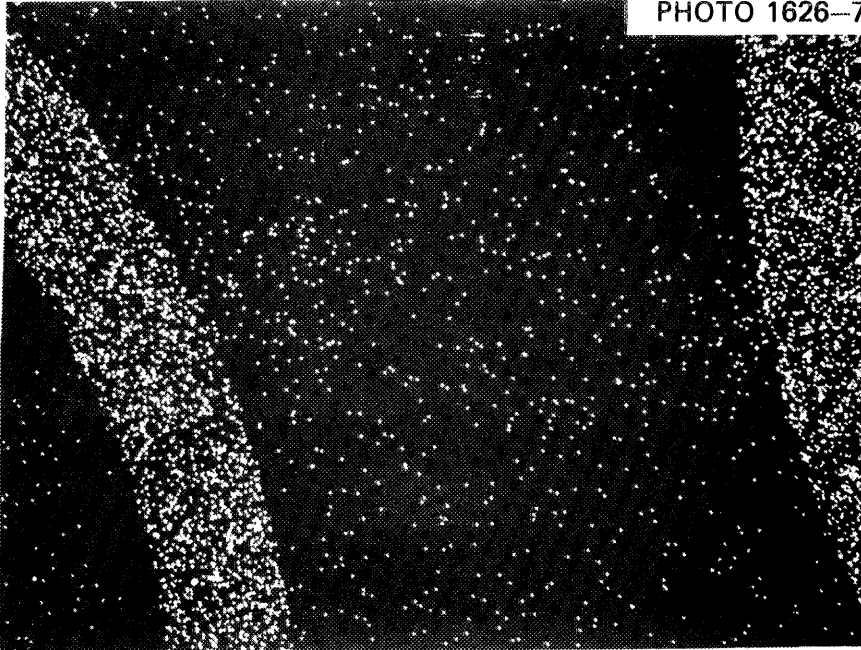
(a) NICKEL X-RAY MAP



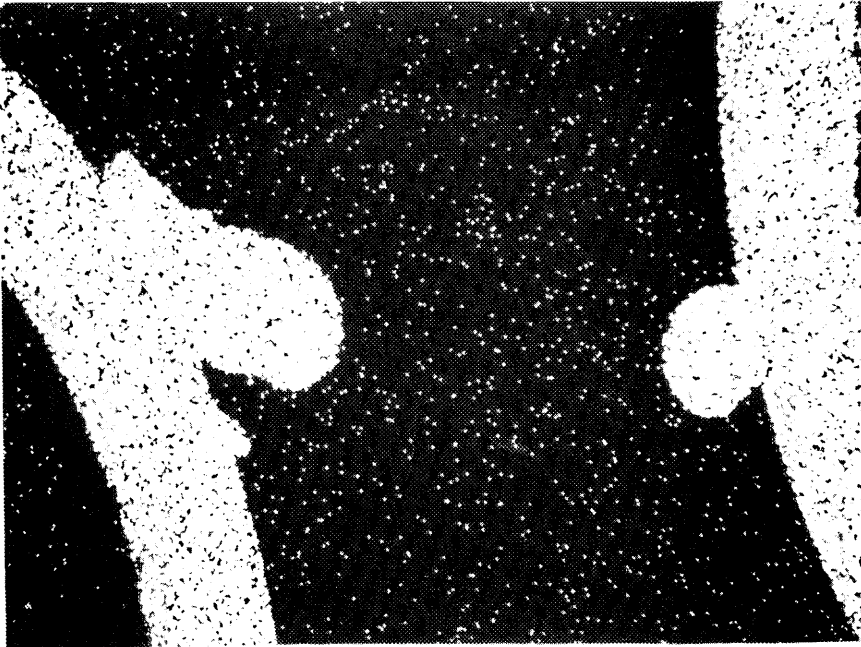
(b) IRON X-RAY MAP

Fig. 5.30. X-ray maps of area of downstream face of slice 60 showing piece of heater 6 stainless steel sheath attached to thermocouple tube of heater 1. The uneven nickel response in (a) may indicate a mixture of stainless steel and Kanthal A1.

PHOTO 1626-76

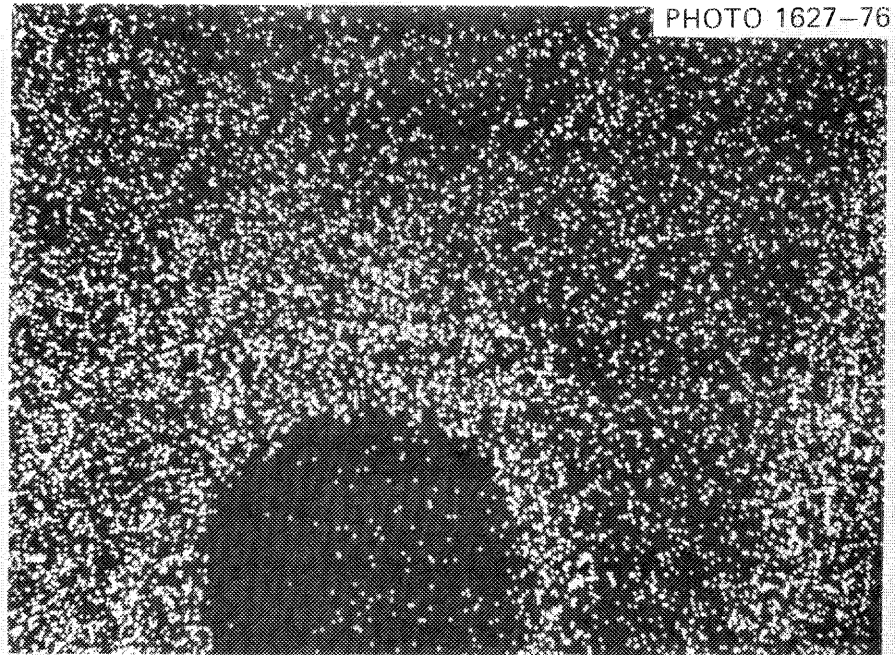


(a)

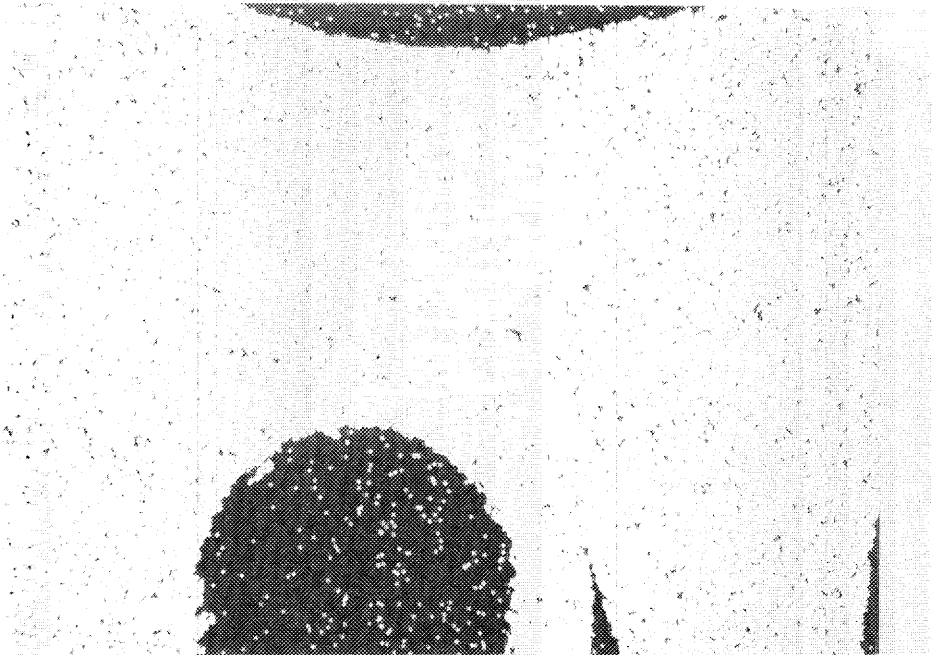


(b)

Fig. 5.31. X-ray maps of area of downstream face of slice 60 showing droplets of Kanthal Al adhering to sheaths of heaters 7 and 17.

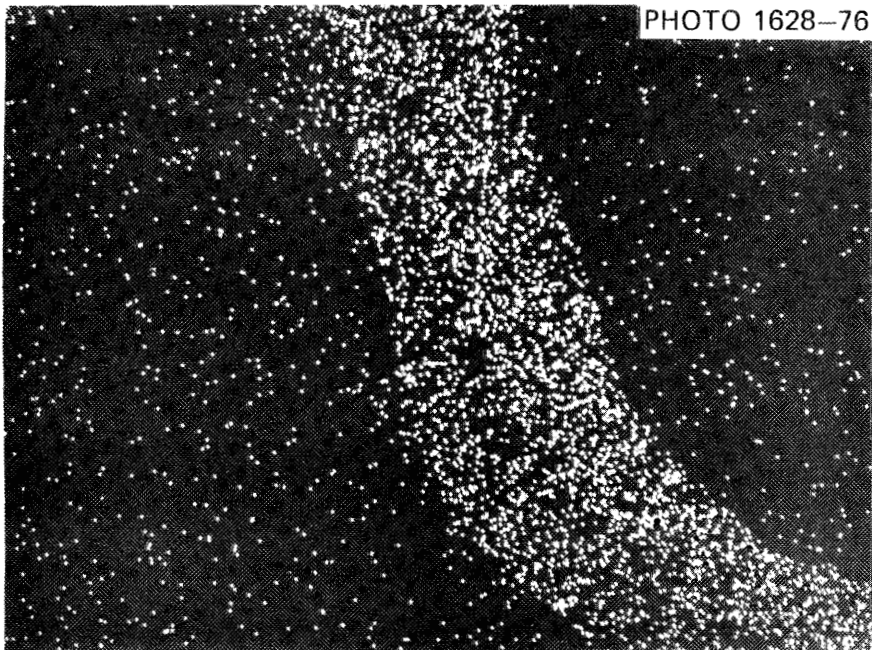


(a) NICKEL X-RAY MAP

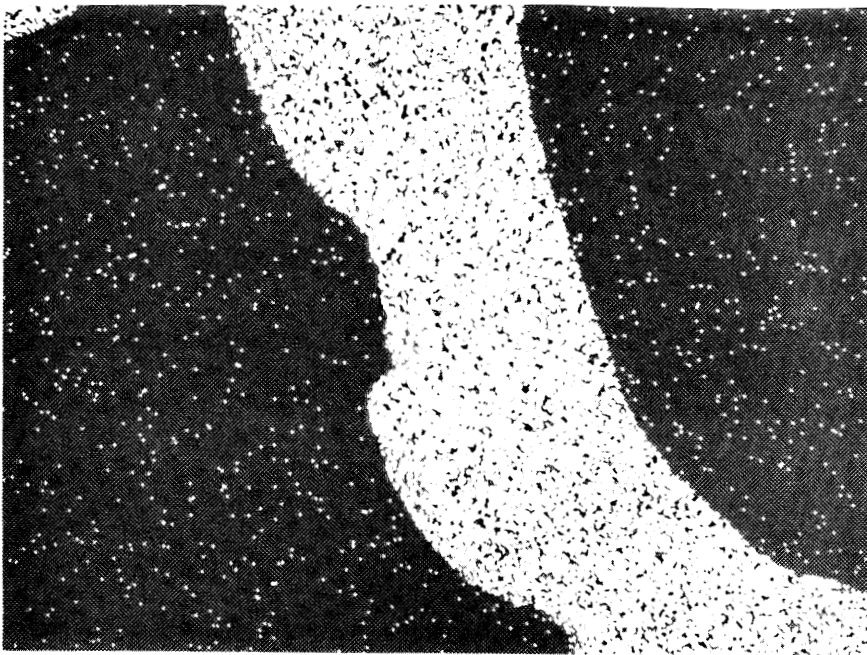


(b) IRON X-RAY MAP

Fig. 5.32. X-ray maps of area on downstream face of slice 61 showing apparent stainless steel bridge between heater 1 (right) and heater 6. Nickel response in (a) is lower on right side of map than on left.



(a) NICKEL X-RAY MAP



(b) IRON X-RAY MAP

Fig. 5.33. X-ray maps of thickened ruptured sheath of heater 6 on downstream face of slide 62 showing stainless steel to be the principal component of the thickened wall. Nickel map (a) indicates flat projections on wall are low in nickel and may be Kanthal Al.

slices nor in any slices to the end of the bundle. This suggests a downstream flow, against gravity, under the influence of the flowing sodium.

An electron spectrographic chemical analysis (ESCA) was made of the Nichrome V bead previously described in an attempt to obtain an insight into the form in which boron was present in the Nichrome V grain boundaries. The ESCA apparatus examines a large area but only to a depth of a few tens of Angstroms. Sputtering of the specimen surface with argon ions revealed nickel, chromium, sodium, chlorine, nitrogen, and sulfur. There were small responses to calcium, titanium, and possibly molybdenum, but no boron was detected. The grain boundary area, compared to the ESCA analyzing area, is small, which may be the reason why boron could not be found.

The study of the locations in the bundle where the alloy residue from the ruptured heaters was found indicated that most of it remained within a few centimeters of its point of origin. This was probably due to the presence of the essentially oxygen-free sodium coolant that flows through the bundles. The sodium cleaned the surfaces of the undamaged heaters, allowing the alloy residue, principally Nichrome V, to wet these surfaces and adhere readily. The sodium also rapidly cooled the molten alloy, thus preventing it from flowing very far and from dissolving or penetrating the sheaths of undamaged heaters.

Since the sodium flows counter to the influence of gravity, the sheath force exerted on any alloy residue opposed the force of gravity, and thus the overall magnitude of the force tending to move the alloy residue either upstream or downstream was reduced.

Another explanation for the relatively small amount of movement of the Nichrome V was the fact that the greatest quantity was released from breaks in heaters 1 and 4. These breaks were located close to the end of the heated zone of the bundle. The flow distance to the unheated ends of the heaters was short, and the lack of heating greatly increased the cooling rate of the Nichrome V.

The ruptures in heaters 1, 4, and 5 were small and occurred while the sheaths were hot and soft but probably not molten. The sheaths of

these heaters were necked down to a knife edge at the points of failure, and only occasional small pieces of sheath broke free.

The catastrophic failure of heater 6 provided the greatest quantity of stainless steel and all the Kanthal Al that was released into the bundle. It seems probable that the Kanthal Al element heated the stainless steel sheath to its melting point, and shear from the flowing sodium caused some of the molten stainless steel to migrate downstream and up the wall of the heater, thickening it in some areas. Then the Kanthal Al may have become hot enough to melt and react with the BN or to heat the stainless steel sufficiently for it to react with the BN, thereby creating pressures great enough to blow the heater apart. The pieces of stainless steel sheath were plastic enough to adhere to adjacent heaters and wraps. There is evidence that some stainless steel melted and possibly alloyed with the Kanthal Al, but in spite of its melting, the stainless steel was displaced not far from its original location and solidified on adjacent heaters and wraps. Large pieces of Kanthal Al were found, but the x-ray maps did not indicate the presence of Kanthal Al, probably because it alloyed with the stainless steel and could not be identified separately.

References

1. M. H. Fontana, LMFBR Safety and Core Systems Programs Progr. Rep. October-December 1974, ORNL/TM-4877.
2. M. H. Fontana, LMFBR Safety and Core Systems Programs Progr. Rep. April-June 1975, ORNL/TM-5076.
3. M. H. Fontana and J. L. Wantland, LMFBR Safety and Core Systems Programs Progr. Rep. July-September 1975, ORNL/TM-5197.
4. Y-12 Development Division Technical Progress Report, Y-1908-3 (June 1975).

6. HEATER DEVELOPMENT

R. E. MacPherson R. W. McCulloch

6.1 LMFBR Heaters

The objectives of this program are to provide heaters for the FFM, to develop both a category II heater that can withstand transients to the point of boiling at the heat flux of $3 \text{ MW}\cdot\text{m}^{-2}$ ($10^6 \text{ Btu}\cdot\text{hr}^{-1}\cdot\text{ft}^{-2}$) and a category III heater that can withstand the temperatures associated with sodium boiling, expulsion, and reentry at the same heat flux.

The fabrication, materials development, and procurement efforts to meet these objectives are reported in this section.

6.1.1 FFM heaters

Simulators for FFM bundle 6A. Analysis of the four 6A simulators with low insulation resistance revealed no significant metallic impurities. The low insulation resistance of the sectioned pieces improved when they were baked in vacuum at 280°C (400°F), which indicates that moisture had been trapped in the simulators during fabrication.

A 6A fuel pin simulator with an infrared (IR) scan similar to those from simulators used for bundle assembly was inserted into the sodium test loop, the purpose being to obtain operation data under conditions both similar to and more severe than those expected in FFM tests. Table 6.1 summarizes this operation. Although a total of almost 400 hr was logged, it was determined later that failure occurred after 21 hr of continuous operation at $2.4 \text{ MW}\cdot\text{m}^{-2}$ ($770,000 \text{ Btu}\cdot\text{hr}^{-1}\cdot\text{ft}^{-2}$) and 800°C (1500°F) sheath temperature with a total of 273 hr of operation. The element and sheath melted at a point $\sim 177.8 \text{ mm}$ (7 in.) from the ground end. This lowered the element resistance by about 10%, but the heater continued to function for the balance of the test.

These test results imply that the 6A bundle should operate at the $16 \text{ kW}\cdot\text{m}^{-1}$ level specified through a major portion of the proposed test program. Another 6A simulator will undergo boiling tests in February in

Table 6.1. Summary of 6A fuel pin simulator 22 sodium loop tests

Hours	Maximum power [kW·m ⁻¹ (kW·ft ⁻¹)]	Total power (kW)	Maximum power [kW·m ⁻² (Btu·hr ⁻¹ ·ft ⁻²)]	Sheath temperature [°C (°F)]
132	20-23 (6-7)	14-16	1.04-1.17 (330-370)	620 (1000)
120	34 (10.5)	24.3	1.86 (590)	730 (1340)
21 ^a	44 (13.5)	31.2	2.43 (770)	900 (1500)
69	20 (6)	14	1.04 (330)	630 (1030)
39	33 (10)	23	1.73 (550)	840 (1400)
6	20 (6)	14	1.04 (330)	620 (1000)
<hr/>				
387 total				

^aSheath melting occurred to end this run (273 hr total).

an attempt to ascertain operational lifetimes under these extreme conditions.

Simulators for FFM bundle 7A. A second 7A simulator that was tested in the sodium loop failed after 2.5 hr of operation at $2.8 \text{ MW}\cdot\text{m}^{-2}$ ($900,000 \text{ Btu}\cdot\text{hr}^{-1}\cdot\text{ft}^{-2}$) and 1100°C (1800°F) sheath temperature. Close examination of all bundle 7A simulator x rays indicated that 27 of the 30 simulators had uncrushed, hot-pressed BN mandrels and gaps in the mandrels as a result. An unsuccessful attempt was made by Watlow to eliminate the gaps by further swaging. Subsequent negotiations were conducted with Watlow concerning simulator resupply, and preliminary indications are that Watlow will remake the bundle at their own expense if ORNL supplies more materials.

Five simulators damaged in shipment were repaired by Watlow and re-shipped to ORNL where they were given IR scans. Two of the five are now acceptable.

Further analysis on the melted area of ribbon from the first failed 7A simulator and grain growth vs temperature studies now indicate that excessive grain growth, which can cause ribbon failure, occurs in less than 4 hr above 1400°C (2550°F). Evidence also indicates that a boron-platinum eutectic is formed at approximately this temperature when pure boron is put into contact with the ribbon. It appears that the large grains make the ribbon susceptible to melting at temperatures well below its 1800°C (3200°F) melting point if free boron is present. Studies are in progress to find a material that can be added to the Pt-8% W alloy in small amounts to retard the grain growth.

Simulators for FFM bundle 8A. The purchase requisition for bundle 8A has been delayed pending further definition of problems with simulators for bundle 7.

6.1.2 Fuel pin simulators for others

Twenty-five ANL simulators have been shipped to ORNL from Watlow to undergo IR scanning, and ANL is in the process of sending an additional 34 to ORNL for IR scanning. All scanning is being done on a cost-recovery basis.

6.1.3 Advanced fuel pin simulator development

Category III fuel pin simulator development. Difficulties are still being experienced in the machining of variable-width Pt-8% W ribbons. Several attempts have been made during this reporting period. Two Pt-8% W ribbons have now been machined, but tool wear was excessive and tolerances were not held as well as expected. The tough and ductile Pt-8% W material plastically deformed, causing a dog-bone-shaped ribbon cross section, and deburring will be necessary prior to winding.

Investigations are in progress on the use of an alumina-template grinding machine to fabricate the ribbons. The machine can grind to tolerances less than 13 μm (0.0005 in.), and no wear or burring occurred on small test samples. In addition, 30 or more ribbons can be machined in a single operation, saving considerable time and cost. However, details of machine fixturing, ribbon rough cutting prior to grinding, and ribbon stacking must be established.

The possibility of failure of the Pt-8% W ribbon at temperatures below its melting point, as well as machining problems, has led to the consideration of Nichrome V ribbon as a backup. Ribbon of this material has been procured and is being prepared for machining.

Preform fuel pin simulator. An effort is in progress to fabricate locally a fuel pin simulator using BN preforms and a variable-width ribbon but initially no thermocouples. The first of such simulators is scheduled to be fabricated jointly by Reactor Division simulator development personnel and the Y-12 Development Division in February. Fabrication techniques will be modified and refined until an acceptable simulator is fabricated. The fabrication techniques will then be relayed to a vendor or vendors through a development contract to permit them to supply a small number of such simulators for test and evaluation.

Conductivity cell testing. Labor and material delays have been experienced in the fabrication of a high-temperature conductivity cell furnace. However, electrical conductivity tests will begin in late January or early February 1976.

Preliminary electrical resistivity data were obtained on cold-pressed BN preforms fabricated from HCM powder. These tests show that

the resistivity is about $10^6 \Omega\text{-cm}$ at 1025°C (1900°F) and decreases at the rate of about one decade per 170°C (300°F).

More detailed resistivity information, as well as thermal conductivity data on both powder and preform conductivity cells, should be obtained in the next reporting period.

BN investigations. The request for capital funds to support commercial manufacture of preforms on a high-volume basis has been approved, and the purchase requisition is now being processed. ERDA is handling the procurement, since one of the possible preform fabricators is the Carbon Products Division of Union Carbide Corporation in Parma, Ohio.

In the interim, to fill the demand for preforms for prototype and conductivity cell use, preforms are being fabricated locally on an as-needed basis. Improvements in the pretreatment of powder have allowed the pressing pressures to be increased to 300 MPa (50 kpsi), but die malfunctions are still occurring frequently and slowing the fabrication process.

One of the primary development goals is a process that will allow high-volume production of preforms having highly oriented crystallites. Orientation is achieved by pressing powders of very fine particle size. However, pressing is difficult because these powders are too fine to pour into dies, and their low "tap" density requires a large die center punch movement to achieve final size.

Metals and Ceramics Division personnel have devised a BN powder pretreatment that partially eliminates these disadvantages. The original TS-1325 powder is ball milled for approximately 3 hr to achieve ultrafine particle size. This powder is then treated with a solution of 1% camphor in benzene, allowed to dry, and pressed at low pressure into 12- to 25-mm-diam (0.5- to 1-in.) cylinders. These cylinders are then broken up, but agglomerates remain that are much larger than the original particles. This yields a powder that still has good orientation properties, can be loaded into dies, and has a "tap" density between that of HCM and the original TS-1325 powder. An additional advantage of this powder is that its lubrication properties are enhanced, making it less likely to cause die lockup during pressing.

Powder pretreatment residues, as well as lubricants used in pressing, can now be completely removed with the anhydrous ammonia baking process developed during the last reporting period. An additional vacuum bake-out process is now used prior to the ammonia bake to enhance impurity elimination. Plans are under way to install a purification process locally that will purify commercially fabricated preforms.

6.1.4 Nondestructive testing

Data Corporation, Inc., is in the final stages of testing the interface and magnetic recording equipment for the automated IR scanning system. The equipment should be operational on the IR scanning system by February 1976.

A voltage offset device that offsets the dc position of a signal resulting from a high-temperature scan has been installed in the IR scanning system. This device makes possible high-resolution IR scanning of sheath temperatures of 600°C (1100°F) or more. In addition, the offset voltage is recorded so that the absolute temperature is also known.

Cost quotations have been obtained on the automation of radiography interpretation. This total system will provide over 300,000 readings per radiograph in a 6-min scan with tolerances to fractions of a millimeter on coil turns per millimeter, concentricity, width, and thickness.

7. NEUTRONICS ANALYSIS OF A DISRUPTED CORE

G. F. Flanagan S. N. Cramer R. A. Lillie

The purpose of this task is twofold: (1) to test and verify neutronics methods for analysis of disrupted LMFBR cores using existing computer codes; and (2) to develop a three-dimensional Monte Carlo quasi-static code appropriate for coupling with existing hydrodynamics codes for use in LMFBR core disassembly calculations.

7.1 Effects of Bubble Collapse on Reactivity

The analysis of the reactivity insertion due to collapse of vapor bubbles in a uniform-density medium was essentially completed, and a summary report is in preparation. A letter¹ summarizing the results of the special variable-density bubble collapse reactivity transport calculations was sent to ERDA.

An attempt was made to analyze the bubble collapse reactivity using modified cell-weighting techniques. These attempts failed after sample problem checks, and theory indicated that the heterogeneity effect was in the square of the mean free path (first moment) and not in the mean free path itself.

All attempts to use Monte Carlo techniques directly to analyze the bubble collapse problem have resulted in large standard deviations ($\sim 100\%$). An attempt to bound the problem based on leakage differences from the Monte Carlo calculations resulted in very small standard deviations but gave a bound only on the magnitude of the reactivity.

A meeting to review the bubble calculations was held on December 4, 1975, at ERDA headquarters and was attended by W. H. Hannum, H. Alter, and F. Tooper. It was concluded at the meeting that Monte Carlo techniques using the upper-bound approach could be used to estimate the upper bound on the magnitude of the reactivity associated with the bubble collapse with small standard deviations. The magnitude of this estimate on a sample problem is approximately half that predicted by Behrens.

Efforts in this area are to be continued to determine the extent of this upper bound and to apply the technique to multiregion reflected systems. The results are to be compared with the transport calculations that were previously discussed.

7.2 Development of a Transient Monte Carlo Code

Coding was started that will use Monte Carlo techniques to estimate the integral parameters [namely, ρ/Λ , β_i/Λ , and Λ (where ρ is the reactivity, Λ is the prompt generation time, and β_i is the delayed neutron fraction for the i th delay group)] used in the quasi-static approach. The adjoint (importance weighting) for the integral parameters was obtained from a discrete ordinate calculation performed on the FFTF Engineering Mockup Critical R-Z geometry model.

7.3 Reactivity Determinations of a Disrupted Core

Work on this subtask was postponed again to allow completion of work on the bubble collapse problem. Information on models for use in the study is being gathered from Appendix F of the Clinch River Breeder Reactor Preliminary Safety Analysis Report.

Reference

1. R. A. Lillie to G. F. Flanagan, Oak Ridge National Laboratory Internal Memorandum, Nov. 19, 1975; Subject: Bubble Collapse Reactivity Effects Using Variable-Density Models.

8. CENTRAL COMPUTERIZED DATA BASE FOR LMFBR SAFETY CODES

G. F. Flanagan E. T. Tomlinson
N. M. Greene V. M. Forsberg

The purpose of this task is to define, develop, and maintain a central computerized data base for LMFBR safety computer codes.

Data forms from the participating organizations were received and compiled into a master list. These data were then cross-correlated, and the maximum ranges for the independent variables for each parameter of interest were obtained. Based on this information, the size of the data storage arrays needed for the data is being determined.

A meeting was held with the ORNL systems staff to discuss the needs of the data base and to determine whether it can be used in a time-shared operation (TSO) mode instead of permanent system monitoring with interactive terminals. It appears it can with some modification. A TSO consultant from the Computer Sciences Division staff will work with N. M. Greene in getting the system operable on the ORNL TSO system as soon as possible.

A meeting with Savannah River Laboratory staff was held on November 14, 1975. The formats and the file description were finalized in such a way as to remain compatible with the JOSHUA computer system.¹ The problems of TSO of JOSHUA with Savannah River Laboratory system personnel also were discussed. JOSHUA, at present, is semioperational at ORNL in the batch mode.

All of the proposed members of the Safety Analysis Data Coordinating Group (SADCG) were contacted. All proposed SADCG subcommittee chairpersons agreed to present a scope and a tentative list of subcommittee members at the organizational meeting, which is to be held on January 22 and 23, 1976. ORNL personnel attending will be G. F. Flanagan, N. M. Greene, and C. Richmond.

Reference

1. N. M. Greene to G. F. Flanagan, Oak Ridge National Laboratory Internal Memorandum, Dec. 17, 1975; Subject: New Formats for SACRD.

Internal Distribution

- | | | | |
|--------|---------------------|--------|---------------------------------|
| 1. | N. J. Ackerman | 47. | F. C. Maienschein |
| 2. | R. K. Adams | 48. | C. D. Martin |
| 3. | A. H. Anderson | 49. | W. J. McCarthy |
| 4. | M. Bender | 50. | R. W. McCulloch |
| 5. | R. Blumberg | 51. | H. C. McCurdy |
| 6. | R. H. Bryan | 52. | C. K. McGlothlin |
| 7. | J. R. Buchanan | 53. | R. L. Moore |
| 8. | R. M. Burnett | 54. | F. R. Mynatt |
| 9. | R. H. Chapman | 55. | F. H. Neill |
| 10. | C. J. Claffey | 56. | L. C. Oakes |
| 11. | D. L. Clark | 57. | L. F. Parsly |
| 12. | C. W. Collins | 58. | P. Patriarca |
| 13. | W. H. Cook | 59. | T. W. Pickel |
| 14. | W. E. Cooper | 60. | H. Postma |
| 15. | W. B. Cottrell | 61. | M. W. Rosenthal |
| 16. | S. N. Cramer | 62. | T. H. Row |
| 17. | F. L. Culler, Jr. | 63. | J. P. Sanders |
| 18. | R. G. Donnelly | 64. | R. L. Scott |
| 19. | G. G. Fee | 65-66. | Myrtle Sheldon |
| 20. | W. F. Ferguson | 67. | J. D. Sheppard |
| 21. | G. F. Flanagan | 68. | W. H. Sides |
| 22-26. | M. H. Fontana | 69. | R. H. Sigler |
| 27. | V. M. Forsberg | 70. | M. J. Skinner |
| 28. | A. P. Fraas | 71. | C. M. Smith |
| 29. | D. N. Fry | 72. | I. Spiewak |
| 30. | P. A. Gnadt | 73. | R. D. Stulting |
| 31. | M. J. Goglia | 74. | J. J. Taylor |
| 32. | N. M. Greene | 75. | D. G. Thomas |
| 33. | A. G. Grindell | 76. | R. H. Thornton |
| 34. | J. T. Han | 77. | E. T. Tomlinson |
| 35. | N. Hanus | 78. | D. B. Trauger |
| 36. | W. O. Harms | 79. | W. E. Unger |
| 37. | R. A. Hedrick | 80. | J. L. Wantland |
| 38. | H. W. Hoffman | 81. | J. R. Weir |
| 39. | P. R. Kasten | 82. | J. S. White |
| 40. | J. W. Koger (Y-12) | 83. | G. D. Whitman |
| 41. | T. S. Kress | 84. | W. J. Wilcox |
| 42. | R. Kryter | 85. | R. Saxe (Consultant) |
| 43. | R. A. Lillie | 86-87. | Central Research Library |
| 44. | D. G. Line | 88. | Y-12 Document Reference Section |
| 45. | R. L. Ludwig (Y-12) | 89-91. | Laboratory Records Department |
| 46. | R. E. MacPherson | 92. | Laboratory Records (RC) |

External Distribution

- 93. Assistant Administrator for Nuclear Energy, ERDA, Washington, D.C. 20545
- 94-95. Director, Division of Reactor Development and Demonstration, ERDA, Washington, D.C. 20545
- 96. Director, Reactor Division, ERDA, ORO
- 97. Research and Technical Support Division, ERDA, ORO
- 98-313. For distribution as shown in TID-4500 under categories UC-79, -79e, -79p (25 copies — NTIS)